Harald Görner

Removal of dissolved elements in aluminium by filtration

Thesis for the degree of Philosophiae Doctor

Trondheim, November 2009

Norwegian University of Science and Technology
Faculty of Natural Sciences and Technology
Department of Materials Science and Engineering

NTNU
Norwegian University of
Science and Technology

NTNU
Norwegian University of Science and Technology

Thesis for the degree of Philosophiae Doctor

Faculty of Natural Sciences and Technology
Department of Materials Science and Engineering

ISBN 978-82-471-1854-2 (printed ver.)
ISBN 978-82-471-1855-9 (electronic ver.)
ISSN 1503-8181

Doctoral theses at NTNU, 2009:225

Printed by NTNU-trykk

Preface

The research presented in this thesis was carried out at the Department of Materials Science and Engineering at the Norwegian University of Science and Technology, NTNU, in close cooperation with SINTEF's department of materials and chemistry in the period from November 2002 to December 2006. The author has been working in the industry since 2007. The interpretation of the experimental results and final compilation of this thesis was therefore not completed before September 2009.

The present work was carried out within the framework of the project NorLight Shaped Castings of Light Metals with the following partners: Alcoa Automotive Castings, Scandinavian Casting Center ANS; Elkem Aluminium ANS; Fundo Wheels AS; Hydro Aluminium Metal Products; Hydro Magnesium; the Netherlands Institute for Metals Research; Norwegian University of Science and Technology (NTNU); and SINTEF (project responsible). The funding was provided by the Norwegian light metals industry and the Norwegian Research Council what is greatefully acknowledged.

Acknowledgments

*Wisdom lies in listening to the people and learning from them. But you must draw your own conclusions for your work. This work would have not been realized without **you**. I am very greatfull for the open environment at NTNU / SINTEF and the warm welcome by the people of this country.*

I am in great debt to my supervisors Prof. Em. Thorvald Abel Engh and Lars Arnberg for offering me the opportunity to specialize in the field of metallurgy. My gratitude goes to them for giving me the freedom to explore the features in process metallurgy by myself and providing guidance whenever it was necessary. Their support and encouragement also across the border of Norway is greatefully acknowledged.

Many people at NTNU as well as SINTEF have been contributing to this work with their expertice, experience and kind assistance. At the Department of Materials Science and Engineering thanks are due to Prof. Leiv Kolbeinson (chemical thermodynamics), Pål Ulseth (metallography), Elin Nilsen (XRD measurements), Reimo Helenius (technical drawings), Tore Jørgensen (technical support), Jan Arve Baatnes (castshop, toolshop), Hilde Martinsen Nordø and Åse Lill Salomonsen (accounting and administration), and Bjørn Olsen and team (machining of experimental setup, sawing of ingots). The cooperation with Øyvind Nielsen (project leader), Martin Syvertsen, Anne Kvithyld, Sean Gaal, Eivind J. Øvrelid, Juraj Chmelar (milling), Kai Tang (Fact Sage calculations), Morten P. Raanes (electron microprobe measurements), Per Ola Grøntvedt (imaging), Arne Nordmark, Freddy Syvertsen, and Alf Sandberg (all castshop) at SINTEF's department of materials and chemistry is gratefully acknowledged.

Particular recognition is deserved by Martin Syvertsen, Anne Kvithyld, Sean Gaal, Eivind J. Øvrelid, Juraj Chmelar, and Kai Tang for their obliging and unselfish support on all topics and through all stages of this work. Your cooperation is most appreciated and the insight I gained with your help is invaluable.

I would like to acknowledge the industry partners and the people there. The economic and efficient technical support by supplying funding, metal for the filtration experiments and the chemical analysis of the sampled melt is highly recognized. My thanks go to Jorunn Voje, Harry Fossheim, Margit Kønigsson, and Dagfinn Nilsskog at Elkem Aluminium; Jorunn Snøan Mæland, Petter Åsholt, Hans Ivar Laukli, Ann Øygård, Bjørn Rasch, and Harald Johnsen at Hydro Aluminium; Jan Ove Løland at Alcoa; and last but not least Asbjørn Prestmo now retired from Fundo Wheels. Offering insight into the "world of production" and showing your interest made the industrial relevance of this work most apparent to me.

Also I do not want to forget my fellow PhD students and "predecessors" many of who became good friends. Thank you Anne, Arjan, Adrian, Christa, Emanuelle, Florian, Hans Ivar, Gustav, Marisa, Maneesh, Reimo and Sorin for an unforgettable time.

My deepest gratitude goes to my parents and my dear Anne for being by my side and for their great belief in me throughout all those years.

Trondheim, September 2009

Harald Görner

Summary

The objective of this work was to show that removal of alkali from aluminium melts by means of filtration is feasible. Therefore, a chemically active filter based on a packed bed of AlF_3 grains was designed and built. Varying parameters like contact area, impurity level, residence time and temperature, pure aluminium melts as well as two different AlMg–alloys containing different levels of Na or Ca were filtered to reveal the kinetics of the AlF_3 filter material. Filtration experiments performed on a laboratory scale using AlF_3 filter grains in a packed bed gave high removal rates for alkali metals such as Na and Ca following first order kinetics. Removal was between ~50% and ~95% for a dimensionless contact area A* increasing from ~1 to ~2, respectively. An empirical expression for the total mass transfer coefficient to be expected for the removal of Ca at a certain velocity of pure molten aluminium was determined. Further it could be shown that the elements removed are retained in the AlF_3 filter.

List of publications

1. Görner H, Engh TA, Syvertsen M, Zhang LF: *"Removal of Na and Ca from Aluminum Scrap through Filtration"* . LF MATERIALS SCIENCE FORUM Volume: 546-549 Pages: 801-806 Part: Part 1-4 Published: 2007

2. Görner H, Engh TA, Syvertsen M: *"Kinetics of an AlF_3 Aluminium Filter"*. LIGHT METALS Pages: 765-770 Published: 2006

3. Görner H, Syvertsen M, Øvrelid EJ, Engh TA: *"AlF_3 as an Aluminium Filter Medium"*. LIGHT METALS Pages: 939-944 Published: 2005

Nomenclature

A	Cross sectional area of filter bed	m^2
ΔA	Area of contact of inclusion attached to filter wall	m^2
A^*	Dimensionless contact area	
a	Average distance between atoms of melt and inclusion	m
a_{AlF_3}	Activity of AlF_3	
A_m	Surface area per unit volume of packing	$m^2\ m^{-3}$
a_{solute}	Activity of surface active element	
a_v	Specific surface area of the filter grains	$m^2\ m^{-3}$
Δa_{v_i}	Standard deviation in specific surface area of the filter grains	$m^2\ m^{-3}$
C	Empirical factor correcting for the porous medium	
c	Concentration at distance z away from filter inlet	ppm
c_0	Inlet concentration	ppm
c_i	Concentrations of species i in bulk	ppm
c_i^*	Concentrations of species i at the melt/filter interface	ppm
c_i^{in}	Inlet concentration of species i	ppm
c_i^{out}	Outlet concentration of species i	ppm
c_{in}	Number of inclusions per unit volume entering the filter, or inlet concentration	
c_{out}	Number of inclusions per unit volume leaving the filter, or outlet concentration	ppm
C_D	Drag coefficient	
D	Capillary slot width,	m
	or diffusion coefficient	$m^2\ s^{-1}$
D_{Na}	Diffusion coefficient for sodium	$m^2\ s^{-1}$
D_{Ca}	Diffusion coefficient for calcium	$m^2\ s^{-1}$
D_{Mg}	Diffusion coefficient for magnesium	$m^2\ s^{-1}$
d	2 times the metallic radius of the solvent atom	m

D_p	Effective particle diameter	m
E	Removal efficiency	
$\overline{E}$	Average efficiency for all measurements of an experiment	
E_i	Single value of E determined during an experiment	
F_D	Drag force exerted on inclusion	N
F_{SL}	Force necessary to separate the liquid from the solid body	N
G	Total free energy of the system	kJ mol^{-1}
	or the mass velocity	kg s^{-1}
ΔG	Gibbs energy of formation	kJ mol^{-1}
$\Delta G_{Stripping}$	Change in Gibbs free energy for stripping	
	an oxide layer of area S	kJ mol^{-1}
g	Gravity	m s^{-2}
H	Height of liquid in a vertical capillary,	m
	or height of the filter bed	m
H_F	Height of the filter bed	m
H_M	Metal head	m
j_M	Colburn j-factor for mass	
K	Equilibrium constant	
k	Boltzmann constant	J K^{-1}
k_c	Mass transfer coefficient	m s^{-1}
Δk_c	Standard deviation of mass transfer coefficient	m s^{-1}
L	Velocity of a liquid along a horizontal slot,	m s^{-1}
	or length of outlet tube	m
L_A	Sum of perimeters	µm $µm^{-2}$
$\dot{m}$	Mass flow	kg s^{-1}
m_1	Atomic weight of solvent	
m_2	Atomic weight of solute	
m_{Al}	Atomic weight of aluminium	
m_{Na}	Atomic weight of sodium	
m_{Ca}	Atomic weight of calcium	
m_{Mg}	Atomic weight of magnesium	

N	Number of data points x_i and y_i	
n_i	Number of moles of component i	mol
$\dot{n}_i$	Flux of species i across melt boundary layer	kmoles s^{-1} m^{-2}
ΔP	Pressure drop	N m^{-2}
Δp	Pressure drop	N m^{-2}
p	Capillary pressure	Pa
p_{AlF_3}	Vapour pressure above solid AlF_3	bar
Pe	Dimensionless Peclet number	
R	Gas constant,	J mol^{-1} K^{-1}
	or radius of filter bed	m
R^2	Correlation coefficient	1
R_0	Inner radius of outlet tube	m
r	Radius of inclusion,	m
	or the capillary radius	m
Re	Dimensionless Reynolds number	
ΔRe_i	Standard deviation in Re for one experiment	
Re_p	Particle Reynolds number	
S	Area of stripped oxide layer	m^2
S_i	Projected surface area of an inclusion	m^2
S_p	Surface area of particle	m^2
S_V	Surface area per unit volume	m^2 m^{-3}
Sc	Dimensionless Schmidt number	
Sh	Dimensionless Sherwood number	
T	Absolute temperature	K
$T_{Furnace}$	Furnace temperature	°C
t	Residence time of the melt in the filter	s
Δt	Standard deviation in residence time	s
u	Relative velocity	m s^{-1}
u_0	Superficial velocity	m s^{-1}
V	Volume of inclusion	m^3
v	Volume of liquid L,	m^3

	or the molten aluminium flow velocity relative to the particle	m s^{-1}
$\dot{V}$	Volume flow	m^3 s^{-1}
V_p	Volume of particle	m^3
V_{V_0}	Voids fraction	%
W_a	Work of adhesion	N m
W_c	Work of cohesion	N m
W_{SL}	Adhesion strength of the liquid and the solid body	N m^{-1}
x	Independent variable in regression analysis	
x_i	Independent variable for measurement i	
X_A	Mole fraction of pure component A	
X_B	Mole fraction of pure component B	
y	Function of C and x_i	
y_i	Efficiency determined for measurement i	
z	Height of filter bed	m

Greek letters

χ^2	Figure-of-merit-function	1
δ	Boundary layer thickness	m
ε	Void fraction (porosity)	
$\Delta\varepsilon_i$	Standard deviation in the void fraction (porosity)	
ϕ	Interaction coefficient given by the ratio ($W_a^{SL}/W_c^S\ W_c^L$)	
Γ^{XS}	Excess surface coverage of surface active element	mol m^{-2}
μ	Dynamic viscosity	Pa s
μ_{Al}	Dynamic viscosity of aluminium	Pa s
μ_i^S	Chemical potential of component i in the solid phase	J mol^{-1}
μ_i^L	Chemical potential of component i in the liquid phase	J mol^{-1}
γ_A	Surface tension of pure component A	N m^{-1}
γ_B	Surface tension of pure component B	N m^{-1}
γ_{LV}	Surface tension of a liquid L in contact with a vapour V	N m^{-1}
γ_{SV}	Surface tension of a solid S in contact with a vapour V	N m^{-1}

γ_{SL}	Interfacial tension of a solid *S* in contact with a liquid *L*	N m^{-1}
$\gamma_{metal/flux}$	Interfacial tension between molten metal and flux	N m^{-1}
$\gamma_{oxide/flux}$	Interfacial tension between oxide and flux	N m^{-1}
$\gamma_{metal/oxide}$	Interfacial tension between molten metal and oxide	N m^{-1}
η	Dynamic viscosity	Pa s
θ	Wetting angle	°
θ_{SL}	Wetting angle of a liquid wetting a solid	°
$\theta_{metal/oxide}$	Contact angle for metal/oxide when in contact with flux/filter	°
ρ	Density of liquid in a vertical capillary	kg m^{-3}
ρ_i	Inclusion density	kg m^{-3}
ρ_{Al}	Density of aluminum melt	kg m^3
σ_{LV}	Surface energy of a liquid *L* in contact with a vapour *V*	J m^{-2}
σ_{SV}	Surface energy of a solid *S* in contact with a vapour *V*	J m^{-2}
σ_{SL}	Interfacial energy of a solid *S* in contact with a liquid *L*	J m^{-2}
σ_i^2	Total error in measurement *I*	
σ_{x_i}	Error in independent variable for a single measurement	
σ_{y_i}	Error in *E* of measurement *i*	
τ	Time,	s
	or residence time	s
υ	Kinematic viscosity	m^2 s
Ω	Additional surface area created	m^2

Abbreviations

AlSCAN	Analyzer for hydrogen in liquid aluminum
BACO	British Aluminium Corporation
CFF	Ceramic Foam Filter
CHAPEL	Direct measurement of partial pressure of hydrogen in aluminium melt
COSMA	Controlled Addition of Sodium Modifiers to Aluminium Alloys
DC	Direct Current
EDS	Energy Dispersive Spectrometer

EPMA	Electron Probe Microanalyzer
GWP	Global Warming Potential
IBT	Initial Bubble Test
LAIS	Liquid Aluminum Inclusion Sampler
LARS™	Liquid Aluminum Refining System
LiMCA	Liquid Metal Cleanliness Analyzer
MTS	Metal Treatment Station
NTNU	Norwegian University of Science and Technology
OEM	Optical Emission Spectroscopy
PoDFA	Porous Disk Filtration Apparatus
Prefil	Pressure Filtration Melt Cleanliness Analyzer
ppm	Parts per million (by mass)
RAM	Removal of Alkali Metal
RPT	Reduced Pressure Test
SEM	Scanning Electron Microscope
SPC	Statistic Process Control
TAC	Treatment of Aluminium in Crucibles
UBC	Used Beverage Cans
USFIRALS	Ultrasonic melt treatment - degassing, filtration, and grain refinement
XRD	X-Ray Diffraction

Table of Contents

Chapter 1

INTRODUCTION

The expanding use of aluminium alloys for high end applications in castings, extrusion, rolling etc. will never let improving melt quality efforts become unfashionable. Thus more companies will have to catch up to current state of the art. Also there is a strong drive from the downstream industries for further improvements and new developments.

The intention of chapter 1 is to provide a theoretical and practical basis for discussing impurities in aluminium and their removal by filtration. Also present trends regarding melt quality in primary/secondary smelting and foundry industry are presented.

This work aims especially at the treatment of scrap. In the handling of primary metal removal of sodium from the Hall-Heroult cell plays an important role. For secondary metal there is no such step. Levels of sodium can be acceptable. However, calcium levels may be high so that Ca must be removed. Filtration to remove inclusions

is required. Therefore it is tempting to combine removal of Ca and inclusions by filtration.

A general term “quality” is introduced and applied to molten metal to find a measure of melt quality. Impurities in the melt are identified to be the main reason for product failure both during production and use. Thus, melt cleanliness becomes a measure of melt quality. Two major types of impurities can be distinguished, (1) dissolved elements, and (2) suspended particles. Sources of impurities can be traced back to the raw metal, various melt processing operations, and the molten metal interactions with the refractory and the environment. Essentially, melt quality can be controlled by the removal of alkali trace elements, H, and inclusions [1], [2]. Various techniques, such as in-line spinning nozzle units, furnace fluxing and packed bed, rigid media and ceramic foam filters are used to control impurity levels. To make sure melt quality standards are met, these processes must be monitored to allow statistical control [1]. Therefore appropriate detection methods are reviewed. Also the problem of melt quality specifications is addressed here.

1.1 Introducing “Melt Quality”

The German Institute of Standardisation has given the following definition of quality: “Quality is a measure of the ability to fulfill defined and presumed demands.” These demands may be regarding a product or a supply of services, and they can be those of the customer, the producer or the society [3]. Refering to the definition given above, quality can therefore never be an absolute measure. It will always be a relative one that is changing with increasing demands. This terminology, also often referred to as “Fitness for Use”, applies to molten metal quality as well.

Aluminium from reduction cells is not a high purity product. For most products, this establishes the lower composition limit for non-reactive elements [4]. Quality compromising contaminants are broadly classified as dissolved and suspended impurities [5]. Their sources range from the charge material, the refractory and its melt interactions, melting, handling and holding methods, temperature control, alloying, modification and grain refinement to the H content due to moisture [6]. Impurities are even introduced by melt cleaning operations.

The extent to which any contaminant renders a particular alloy “unfit for use” is situational, and a function of the processing techniques employed, specific chemistry, and product application. For example in aluminum ingot extrusions Na and Ca concentrations significantly in excess of 10 ppm are usually allowable whereas for some qualities of rolled aluminum products Na levels below 1 ppm are required to prevent edge cracks [5], [7].

A lot of money, time and effort goes into controlling the melt impurity levels, i.e., H, alkali metals, and inclusions, in companies producing aluminium alloys and shaped castings. However, there is a problem with melt quality control; there is often a lack of specifications. A specification is a guarantee that a certain product attribute is within certain limits [1]. For example, it is normal for customers to specify the chemical composition of their ingot products since the relationship between composition, product performance and final properties has generally been recognised [8]. The chemical composition of products is specified for every batch and, in most cases, controlled to within the required limits. If the composition is outside the limit, then the product is scrapped [1]. As soon as we move away from chemical composition, the picture is not as clear regarding the exact relationship between H and inclusion content on the product performance and final properties. In general, we know when the levels of H or inclusions are too high due to complaints for blisters, porosity, tear-offs, splits, holes, etc. The dilemma is in fixing appropriate specifications for hydrogen and inclusion content for any given product [8]. Most companies aim for internal melt quality limits, but since not every batch is routinely measured for H and inclusions (and sometimes Na), there is no guarantee the product is within those limits [1].

Deriving useful melt quality specifications can be somewhat difficult. A specification should be based on product performance in some logical way, which means that the effect of contaminants on properties must be specified. For many semi-finished products, the number of inclusions is not of critical importance, rather the maximum size [9]. Therefore the relationship between the defects and the impurities needs to be known not only qualitatively but also quantitatively, to know to what extent the impurity needs to be controlled. In practice, this is sometimes difficult to establish. Sometimes only by monitoring the product and the customer’s experience can the critical parameters of impurity be established. There have been few attempts to predict

defect rates from first principles. In some cases the degree of effort spent on melt quality control may be excessive for certain products [1], resulting in a too expensive and thus not very competitive product.

Generally the number of defects in the product increases as the level of impurity in the melt increases. Melt quality can be quantified by the composition and level of impurity, as well as particle size and number size distribution of the inclusions.

1.1.1 Dissolved Elements

Dissolved impurities include alkali elements and gas. Na, Ca and Li are typical examples of the former, while H_2 is the only known gas with appreciable solubility in molten aluminum [5]. Elements such as Na and H are also regarded as volatile elements due to their high vapour pressure. Impurities as Ca and Li, but also Ti for instance, can be removed by adding a variety of chemicals to the melt, and therefore they are referred to as reactive elements. Examples of non-reactive elements are Fe and Si, which are very difficult to remove from aluminium by ordinary processes. One way of refining is to use three-layer electrolysis where the impurities are absorbed in another liquid. A second method of separation is zone refining utilizing fractional melting/solidification. This aluminium product has a very low content of non-reactive impurities, namely less than 10 ppm [7]. To produce a relatively clean metal in the industry, high purity metal has to be added or metal from reduction cells must be selected to lower the contents in Fe and Si [4]. For this reason particular attention must be paid to prevent additional Fe contamination during melt operations. Fe is usually found in intermetallic precipitates which form during solidification. In one case, the shape of an Fe containing Al-Si phase often poses problems. This particular precipitate often embrittles, or otherwise causes deleterious mechanical properties. Fatigue strength, ductility, and impact strength are compromised when this phase is either needle-like or blocky in shape. However, the morphology of this phase can be modified by “balancing” the Fe content with Mn in the ratio of 1Fe:0.5Mn. In this way, the shape of the microstructural constituent is changed to a more acceptable “Chinese Script” appearance. Another case which mainly occurs in pressure die-casting alloys is commonly known as “sludge”. This is an intermetallic

compound consisting of Fe, Cr, and Mn elemental constituents in an Al-Si matrix. For high pressure die-casting, management of such impurities has given rise to an expression called the “sludge factor” [10]:

$$Fe + 2Mn + 3Cr = 1.8 \quad (1.1)$$

If the concentrations of the above elements exceed 1.8 by mass, then, as a general rule, sludge formation is likely to occur. Sludge formation is both temperature and composition dependent. Sludge is very detrimental as this phase is extremely hard, creating tool wear, breakage, and machining inconsistency when producing precision machined castings.

Na and Li can cause edge cracking during hot rolling by creating low melting point phases at the grain boundaries. For most products Na levels are kept below 10 ppm. For Al-Mg alloys which are more sensitive, levels are kept in the 0 – 5 ppm range. Additions of Si in Al-Mg alloys of more than 1000 ppm suppress the high temperature embrittlement caused by Na, and also Sr. Such additions may compensate for concentrations of up to 2 ppm Na or Sr [11]. Also extrusion defects are linked to certain Na levels. Whereas the author of Reference [5] sees no concern in Na levels significantly in excess of 10 ppm for common alloy extrusions, Reference [12] reports a 50% decrease of extrusion speed for an increase in Na from 7 to 17 ppm. In the production of shaped castings, Na is commonly added deliberately in order to promote the plate-to-fibrous transition for eutectic Si (modification). In such products, a stable Na content is crucial for the mechanical properties of the end product. Alternatively, Ca may be added to facilitate the eutectic modification. However, it has a somewhat weaker effect compared to Sr, but the Ca additions keep their level easily unlike Na. If Sr is used as the eutectic modifier, then any Ca present will act as an impurity impairing the positive effect of Sr. All these modifiers (Sr, Na, Ca) increase porosity in castings [13]. H_2 causes porosity as it comes out of solution during solidification. The porosity can cause blisters in extrusions or during hot rolling of sheet metal. As the inclusion content increases and cooling rate decreases, the formation of pores increases [14], since the impurities act as nucleation sites for hydrogen pores to form. Also interdendritic regions are more spacious due to the coarser dendritic network at lower cooling rates,

giving the pores more room to grow. In general, values below 0.2 ppm and preferably less than 0.1 ppm H are aimed for [1]. Below about 0.03 ppm no porosity is found [14]. Some foundries aim at stabilizing the H content at about 0.15 ppm rather than to minimize it, as this results in a better distribution of porosity and thus a reduced reject rate. Such stabilizing can be obtained by degassing the melt with a mixture of argon and 5-10% hydrogen [15].

1.1.2 Suspended Particles

Suspended impurities are physically distinct and mechanically separable phases referred to as inclusions [5]. Inclusion particle sizes in unprocessed aluminum melts range from MgO and Al_4C_3 dispersoids of a few microns in size to Al_2O_3 and $MgAl_2O_4$ films and clusters that extend several millimeters [2]. Concentrations are in the range of part-per-million levels to fractional percentages [5]. For example, a dirty aluminum melt from a melting furnace may have on average about 10,000 inclusions equal to or larger than 15μm in diameter per kilogram prior to settling in a holding furnace. As expected, the number of inclusions greatly increases for small particle sizes of about 1-5μm [16]. Inclusions can be solids, immiscible liquids (e.g., halide salts), or combinations thereof. The former usually consists of oxides, but can include carbides, nitrides, borides, and intermetallic compounds [5]. The intermetallic phases are chemically more active than most of the non-metallic inclusions as they can go partly or totally into solid solution during annealing of the metal at high temperature [7].

The presence of non-metallic inclusions, which can affect mechanical properties, machinability, porosity, corrosion resistance, electrical conductivity and even cosmetic appearance, is one of the most serious problems not only in aluminum castings but also during hot rolling (pinholes in foil and beverage cans) and extrusion [17]. As for melts of Al and Mg alloys actively interacting with H and O, these inclusions consist of, mainly, their oxides, i.e., stable chemical compounds with a low degree of thermal dissociation. It is well known, that these dispersive particles are not wetted by melts and do not take part in the solidification process [18]. Investigations, reported in References [19]-[21], thoroughly deal with the manifestation of different casting defects and their ways of formation. Oxide skins and intermetallic phases have been identified to be the

primary casting defects of capital importance which again have secondary effects like the blocking of interdendritic feeding or a decrease in fluidity. The authors observe an increase in intermetallics with increasing cooling rate. Thereby positive effects from a high cooling rate and short dendrite arm spacings (DAS) on elongation after fracture will be impaired. On the other hand, these dispersive non-metallic impurities are perfect nuclei for degassing of the melt [18].

1.2 Sources of Impurities

1.2.1 Bulk Metal

Molten aluminum comes from two sources:

- *Virgin or primary metal* from electrolytic reduction of alumina (dissolved and reduced in cryolite) in the Hall-Heroult electrolytic cell.
- Recycled aluminum products (*Secondary metal*) remelted

Impurity levels of metal deriving from single electrolysis are compared with those which are possible to attain using three layer electrolysis in Table 1.1. The chemistry of recycled aluminum products from a remelt furnace operation is quite different from smelter metal as can be seen by the comparison provided in Table 1.2 [4]. But the source of the elements does not matter as long as they are within the specified compositional range. The difficulty with a scrap-based alloy is in avoiding the elements you do not want. Almost any alloy can be made from a scrap base. A competent secondary processor can meet the challenge of hitting the compositional target through scrap purchasing, blending programs, and processing techniques. The crucial factor on choosing a metal source should be the economics of using scrap versus prime metal and alloying agents coupled with the manufacturing costs associated with the different feed materials. If compositional concerns are taken care of, then the next level of concern for a foundry or cast house is the contaminants [22].

Table 1.1: Typical impurity levels from pot-line versus three layer electrolysis [4].

	Typical Concentrations (ppm)	
Impurity	***Smelter***	***3-Layer Electrolysis***
Mg	10 - 40	< 1
Na	30 - 50	< 1
Ca	2 - 5	< 1
Li	0 - 20	< 1
Si	300 - 700	1 - 5
Ti	30 - 50	< 1
V	100 - 200	< 1
Fe	500 - 2000	< 1
Ni	10 - 30	
Cu	5 - 30	
Zn	20 - 200	
Ga	80 - 180	
(Oxides)	0 - 60	
(Borides)	0 - 60	
(Nitrides)	0 - 60	

Table 1.2: Typical melt chemistry from smelter and remelt operations [4]

	Molten Metal Source	
Characteristics	***Smelter***	***Remelt***
Composition	Primary metal unalloyed	Alloyed at or close to final composition
Dissolved Hydrogen	0.1 - 0.2 ppm	0.2 - 0.4 ppm
Alkalis Na	30 - 50 ppm	≤ 10 ppm
Ca	2 - 5 ppm	≤ 10 ppm
Li	0 - 20 ppm	≤ 1 ppm
Inclusions	≥ 1.0 mm^2/kg Al_4C_3 or (15 - 40 ppm Al_4C_3)	≥ 0.1 ≤ 1.0 mm^2/kg Al_2O_3, MgO, TiB_2, Al_4C_3, $MgAl_2O_4$

As seen, dissolved H_2 is usually present at levels of one tenth of 1 ppm or more, while recycled metal is generally higher (e.g. double). By contrast, inclusion levels from smelter stock run higher, at ≥ 1mm^2/kg (15 – 40 ppm Al_4C_3) versus levels ranging between 0.1 and 1mm^2/kg for remelt. The units of mm^2/kg derive from the PoDFA method of cleanliness assessment where the mm^2 area of inclusions trapped is rated versus the amount of metal passed. Finally, smelter metal is associated with a higher level of dissolved alkalis (Na, Ca, Li), totalling 20 – 100 ppm [4].

The metal from the reduction cells contains commonly 100 ppm Na before [7] and 0.3-0.6 ppm H_2 after it has been siphoned to the transfer crucible. There it is further reduced in H_2 and Na content when the melt is poured into the mixing furnace. The rapid reduction in both contaminants is caused by the drop in melt temperature and by a rapid evaporation of those elements. The metal from the reduction cells seems to approach the equilibrium H_2 value dictated by local humidity and melt temperature, whereas the Na level fades with time [4].

The origin of the dissolved alkalis derives from the presence of fluoride salts; NaF, CaF_2, and LiF, in the electrolyte. Additionally, the smelter metal supply is generally contaminated with “bath” (electrolyte) material during metal transfer from the Hall-Heroult cell. Further reaction with aluminum alloys containing Mg can take place. During this reaction Na goes into solution and the insoluble salt MgF_2 is accumulated as a product [4].

Remeltet scrap such as used beverage cans (UBC) or swarf often contains hydrocarbon surface contaminants like paint, oil or residual lubricants which will pyrolyze at melt temperatures. Although hydrocarbon pyrolysis products can not be considered directly as potential inclusions, the reaction of aluminum with carbon does yield aluminum carbide, Al_4C_3 [5]. Furthermore, if “cracking”of hydrocarbons immersed in molten metal resulted in 1 bar partial pressure of H_2, at equilibrium at 700°C this would give around 1 ppm dissolved hydrogen. This is much higher than about 0.2 ppm found in primary aluminium [23] and higher than the value shown in Table 1.2. Aluminum carbide is also frequently found in primary ingot; originating from anode reactions in the aluminum reduction cell. Unless agglomerated, however, this form of aluminum carbide is generally innocuous in most extrusions due to the small

particle size (< 5 microns). Oxygen present in silicone-based lubricants (e.g., dimethylpolysiloxane) also can potentially form inclusions [5]. Secondary metal, which commonly has moisture on the surface, can also be a source of H, if there is no preheating of the secondary metal prior to submersion in the melt. Secondary metals contribution of oxides will be proportional to its ratio of surface area to volume [4]. In general scrap metal should be conditioned before charging the furnace. Processing can include controlled crushing, cleaning and compacting depending on the quality of the secondary metal [24]. Light gauge scrap should be meltet submerged in a stream of molten metal and not in a direct fired melter [25]. Resurfacing of immersed scrap, enhancing oxidation has to be prevented.

1.2.2 Melting, Holding and Transfer

H_2 pick-up and oxide generation present the main problems in melt/furnace and melt/environment interactions. Selecting the correct furnace for melting and holding is of prime importance. The layout of aluminium foundries depends on the through-put of molten metal required. A wide range of furnaces are available, for example: crucible, reverberatory, shaft, electric resistance radiant roof, and barrel furnaces [26]. There is also a number of methods especially used to melt secondary scrap such as Reverb Dry Hearth Melter, Side-bay Hearth Melter, Stack Melter, Rotary Furnace or Induction Furnace. Each method has its own strengths and weaknesses such as impact on final oxide content of metal which are examined in [22]. What is important is that whichever furnace is selected, accurate temperature control is used during all stages of melting and holding. High gas absorption and dross levels can all be traced back to the furnace design/operation (open charging or not, wet well or dry hearth, melt surface area exposed, volume of metal, melting time and temperature, etc.) [26] and overheating of the melt. In some cases some of the alloying elements in the aluminium alloys are lost, especially alloys containing Mg. Equally, an alloy too low in temperature can cause the formation of sludge. This problem mainly arises in high pressure foundries. There it is common practice to use the aluminium at the lowest possible temperature which can be cast. We must take into account the size and type of foundries ranging from the jobbing foundry which uses many different alloys to the larger single or two alloy foundries. The latter uses separate bulk melting furnaces and later transfers the molten aluminium

to separate holding furnaces. In contrast, the jobbing foundries tend to melt and hold in the same furnace, and these are usually the crucible type [6]. Tilak et al. [27] demonstrate that by using LARS™ system (Liquid Aluminum Refining System), a plant can successfully eliminate the requirement of a holding furnace in the typical cast house set-up. Crucial for the economic success of a smelter or remelter is to minimize metal losses by oxidation during storage, transport and handling, in particular while melting, holding and casting [24]. In study [26] it was important to note that the melt loss had a stronger economic impact than the fuel costs. New furnaces energy consumption was decreased to about 50 per cent of its original value.

Water vapor in the surroundings, either from humidity or as a product of combustion in gas-fired reverberatory furnaces, is a prevalent H source and is readily chemically reduced by aluminum to produce an oxide (Al_2O_3) and nascent H. H in this form is monatomic and rapidly assimilated by the melt [5]. With time and temperature, adsorption of H results in increased dissolved H up to an equilibrium value for the specific melt, temperature and the current level of humidity. Also, with time and increased temperature, oxidation of the melt proceeds causing an increase in oxides and inclusions in the melt. Al_2O_3 unless disturbed is a protective oxide and the quantity of oxide formed will therefore be limited. There can be traces of N, Mg, Fe, Mn, Zn, Na, K and fluorides contained in the films. With increasing temperatures (>700°C) the γ-Al_2O_3 layer transforms to α- Al_2O_3 (corundum), which occurs with some delay in time and is accompagnied by a decrease in volume. Thereby cracks are caused, and hence oxygen can enter more easily, favouring further oxidation. Alloying elements influence the amount of oxide generated and also the structure and composition of the oxide layer. This is especially true for elements like Ca, Na, Se, Sr, Li and Mg which have a higher affinity for O_2 than aluminium and, therefore, will be lost due to selective oxidation [28].

Also Cu, Fe, Si, Mn and Zn come into play in the given order at increased temperatures around 800°C, instead of 700°C. For example, alloys containing Mg in excess of 0,08 wt% produce unprotective oxides (MgO, $MgAl_2O_4$) and hence oxidation losses. The formation of complex oxides as the $MgAl_2O_4$ spinel may not be self limiting. Mg contents exceeding 3 wt% will generate spinel only. An Al-Mg alloy's rate

of oxidation does not appear to occur in a logical fashion. In some cases, it is almost non-existent. In other cases, the molten bath surface is completely covered with a thick insulating oxide coating, and the bath cannot be heated to the temperature for casting or transferring to downstream processes. This phenomenon known as “breakaway” oxidation had been identified in the 1950’s in industrial melt furnaces. An early reference to this phenomenon is found in the paper by W. Thiele [28] published in 1962. Continued heating without melting the remaining solid, can result in thermiting of the dross present leading to extremely high melt loss for the batch. Oxidation of Na in pure aluminium melts is additionally enhanced by the evaporation of Na, which is suspected to destroy the dense and protective Al_2O_3 layer. Be additions, inhibiting atmospheres of non-reactive gases (dry nitrogen and argon), SF_6, CO_2, and low melt holding temperature significantly reduce the formation of oxides. But due to the toxicity of Be its applications are limited. A collateral benefit of gas covers is that hydrogen and its sources are also excluded. [2], [5], [24], [25], [29].

Chlorides (NaCl, KCl) and fluorides partly stem from salt fluxes added to separate surface attached impurities, to enhance coagulation of drops of melt, and to protect the bath surface against oxidation. Thus the fluxes serve to release aluminium from the dross layer that contains 60-90% Al droplets. The term dross refers to any solid or liquid scum floating on top of a metal bath that comprises metal oxides, sulphides, halides, metallic compounds and so on [7], [24]. Dross must be skimmed off from time to time. Appropriate dross treatment processes can recover a major portion of the metal content of the dross. Typically, 65-75 % of the dross weight is returned by dross processors as recovered aluminium metal. Further improvement may be envisaged as the metal content of dross on removal from direct fired melt furnaces can attain 90 +%. Improvement in metal recovery by dross processors is at least partly due to the development of better controlled processes, including improved rotary salt furnace operations and the rotary plasma dross furnace process [30]. In the casthouse, more care is taken to maintain the metal values in the dross removed from furnaces, through the use of appropriate dross cooling techniques. The dross removed from the furnaces must be handled, cooled, delivered to the treatment facility and treated. The recovered metallic content is shipped back to the plant where it still must be remelted. The cost for this treatment has been evaluated to ~ $250/tonne. This number is highly variable site-

to-site and many factors are involved that will determine a given plant's actual cost. Note that the metal content of the dross is reduced if fluxing is carried out in the melting furnace [25]. Excessive temperatures during melting accelerates the oxidation of aluminum, especially when fluxes are used. If the flux material is not removed properly at the correct temperature, separation of the salts occur, resulting in contamination of the melt and in salt-wetted oxide inclusions [2].

Many of the refractory materials that are successfully used in molten aluminium processing are not thermodynamically stable [31]-[33]. Rather they owe their usefulness to poor wetting by the pool of molten alloy under the given set of process conditions [34]. A good example is the well known agressiveness of aluminium alloys containing magnesium [35]. Elements like Mg alter the structure of the oxide film and promote penetration of refractories by aluminium [36]. Oxides, H, Na, and Ca originate from the interaction between the melt and the refractory linings in the furnace. Maintaining the minimum practical melt superheat discourages refractory wetting and chemical deterioration by molten halide salts. The wetting characteristics and reactivity of molten halides increases significantly above 718-732°C. The refractory material itself and its degradation products such as silicates ($CaSiO_3$), aluminates ($CaAl_2O_4$), and carbides (SiC) are sources of inclusions [2], [5], [24].

Inclusions accumulate in the furnace heel and can reach high levels with time. Thus, if more than 90-95% is decanted off a holding furnace, it can be expected that the last part of the cast material has a high inclusion content [4].

Melt agitation and turbulence disrupt normally coherent and protective oxide layers. A continuously renewed nascent metal surface is thus generated, substantially increasing the overall oxidation rate [5]. Turbulence creates a high melt-surface-area-to-volume ratio and intimately mixes the surface oxide films with metal to become inclusions [5]. Metal transfer turbulence is the most common form of melt agitation. From melting to casting the melt has to be transferred several times either by ladle tapping or through a launder system, since there are different types of furnaces involved for melting, mixing, holding and casting. Inclusion levels increase while transfering the melt. This is more apparent for ladle tapping since the maximum drop level of the melt usually exceeds the critical fall height (0.01 m). Above 0.01 m the melt surface has enough energy and velocity (> 0.5 m/s) to overcome surface tension and continuously

expose fresh layers of melt to the atmosphere. At exceedingly high drop levels this not only excessively creates oxides throughout the melt, but also entrains further moisture and air during the splashes [17]. The same can be observed in casting machines where the higher gas level of the melt is due to the turbulent filling process [17].

1.2.3 Alloy Additions

Alloy additions to metals such as aluminium or magnesium often belong to the class II category. For class II alloys the melting range lies above the bath temperature. They dissolve into the melt by diffusion which is usually a slow process. Depending on their density relative to the melt, they may float up to the surface or settle to the bottom. In the first case there may be considerable losses due to oxidation or evaporation which are potential sources of impurity. In the second case dissolution rates may be prohibitively low, and the yields may vary from charge to charge. The most important methods to tackle these problems include: (1) bulk additions to a furnace or to the ladle during tapping; (2) powder injection by dense or dilute phase transport to the ladle; and (3) wire feeding to the ladle or the tundish and even in some cases to the casting mould. Usually stirring is an advantage, either process-inherent or provided in addition. But it may become a problem if top slag or dross is entrained.

These methods can be supplemented by the use of ingots or waffles, held immersed in the melt with baskets or cages in the case of bulk additions. A different approach is feeding of master alloys. They contain at least 50 per cent aluminium besides the alloying elements. The rod of master alloy is best added where turbulent mixing occurs, in order to speed up the dissolution of the aluminium matrix and to disperse the alloying elements. This is also common practice for adding grain refiners (Ti, B) and Na or Sr for eutectic modification. Clustering of the TiB_2 particles caused by turbulent stirring may be a problem [7]. The interaction of modifiers must be considered, especially in remelt operations. Modifier interactions usually compromise performance, as intermetallic compound formation between competing modifiers removes the modifier elements from solution, reducing their ability to function as proper nucleants [10]. At certain levels P mainly present as AlP detracts the modification effect of Na in Al-Si melts. In hypereutectic Al-Si alloys P is added to initiate the crystallization of silicon first before aluminium. Therefore contents both in

Na and P have to be adjusted to attain an optimal modification of the eutectic structure. The so called COSMA – Process, described in [37] and [38], can help to optimize the addition of Na when preparing aluminium melts. Sb has a negative impact as well, especially in the presence of Sr and in magnesium containing alloys [24].

Another source of impurity while alloying are the alloying elements themselves. For instance, an alloy addition which is rather impure is commercial Si. It contains commonly 0.1-1% Al, 0.1-1% Fe, 0.1-0.5% Ca, ≈0.1% Ti, and ≈0.1% C. Aluminium alloys produced from one or several of these alloy additions may form intermetallic phases or carbides during solidification. An example is particles of Al_3Fe and α-AlFeSi and other phases in aluminium [7]. Alloy additions can also be a major source of H_2. Mg contains from 0-5 ppm H to 8 ppm H depending upon the metal treatment and the production. Other metals such as Ti, Mn and Fe contain H_2 as well. Finally most alloy additions contain oxides and other inclusions. Magnesium is reported to contain 10-40 ppm oxides, 15-60 ppm nitrides, 1.5-7 ppm Al_4C_3 [4] and without careful submersion can give insidious quality consequences. The cause is a submicron particulate dispersoid of MgO that gets distributed throughout the melt and which is difficult to remove [5]. Also MgF_2 and MgS particulates have been observed to form when “dirty” magnesium is added to the melt [39]. As mentioned previously Al-Mg melts can oxidize rapidly when the alloying is carried out above 760°C or held for a long time. After alloying and stirring of the melt the dross must be removed, otherwise it will be re entrained during further operations [4]. Many of the alloying elements of commercial aluminum alloys (Ca, Li, Mg, Zn) are volatile and therefore change the nature of the oxide film, which contributes to dross formation, refractory corrosion and inclusion generation, and cast surface quality [40]. For example, Ca exceeding concentrations of ~20ppm in Al foundry alloys deteriorates the castability of these alloys. Hence, higher reject rates are a consequence [41].

1.2.4 Salts

Liquid salts like $CaCl_2$, NaCl, KCl or $MgCl_2$ in the presence of Mg, but also halides ($AlCl_3$) arise from the use of Cl_2 during gas purging to remove class I and II elements from aluminium. These salts may also contain fine solids such as NaF, AlF_3,

and CaF_2 originating from furnace additives or potroom metal [42]. These liquid phase inclusions affect interfacial energies of the system; for example, borides which are used as grain refiners agglomerate when coated with liquid salt phases [43]. The salts are implicated in collateral reactions, such as spinel and aluminum carbide formation. These molten and solid chloride salts are particularly difficult to remove from the melt. Liquid inclusions must physically wet the filter in order to lower their interfacial energy in the melt (increase the work of adhesion to the filter). The effectiveness of ceramic foam filters can be significantly reduced by the presence of fluxing salts [44]. Molten salts, such as $MgCl_2$ and eutectic mixtures thereof, promote contact and ion exchange with carbon sources. It is important to minimize the use of Cl_2 in the fluxing of magnesium containing alloys to concentrations usually under 10-volume-percent of the total fluxing gas [5], [7]. As a similar but less severe side effect nitrides (AlN) occur when employing N_2 as a purge gas [24]. The presence of $MgCl_2$ also introduced by salt fluxing for melt cleaning purposes can produce MgO through a hydrolysis reaction [5]. Gas and salt fluxes may be also a potential H_2 source if not dry [24].

1.3 Melt Cleaning

As previously stated, the control of alkali trace elements, H_2 reduction, and inclusion removal are the critical “tasks” during molten metal processing since they determine the final metal quality [2]. Refining of molten aluminium typically involves fluxing out dissolved alkali impurities using Cl_2 or salts of Cl_2 or F, Ar degassing for H_2 removal and, finally, flotation/settling/filtration operations for the removal of inclusions [4]. Alkali metal salts typically pose the strongest challenge to any refining system. This is due to their high fluidity, non-wetting surface and similar density to liquid aluminum [27]. An article by Fielding and Kavanaugh [45] has provided an overview of degassing and filtration technologies. The various in-line fluxing degassing technologies, when operated correctly, basically all provide roughly equivalent metal treatment performance. Refining systems with high vortexing tendency and insufficient gas bubble dispersion fall short of removing alkali and alkaline earth metal salts [27]. However, the choice of which unit to install will depend mainly on the capital cost,

operating cost, floor space requirements and ease of alloy change with the chosen technology [8].

In-line degassing/fluxing processes are proportional in nature and as such, will remove a relatively constant fraction of the incoming impurity [46]. Optimization of these units to achieve the maximum efficiency with respect to H_2 and inclusions removal can only be achieved via properly designed experiments and accurate measurements of the inlet and outlet impurity values. It is known that rotor speed, gas and metal flowrates, % Cl_2, etc., all affect the metallurgical efficiency of these units [8]. LARS™ (Liquid Aluminum Refining System) which is designed around three novel concepts; viz, in-situ preheating of inert process gas, attrition mixing of gas in liquid metal and prevention of bubble coalescence, takes also thermal expansion of the gas, volume expansion of the ascending bubbles due to reduced metallostatic pressure and the vortex forming tendency of the rotor into account [27].

If one can not measure the efficiencies, then one can not truly control the process or improve it. You must then be content to take the manufacturer's word that the equipment is doing its job.

The proportional nature of the inclusion removal efficiency of in-line degassing/fluxing units has put the emphasis back on proper furnace practices [8]. For certain end products, the metal cleanliness of the melt exiting the furnace after a holding/settling period is acceptable if the furnace practices ensure a consistently low level of inclusions from batch to batch. With a fixed furnace practice, low H_2 levels can not be guaranteed due to hydrogen absorption from the atmosphere and variability of temperature [47].

There has been a strong demand for the development of highly efficient compact in-line degassing and filtration systems combined with maximum operational flexibility. One of the driving forces is that many of todays aluminium cast houses were constructed before the 1980's with casting centres which have insufficient space for elaborate in-line treatment systems. Also, traditional in-line treatment systems such as the spinning nozzle degassers combined with either bed or rigid media filtration require a significant quantity of metal to be held between casts. The metal retention in these systems is a serious economic limitation for multi-alloy casting centres due to the costs of draining the units for each alloy change [48].

In 1993 so called rotary flux injection machines became generally available. The so called MTS (Metal Treatment Station) is an example for joining together previously separate treatment steps [37]. These machines combine rotary degassing with the ability to inject a measured amount of specially developed flux into the melt. They increased the efficiency of flux treatment by up to tenfolds in terms of flux usage, with significant improvements in oxide removal, the environment and reduction in treatment times as a consequence. Since that time, new treatment technology has evolved with the introduction of combined melt treatments such as sodium modification and phosphorus refinement, calcium removal and grain refinement [49].

1.3.1 Removal of Dissolved Impurities

Basically for removal of dissolved impurities three principles or combinations thereof are utilized industrially, neglecting here methods of less importance such as three-layer electrolysis and fractional melting/solidification: (1) An impurity can be transferred to another phase where it has a high solubility. This second phase is not soluble in the molten metal. (2) Also possible is the reaction of an impurity with a second phase that may be solid, molten or gaseous. For instance, due to its high vapour pressure Na can be removed from molten aluminium by burning with O_2 in the air at the bath surface. Although this may be an effective way of removal and is inevitable during melt processing, it is rather not desired due to the increase of the amount of dross, and hence, metal losses. (3) And again, an impurity may as well react with another element (added to the melt). The reaction product whether solid, liquid, or gaseous has to be removed from the melt. This removal may be achieved by the effect of gravity or buoyancy forces, inertial forces, or forces generated by stirring the melt, hence flotation, settling and filtration operations [7]. Based on the melt processing temperatures involved (≈660-770°C), contaminants such as Na, but also H_2 and Zn become volatile [4]. But now, what determines the final levels of an impurity in the melt? Is it the equilibrium between the impurity content in the metal and in the extracting phase and hence thermodynamics? Or is it mass transfer, a mechanism that is ruled by kinetics? This is one of the main problems that we are adressing here. Whatever the case, some impurity will remain. If the equilibrium is controlling, the chemical activity of the impurity element is the same in the two phases. Which means even at a very low

activity coefficient in the extracting phase, some residue of the impurity must remain in the metal due to equilibrium. If removal is determined by mass transfer, the removal rates are governed by the driving force. With decreasing concentration the time required for removal may increase exponentially, and the cost of attaining low impurity levels becomes prohibitive [7].

Mixing, if producing heat, can accelerate the purification of molten metals. It has a positive impact due to temperature and composition homogenization as well as an improvement of flux – metal bath reaction rates. One also speaks of complete mixing when the impurities become evenly distributed throughout the melt. This can usually be taken as an assumption when doing calculations. Mixing may be performed by the use of mechanical stirrers, gas stirring, electromagnetic stirring, pouring from one ladle to another (Perrin process) or pumps (mechanical or vacuum) [7], [50].

1.3.1.1 Degassing

It is common to remove H from aluminum by gas purging or vacuum treatment. In both cases also suspended particles will be partly removed by flotation. Argon and N_2 are the main components in the gas [51]. Degassing is accomplished by inert gas alone or together with small amounts of halogen gases like Cl_2 or SF_6. However, SF_6 has a global warming potential (GWP) of 23000 compared to CO_2 (GWP = 1). Studies have shown, that if the purge gas bubble is sufficiently small (usually 5mm or less) then degassing efficiency is relatively unaltered by adding the surface-active reactive halogen gases. Rather, the latter serve mainly to de-wet solid inclusions from the melt, and thereby contribute more to melt cleanliness than to H removal per se. Choice of purge gas also affects resultant dross formation during the degassing process. Argon creates a drier (less metallic content) dross than N_2. N_2 plus SF_6 produces a relatively wet (metal rich) dross [10]. Where degassing with N_2 is carried out continuously, as in some large holding furnaces, and where the alloy contains some Mg (which is often the case), there is an additional danger from the build-up of nitrides in the liquid. They can become so prolific that the melt takes on the appearance of a slurry such as porridge or cement. The mechanical properties of the resulting castings are lamentably low because of the embrittling effect of the large concentration of nitrides. The only way to avoid such problems when attempting to degas continuously is to use a truly inert gas such as

Ar [52]. An important criteria regarding the quality of the purge gas is its content of water vapour [24]. If trace amounts of oxygen and moisture which are found in commercial grades of nitrogen and argon are not removed (they can virtually never be removed to the levels required to be non-oxidizing), an alumina film can form along the bubble/melt interface that hinders mass transport. Chlorine can also be added to the inert gas since the violence of its reaction to form chlorides disrupts the oxide film [40].

There are different ways of injecting the purge gas, for example with lances, nozzles, porous or cone plugs, and rotors. Rotor- or impeller-units incorporated in batch or continuous back-mix reactors ("in-line") are broadly used for this purpose, since they are able to generate gas bubbles with radii in a range of 2-5 mm [53]. The rotary technique typically reduces H to very low levels in only 10 minutes [52]. The smaller the gas bubbles, the larger the specific bubble surface area per volume gas and hence mass transfer. In a back-mix tank, the driving force for transport of hydrogen to the purge gas is reduced because untreated aluminum mixes with purged melt. This is compensated to some extent by the use of two or more tanks in series. A more efficient way of removing hydrogen is to use bubble columns run either co-current or counter-current, where mixing of treated and untreated melt is reduced and, therefore, the driving force is retained. Some advantages of these bubble columns are simplicity in structure, no mechanically moving parts and good mass transfer properties [53]. Reference [24] gives a schematic survey over different commercial gas purging systems available.

The physical-chemical process of hydrogen removal (gas purging) is based on the shift of the solubility equilibrium towards the gas phase. Driving force of the reaction is then the gradient of hydrogen concentration between the melt and the gas phase. The pressure of H_2 is so low in the gas bubbles that the dissolved monoatomic hydrogen $\underline{H}$ leaves the melt and enters the bubble or vacuum phase. The transport process may be separated into four steps [24]:

1. Transport of H by convection and diffusion to the vicinity of an inert gas bubble.
2. Diffusion of H through a thin laminary melt boundary layer into the bubble.
3. Reaction at the melt-bubble-interface to molecular H and desorption into the gas phase.

4. Rise of the gas bubble to the melt surface while the absorption of H is continued.

Step 2 is probably the slowest one – at least for gas purging - and will be regarded as rate controlling for H removal [54]. Bertherat et al. [55] state that the metal to bubble H transfer is not diffusion limited as proposed by Sigworth [56] but is mainly controlled by an interfacial reaction.

Degassing processes can affect the behaviour of modification and grain refining response. Increased degassing treatment times, and higher gas flows tend to compromise modification/grain refinement results achieved prior to degassing. Consequently, degassing is usually employed first [10].

Vacuum melting and vacuum degassing are rapid and effective ways of removing gases from metals. Vacuum degassing differs from vacuum melting only in that the metal is melted in air and subsequently exposed to vacuum. For best efficiency, it is desirable that bubbles form within the melt, not just that the gas diffuses out of the top exposed melt surface. To form these bubbles it is important to reduce the metallostatic head on the metal. This can be done by stream degassing (pouring metal through a vacuum), by processes which repeatedly draw a small amount of metal out of a large bath and expose it to vacuum, and by vigorous stirring of the melt (to bring the gas-containing liquid to the melt surface) [57]. An extreme type of stream degassing is the recently proposed spray degassing method [58]. There, melt is sprayed into a tank containing argon gas which gives a maximum in contact area. Treatment times and consumption of argon are much reduced in comparison to the established spinning nozzle degasser. Further benefits are the recovery and reuse of the purge gas as well as preventing the pick up of “ambient” hydrogen due to the closed nature of the system.

1.3.1.2 Fluxing

The term fluxing as addressed here refers to the use of salts and reactive gases for melt protection, and melt cleaning operations removing alkali elements and Mg, but also for the recovery of metal from dross or slag.

Major application for salt fluxing is in remelt operations to process feedstock of contaminated aluminium and to maximize the rate of yield. During remelting the salt has to fulfil several tasks: (1) Detach surface attached oxides and impurities, which then will be absorbed in the molten salt. Thereby (2) enabling coagulation of drops of melt. And finally (3) protection of the melt against further oxidation by the covering molten salt. Therefore suitable salt fluxes must have the following properties when they are in the molten state at operating temperature: (1) thermochemical stability towards molten aluminium; (2) high thermal stability, meaning high resistance against dissociation and evaporation; (3) sufficiently lower density compared to aluminium alloy melts; (4) low viscosity; (5) optimal interfacial tension towards Al_2O_3 and molten aluminium; (6) high capacity for absorbtion of non-metallic impurities, in particular Al_2O_3; (7) no reaction with refractory linings. In any case, the yield of metal will never be 100 percent. In principle, metal losses during remelting of aluminium using salt fluxes can be caused by: (1) the solubility of metal in the molten salt, and subsequent oxidation of the dissolved metal due to exposure to the atmosphere, (2) chemical reaction of aluminium and alloying elements with components of the fluxes as well as (3) retention of suspended metal drops in the salt phase, which is the main problem [24]. Point one is negligible due to the low solubility of aluminium and its alloying elements in NaCl-KCl-melts [59]. The relevance of point two is limited to Mg containing scrap and contaminated salt fluxes. In the presence of F additions the thermodynamic stability of the salt compared to MgF_2 is of main interest. Only CaF_2 is more stable [60]. Metal losses due to contaminated salt fluxes, containing water from reprocessing or $CaSO_4$ from a natural salt source, can be considerable. In Germany commonly a mixture of 65 to 75 wt% NaCl and 25 to 30 wt% KCl with additions of 2 to 5 wt% CaF_2 is in use for salt fluxing. In Canada and the USA they mix 40 to 60 wt% KCl together with 40 to 60 wt% NaCl and supplements of up to 5 wt% cryolite and/or alkali fluorides. Salt additions range from 0.4 – 0.8 times the amount of non-metallic fraction in the scrap (for strongly oxidized feedstock, especially dross), giving a dry cake of salt, to 0.8 – 1.2 times the amount of non-metallic fraction in the scrap, forming a thin molten layer of slag. Even though the use of salts for fluxing offers indisputable technological and economical advantages, energy consumption, use of raw materials and residue reprocessing present an expenditure that can not be neglected. An optimization

according to the amount and the composition of the salt fluxes is therefore indicated [24].

The treatment of aluminium melts with inert purge gasses only to some extent removes Li and Na by evaporation and oxidation [24]. This is due to the low vapour pressure of alkalis at low concentrations in the bath. Such a practice would therefore require very large quantities of Ar for effective removal [4]. An effective removal of dissolved alkali/alkaline earth impurities and Sr, but often also Mg can be achieved only by the use of AlF_3 additions or reactive gases like Cl_2 or mixtures thereof with inert gases such as Ar [24]. Due to the high chemical affinity of Cl_2 for Sr, but also its time depending fading behaviour, Sr modification should be carried out after gas fluxing prior to casting.

In the process of producing foundry/die cast specification Al-Si alloy ingot, it is often necessary to remove Mg from recycled melts. This is also referred to as de-magging. The initially high Mg content results from scrap blends, and better availability of higher Mg content materials in the scrap stream. Mg can be removed from aluminum favorably by a reaction with Cl_2 to first $AlCl_3$ and subsequently $MgCl_2$. Unlike other melt treatment processes, economically effective de-magging requires high concentrations of Cl_2, e.g. 90 per cent, which far surpasses the concentrations used for degassing (3-5% Cl_2) [5] or alkali removal (Cl_2 <15%) [24]. In the secondary smelting industry, the application of the gas injection pump has become the most cost effective technology for de-magging [61], [62]. The gas injection pump provides forced convectional heat transfer and great metal mixing capability, and the rotating impeller of the pump creates a very high degree of bubble shear. This results in excellent mixing of metal with process gas and efficient reaction kinetics, respectively, even at low concentrations of Mg. In previous studies, the gas injection pump has been shown to be near-perfect in de-magging efficiency (Cl_2 utilization versus theoretical amount required). No free Cl_2 was observed in this study, when sought by a variety of analytical effluent capture techniques [61], [63]. Another promising just recently reported [64] de-magging technique under development removes Mg from molten aluminum alloys by using submerged powders injection of SiO_2 particles. The main attraction of such a process is the non-pollutant nature of the reagents employed. The main reaction product is $MgAl_2O_4$, a so-called spinel. On a laboratory scale removal efficiencies close to 90%

together with low inclusion contents could be achieved. A validation on an industrial level gave somewhat lower removal efficiencies.

1.3.2 Removal of Suspended Particles

The removal of non-metallic and intermetallic particulate suspensions present the most significant challenge in molten metal treatment. The solid inclusions, present in molten metal prior to casting, are an inevitable feature of the process of manufacture. Inclusion removal and separation from aluminum melts can be carried out by sedimentation/settling while holding the melt, flotation using small bubbles, and filtration employing deep-bed or rigid media filters. There are at least three participants in the removal process: the inclusions, the molten metal, and a collector (filter medium, or purge gas). The solid or liquid inclusions are described by their size distribution, composition, density, and shape. The properties of the fluid depend on alloy composition, kinematic viscosity, and density [7]. Non-metallic inclusion removal techniques depend on body force driven separation methods and on screening. As a result, each of the melt treatment systems is suitable for removing a specific type and size range of inclusions. Most characteristic for the performance of such a system is the removal efficiency, E:

$$E = 1 - \frac{c_o}{c_{in}} \tag{1.2}$$

c_o – number of inclusions per unit volume leaving

c_{in} – number per unit volume entering the filter

Fifty to ninety five percent reduction in the oxide content has been reported when filtration, flotation or a combination of these methods has been used [2], [4]. One has to be aware of that in case the oxide content is reduced by 95% but the H content is reduced only by 75%, then roughly 25% of the remaining gas precipitates on 5% of the remaining nucleation sites. In general porosity in the casting is reduced, but it may be 5 times worse in areas to be formed [52]. From industrial observation it has been reported that the majority of the particles, which are deleterious to product quality, lie in the range of 1-30 microns and are dilutely suspended [66], [67]. Sometimes only one single

particle larger than a critical size can cause a product to fail. Most notably this example refers to the fracture of mechanical parts.

1.3.2.1 Sedimentation/Settling

Inclusions may be lighter than the molten metal or they may be heavier than the melt. The inclusions that float up are collected by a slag or dross phase while heavy inclusions accumulate as a slurry in the lower parts of the furnace (a holding or settling furnace). In either case the removal mechanism is gravity coupled with the density difference (negative or positive) between the particle and the surrounding melt. The term `settling´ is used both when particles sink or float up [7]. The fundamental equation governing the rising, or settling, of a small inclusion in a melt is Stokes Law. Stokes Law is valid at low Reynolds numbers such that viscous forces far exceed inertial forces. The drag force experienced by a sphere is 6π rμU in a fluid extending in all directions, while the buoyancy force is $(\rho_i-\rho_{Al})$gV, where [4]:

μ = Viscosity of aluminum melt
r = Radius of inclusion
V = Volume of inclusion
g = Gravity
ρi = Inclusion density
ρ_{Al} = Density of aluminum melt

A balance between drag forces and buoyancy forces then gives [4]:

$$6\pi r\mu U = (\rho_i - \rho_{Al})g\left(\tfrac{4}{3}\pi r^3\right) \tag{1.3}$$

Gravity sedimentation methods are practically limited to relatively large inclusion sizes, due to the high drag forces encountered and the inordinately low particle terminal velocities [2]. [68] reports that sedimentation as a practically viable separation method is limited to inclusion diameters greater than 90μm, for those operations limited to interval separation times of 30 minutes or less. Further reduction of the level of small inclusions requires extra holding time, which will result in a reduction of furnace productivity [69].

Particles may be removed not only by gravity effects but also by various other mechanisms: Brownian diffusion, inertial and turbulent removal to walls, and so-called hydrodynamic effects [7]. Stirring and moderate turbulence stimulates particle agglomeration and thus may enhance sedimentation efficiency [70], [71]. Particle removal at a free surface occurs in the flow separation region which is illustrated in Figure 1.1. The rate of agglomeration is generally higher than the overall rate of removal. The overall rate of particle removal is dictated by both particle entrapment within the flow and the kinetics of particle removal at the flow separation region. The nature of the particles has a significant influence on the removal and agglomeration kinetics of inclusions [69]. Studies of the level of turbulence necessary to optimize inclusion agglomeration and subsequent separation have been carried out at the Metal Processing Institute [72], [73]. The molten metal bath may be stirred mechanically [74], [75], by bubbling [76], [77], [78] or electromagnetically [79], [80], [81]. Also temperature gradients, owing to heat losses throughout the holding vessels side walls, or concentration gradients can induce convection [7], [4]. Another technique that could enhance sedimentation is the application of an electromagnetic force upon the melt. Responding to this externally applied force, the inclusions move opposite to this force – as a result of Newton's third law – and are thus separated. In laboratory-scale experiments, large force densities can be achieved. For a spinel particle, an electromagnetic force value of about 30 times greater than the gravitational force can be accomplished. This allows sedimentation of smaller particles to take place [16]. It must be pointed out that large force densities in large volumes are difficult to achieve, mainly due to the complexity of producing strong, highly homogeneous magnetic fields. For this reason, separation efficiencies are quite low when the inclusion size is below 50μm [65]. This is probably why electromagnetic separation has not been widely utilized. The use of high DC magnetic fields generated by modern superconducting coils can considerably improve the separation efficiency and move the size limit towards smaller particles [82]-[84]. For large force densities the main problem remains the homogenity of the force distribution through the volume. If the force field is not uniform, very strong electromagnetically driven fluid motion and turbulence may appear, thus creating an uncontrollable situation [16].

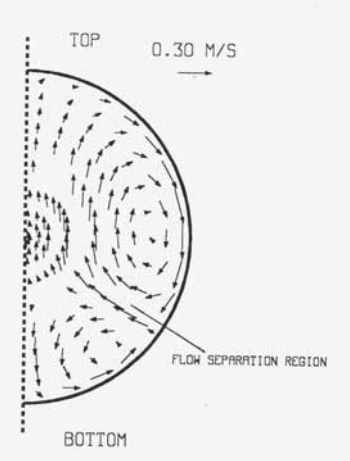

Fig. 1.1: Computed velocity field in an aluminum levitated spherical droplet [69]

1.3.2.2 Flotation

As mentioned previously, gas purging of aluminium melts not only decreases the levels of dissolved hydrogen and alkali but also is the cause of reduction in content of suspended particles [24]. If a gas is bubbled through the melt, the particles may come into contact with the bubbles. Furthermore, if these particles or inclusion are wetted by the bubbles but not by the melt, there is a high probability that particles remain trapped at the bubble-melt interface. They are then carried by the bubbles up to the dross layer. This is a process referred to as flotation [7]. Particle flotation mechanisms have been extensively investigated by Szekely [85]. Flotation is found to be a result of three elementary capture operations: inertial impaction, peripheral interception and gravity forces. If attachment to the bubble occurs and viscous shear forces do not cause detachment, the inclusion is separated from the melt by flotation. Inertial impaction occurs when the inertia of an inclusion particle exceeds that of a local fluid volume element, resulting in departure from fluid flow streamlines around a rising gas bubble. This mechanism results in the impaction of an inclusion on the gas bubble surface. Since inertial impaction is gas bubble and inclusion diameter dependent, Szekely concludes that particles larger than 80μm can be removed by inertial effects with bubble diameters as great as 10 mm. [68] shows that inclusions greater than 30-40μm may be reliably separated from the melt by flotation. The second mechanism of particle

flotation, peripheral interception, depends on equatorial contact of an inclusion and a rising gas bubble [2]. The inclusions elude capture by the bubbles, if the bubbles are significantly larger in size relative to the inclusions. Even bubbles of 1-10 mm in diameter are not sufficiently small to trap inclusions in size of a few microns (< 10 μm) [24].

Flotation properties of non-metallic inclusions in aluminium melts in the case of inert gas purging are influenced by the wetting conditions between inclusion, melt and purge gas, i.e. the wetting angle θ [24]. Practically all non-metallic inclusions that have a wetting angle larger than 90° in relation to the melt should be removable by inert gas purging. Thus an Ar purge is capable of removing oxides but rather less nitrides, carbides and borides [86]. Chlorine can increase the wetting angle between oxides and melt [87]. Therefore it is valuable as a reactive gas for inclusion removal, skim control, and in certain instances, degassing. Three- to five-volume-percent chlorine is appropriate for enhancing inclusion flotation and producing an acceptably dry skim. Efficient phase contactors should also be used for chlorine fluxing [5]. Mattocks and Frank [88] consider amounts of chlorine of already less than 0.5% of the process gas as sufficient to separate non-wetted, non-metallic inclusions from aluminium.

1.3.2.3 Filtration

Removal of non-metallic inclusions may be accomplished by filtration [66], [67]. The filter material is characterized by its geometrical dimensions: the size of the structural units, their distribution and arrangement in the filter, and by their porosity [7].

Liquid metal filtration processes are inevitably transient in nature. That is to say, the filtration processes as well as the parameters pertaining to them, change with time. This is because the particles captured inside the filter alter the filter's properties – a process that has been referred to as `filter aging´. By definition, a filter starts aging as soon as particles start to accumulate within it or on it. The most important issues of interest during the aging period are changes in filtration efficiency, E, and pressure drop, Δp, as a function of time. The efficiency, E, directly concerns the quality of the filtered metal, while the latter determines whether a filtration process remains operable. In that period, the filters internal structure changes. These changes cause some of the

independent variables on which the filtration efficiency depends, to change. The most obvious is filter porosity, which decreases with time. The specific surface area, or equivalent filter web diameter, also changes [89]. Filter capacity is defined as the quantity of deposited particles (usually expressed in grams or kilograms) which the filter is capable of accumulating before reaching a certain pressure drop (loss of metallostatic head). The filter capacity clearly depends on the type and size of the particles [7]. But all these parameters do not tell how effectively each particle size is captured by the filter. To be on the safe side one could choose a filter pore size that is just below the critical particle size. But this is only a solution when the appearance of large particles is an exception and not the rule in the casting process.

Basically two different types of filtration have gained a wide scale of industrial application: deep-bed and cake filtration [2]. The two filter mechanisms are illustrated in Figure 1.2.

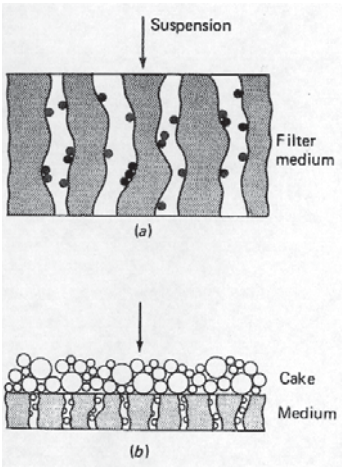

Fig. 1.2: Mechanisms of filtration: deep-bed (a) and cake filtration (b)

A deep bed filter relies on the tortuous path the melt must flow through [66]. Filter efficiency is inversely proportional to the size of the filter grains and directly proportional to the depth of the filter bed [90]. The inclusions deposit both onto the grains and in the voids between the filter medium. Also they may become dispersed through a part or all of the filter volume [2]. The filter thus has the advantage of having

a large surface area for inclusion capture and can trap particles much smaller in size than the pores of the filter bed. Additionally, the head loss over the filter is only in the order of a few psi or roughly 0.1 bar [66]. Mechanical entrapment has been observed to be responsible for filtration of inclusions larger than 30μm, whereas it is believed that surface forces are responsible for the retention of inclusions smaller than 30μm. Therefore, the filtration process here is not only one of physical separation as in screening and separation, but rather melt filtration is a two step serial transport process. First, as a result of bulk fluid flow the inclusions are transported to the filter surface. In the second step inclusion capture occurs due to interfacial or surface forces. Figure 1.3 shows a schematic representation of the inclusion size with respect to the average filter pore diameter. It is quite evident that physical separation is not the only mode of capture.

In general as for removal by flotation, particle removal in filters can arise from impingement, interception, sedimentation, diffusion, and hydrodynamic effects. Particle attachment can be a result of forces developed through pressure, chemical, or Van der Waal effects. The relative dominance of each mechanism is a function of particulate type and size, fluid approach velocity, as well as temperature and filter media characteristics. The inclusion removal efficiency can be improved by either increasing filter length or by decreasing melt velocity [2]. As previously mentioned, particles accumulate (or porosity decreases), flow resistance increases, causing pressure drops to rise and, in turn, interstitial velocities increase, if the flow rate is to be maintained constant. As a result, drag forces exerted on either contacting particles or particles already captured will increase. This can lead to lower adhesion efficiencies since particles may not be able to adhere to the filter surface due to increased drag, even if they are able to make a contact with them. Similarly, increased drag forces may dislodge previously captured particles if the forces of adhesion are overcome. The particles scoured from one location may be recaptured downstream, within the filter, or, in the worst scenario, be released into filtered liquid metal [89]. This release can occur during a continuous flow or during a flow interruption which is the case for aluminium filtration during cast stop/start periods. During the re-start, a significant quantity of inclusions may be released [91]. The inclusions released may as well originate from the

filter or other melt cleaning equipment. X. Wang [92] describes several inclusions found in D & I can stock that originated from interactions with cone plugs and glass cloth materials.

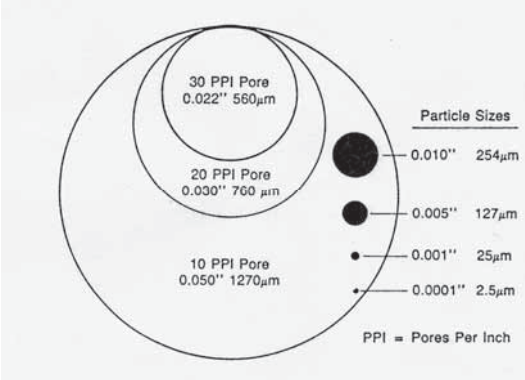

Fig. 1.3: Schematic representation of the inclusion size with respect to the filter pore diameter [2]

In cake filtration there are two scenarios that can be distinguished. Either the inclusions are deposited at the upper surface of the filter and hence, the size of the filter pores must be smaller than that of the impurities [66], or the cake evolves out of a transition from deep bed to cake filtration where an inordinately high solid fraction of inclusions smaller than the pore size gradually clogs the filter and leads to an unacceptably rapid filter head build-up, respectively. The latter warrants pre-treatment clarification methods such as sedimentation and flotation. In either case the aggregate of inclusions acts as a “second” filter, rendering an additional resistance to flow and thus causing separation of the particulates from the melt. Particle capture is almost exclusively determined by the nature of the cake formed. Generally the occurrence of the cake mode is not appreciated throughout the aluminium manufacturing industry. This is because the production is slowed down considerably due to the large flow resistance experienced by the metal and the subsequent necessity of filter change. Therefore cake filtration is limited to occasions in aluminum melt clarification when (1) the inclusion concentration is high and/or (2) cast shop floor space is limited. Filter cakes can be broadly classified into two types: incompressible and compressible.

Qualitatively, an incompressible cake is one in which the void fraction, ε, of the cake is essentially time invariant within the filtration pressure limits. Changes in metal flow resistance imparted by the incompressible cake is caused principally by increases in cake thickness. The particular form of D'Arcy's Law describing flow in incompressible cakes can be represented as a function of processed metal volume. One expects hard, nondeformable inclusions of relatively narrow size distribution and similar shape to form incompressible cakes. On the other hand, compressible cakes typically develop when the separated solids are highly deformable and represent a broad size distribution. Thick cakes may also exhibit compressibility over a broad range of operating pressure. Cake mode filtration is a dynamic process resulting in an increasing cake thickness as filtration progresses. Hence, the cake length will be expressed as some function of time in a model. Knowledge of this functional relationship is important to investigators because it characterizes filter performance and associated pressure drops. Since in metal systems, the cake thickness is believed to be in the order of 10^{-1} to 10^{-2} cm, it is impossible to measure it directly. Alternatively, this functionality can be obtained through mathematical relationships and experimental data, as presented by the authors [2].

At present, there are five major types of filters which are used for aluminum filtration [93]. These are: (1) woven glass or ceramic fiber screens; (2) packed bed of unbonded tabular or spherical alumina particulates; (3) ceramic foam filters; (4) bonded alumina particulates in various shapes; and (5) extruded ceramic monoliths [66]. One can destinguish between single use filters (1, 3, 4, 5) and multiple use filters (2, porous tube filters, heated single use filters) [8]. Bed filters and porous tube filters tend to be used for high volume, single alloy (or family) of inclusion critical products such as can body, can-end and thin foil. While being suited to these applications, they are not cost effective where many alloy changes are required or where floor space is greatly limited. The single use filter has filled the needs for moderate filtration efficiency, ease of alloy changes and a small footprint [8]. Filtration with ceramic foam, developed by SELEE in 1974 [94], is a process that is complementary to existing metal treatment practices and is extensively used both in ingot making as well as for shaped castings. For the latter, placed in the runner, it does not only hold back inclusions but also promotes smooth, non-turbulent mould filling, so that reoxidation and dross formation does not occur

down-stream of the filter [29]. The ceramic foam filter (CFF) consists of a sheet of open pore ceramic foam of varying thickness and cross-sectional area. Typically it would have 85% volume fraction of inter-connected voids [2]. Filters are made in various grades of fineness, usually 10, 20 and 30 ppi (pores per linear inch) with a trend to finer pores (50, 60 ,80 ppi). The filtration efficiency (E) together with the reliability of the filtration systems, i.e. smaller standard deviations of E, is reported [9] to increase with finer pore sizes. Another interesting observation filtering very clean metal, was a poor performance of the filter regarding small particle sizes (15-30 μm) compared to particles in a range of 30 to 60 μm. In this particular case the filters did not face the usually high inclusion loadings that occur in the initial stages of a casting. The results might to some extent be due to an increase of the relative error of the LiMCA measurements with low inclusion levels and the greater impact of electrical noise disturbing the LiMCA [9], [29]. The results correspond well with water model tests. There it was found that for coarse sand filtration efficiency increases with flow rate, filter size and low porosity, while for fine sand efficiency increases when flow rate decreases [95]. Figure 1.4 shows schematically the flow pattern in a ceramic foam filter. In the interstitial channels particles also get captured in so-called “backwaters” under conditions of quiescent flow. There the inclusions may form lightly cohering, loosely packed suspended masses and stay without any effect of adhesion so long as the metal flow is not unduly disturbed [96]. A reason for particle release can be a change in flow velocity or vibrations. Therefore, particle capture may be controllable only to a certain extent in the range of 1-30 microns, and re-entrainment of already captured particles can not be excluded. This uncertainty may explain the harmfulness of these particles rather than their size. A ceramic foam filter can be installed prior to the casting station with minimal capital expenditure. However, it only has a limited life because with use the inclusions form a filter cake, which increases the flow resistance. Thus, ceramic foam is a good example of a filter medium which at the onset operates as a depth filter and at the end of its “useful life” operates as a cake filter [2]. In [48] the authors report the development of a compact dual stage ceramic foam filtration system, utilising two standard ceramic foam filters in series, which offers significantly higher filtration efficiency, while maintaining all the well known advantages of normal CFF systems.

These systems are used in a wide range of casting processes (rolling slab, extrusion billet, continuous casting, rod casters) and for a wide range of end products (rigid and flexible packaging, automotive condenser tubing, copier drum and wire rod). The paper also discusses the design requirements for a compact filtration system, equipment development and the results of LiMCA evaluations.

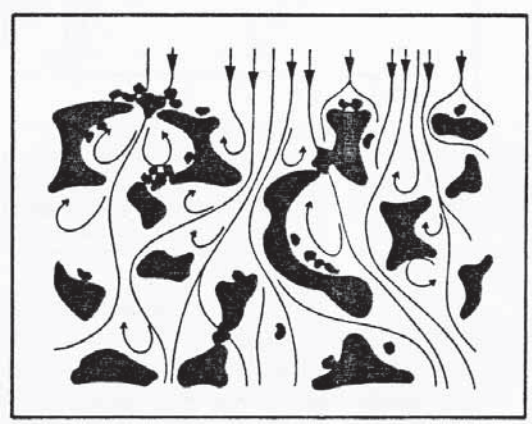

Fig. 1.4: Schematic representation of the flow in a ceramic foam filter [29]

Filtration in an acoustic cavitation field employing a 3-5 layer filter from 0.4 x 0.4 mm cell fibre glass, which is placed in the runner, provides not only melt degassing but also a high degree of melt refining for hard inclusions due to the sound-capillary effect [97]. The USFIRALS-process which is based on this principle allows a very effective refining of dispersive particles down to 1-3 μm by a multi-layer filter. It allows production of high quality blanks for magnetic disks from 5xxx alloys, fine foils, sheets and other semis from 6061-type alloys sensitive to impurities. Fine filtration according to the "USFIRALS-process" technique results in an improvement of service-life performance in the short transverse direction. According to the data, fracture toughness in the short-transverse direction and durability at LCF (160 Mpa) of D16ch (2324) alloy extruded strip of 65 x 200 mm in cross-section were increased from 29 to 39 Mpa.$m^{1/2}$ and from 162 to 259 kilocycles respectively [18].

Recently interesting results are reported in the literature [98] and [99] regarding so-called “Active Filtration” where active coatings form an adhesive layer on the filter substrate. The coatings consist of NaBr or a mixture of KCl-NaCl and small quantities of F, CO_3, SO_4, for example. Alternatively, coatings may consist of glassy enamels. The filtration efficiency is much higher compared to uncoated filter material. However, the content of trace impurity elements such as alkali is not reported to be affected by this filtration mechanism.

1.4 Measuring Melt Cleanliness

The use of quantitative measurement techniques is at the heart of gaining understanding and improving metal treatment processes [8]. To describe conditions in an aluminium melt, a set of different melt parameters including temperature and chemical composition of the melt, the gasses dissolved in the melt (mostly hydrogen) and the inclusions should be measured [100]. For the measurement techniques one must distinguish between on-line and off-line modes. The former enable the foundry staff to attain real-time measurements directly by implementing the measuring device into the process chain. In the latter case it is a process of first sampling and a subsequent analysis of the samples taken, which often is rather time consuming.

1.4.1 Chemical Composition and Trace Elements (Alkali)

It would be hard to imagine an ingot producer that is not equiped with instruments to analyze the chemical composition of the melt. Since its development in the early nineteen twenties, optical emission spectroscopy (OES) has become the industrial standard for measuring alloy chemical composition at the level of alloy element additions, as well as at the ppm level of trace elements. Automated sample preparation and automated, stable OES instruments have allowed the transfer of these instruments from laboratories to the shop floor. The analyses are not yet truly on-line but the time delay between sampling and results is so short that chemical analysis seems to be “on-line” [8]. The setup of a spectroscope principally consists of a light source (argon, hydrogen, xenon or discharge lamps etc., laser), a probe container, a dispersive media or monochromator, respectively, to disperse radiation as well as a detection

system with an attached data processing unit. Emission of radiation can be observed when excited particles like atoms, ions or molecules fall back to a lower energy level thereby releasing the excess energy as photo-electrons. The state of excitement can be attained in many ways, for example by absorption of radiation, thermic in flames or plasma as well as through ion or electron bombardment. Optical emission spectroscopy is not limited to the visible spectrum but also includes the spectra of the ultra violet and infra-red range [101].

1.5 Resume

The intention of this chapter was to survey the literature to shed light on different aspects concerning “melt quality”. The general term “quality” was introduced and applied to molten metals. Impurities in the melt were identified to be the main reason for product failure both during production and use. Thus, melt cleanliness becomes a measure of melt quality.

Sources of impurities can be traced back to the bulk metal, various melt processing operations, and the molten metal interactions with the refractory and the environment. Especially sources of dissolved elements are tried to be identified.
Refining methods such as degassing, fluxing, settling and filtration are reviewed with emphasis on possibilities for removal of dissolved elements. However, melt cleaning procedures, especially fluxing represent a potential source of impurity. Finally the typical measuring technique for dissolved elements is commented.

Bibliography

[1] J. F. Grandfield: *"Melt Quality Specifications"*. Aluminum Melt Treatment & Casting, Edited by M. Nilmani, The Minerals, Metals & Materials Society, 1993, pp. 80 – 82

[2] D. Apelian and S. Shivkumar: *"Molten Metal Filtration – Past, Present and Future Trends"*. 2nd International Conference on Molten Aluminium Processing Proceedings, Orlando, Florida, 6. – 7. November 1989

[3] *"DIN ISO 9000 – 9004 und die Auswirkungen für das Marketing im Business-to Business-Sektor"*. IO – Management Zeitschrift, Ausgabe vom 01. 09. 1996

[4] R. I. L. Guthrie, M. Nilmani: *"Impurity Sources and Control – General Principles of Melt Treatment"*. Aluminum Melt Treatment & Casting, Edited by M. Nilmani, The Minerals, Metals & Materials Society, 1993

[5] C. Edward Eckert, Jr.: *"Molten Metal Quality Considerations for Aluminum Extrusion Ingot Product"*. Profiles of Change. 6th International Aluminum Extrusion Technology Seminar. Vol. I; Chicago, Illinois; USA; 14-17 May 1996, pp. 477-486

[6] T. M. Paterson: *"Total control of melting and holding aluminium in the foundry"*. Foundry & Heat Treatment SA (South Africa), 5, (6), ti1-ti4, Nov. – Dec. 1997, pp. 379 – 381

[7] T. Abel Engh: *"Principles of Metal Refining"*. Oxford University Press, 1992, pp. 2 – 3, 15, 76, 77, 132, 345 – 347

[8] C. Weaver: *"Future Trends in Melt Quality Control"*. Fifth Australasian-Asian Pacific Conference on Aluminum Cast House Technology: Theory & Practice**,** 1997, Edited by M. Nilmani, P. Whiteley, and J. Grandfield, The Minerals, Metals & Materials Society, 1997, pp. 105 – 109

[9] N. J. Keegan, W. Schneider, H. P. Krug: *"Evaluation of the Efficiency of Fine Pore Ceramic Foam Filters"*. Light Metals 1999, Edited by C. Edward Eckert, The Minerals, Metals & Materials Society, 1999, pp. 1031 – 1040

[10] David V. Neff: *"Metallurgy and Melt Treatment of Aluminum-Silicon Alloys"*. 5th Australasian Asian Pacific Conference on Aluminium Cast House Technology, Edited by M. Nilmani, P. Whiteley, and J. Grandfield, The Minerals, Metals & Materials Society, 1997, pp. 155 – 177

[11] K. Horikawa, S. Kuramoto, M. Kanno: *"Intergranular Fracture caused by Trace Impurities in an Al-5.5 mol% Mg Alloy"*. Acta Materialia, Vol. 49, 2001, pp. 3981 – 3989

[12] A. Annenkoff, in 4th Proceedings Int. Al. Extrusion Technol. Seminar, pp. 97 – 103.

[13] Abdollahi and Gruzleski: *"An evaluation of calcium as a eutectic modifier in A357 alloy"*. Int. J. Cast Metals Res., Vol. 11, 1998, pp. 145 – 155.

[14] Q.T. Fang, P.N. Anyalebechi, D.A. Granger: *"Measurement of Hydrogen Porosity in Unidirectional Solidified Aluminum Alloys"*. Light Metals 1988, 1988, pp. 477 – 486

[15] Øyvind Nielsen, SINTEF, Materialer og kjemi, Metallurgi, Oslo (Private communication).

[16] S. Makarov, D. Apelian, R. Ludwig: *"Inclusion Removal and Detection in Molten Aluminum – Mechanical, Electromagnetic, and Acoustic Techniques"*. Metal Processing Institute, Worcester Polytechnic Institute, To be published in AFS Transactions 1999.

[17] Darius P. K. Singh and Dave J. Mitchell: *"Analyzing Aluminum Melt Quality from Furnace to Mold"*. Modern Casting (USA), 91, (5), May 2001, pp. 44 – 46

[18] G. I. Eskin: *"Principles of Ultrasonic Treatment: Application for Light Alloys Melts"*. Advanced Performance Materials (1997), 4(2) pp. 223 – 232

[19] High quality aluminium castings conf., Otaniemi, 1992, Lecture 3

[20] High quality aluminium castings conf., Otaniemi, 1992, Lecture 7

[21] 60th Foundry World Congress. Den Haag, 1993, Lecture 30

[22] Ray D. Peterson: *"The Secondary Metal Supplier and Metal Quality"*. Light Metals 2003, Edited by Paul N. Crepeau, TMS, 2003, pp. 1075 – 1081

[23] F. Frisvold, P. Bakke, E. Øvrelid, N. E. Hald, T. A. Engh: *"Hydrogen and Inclusion Content in Recycled Aluminium at Holmestrand Rolling Mill"*. Light Metals, 125th TMS Annual Meeting, Anaheim, California, pp. 1011 – 1016.

[24] K. Krone: *"Aluminiumrecycling "*. Vereinigung Deutscher Schmelzhütten e.V., Düsseldorf, 2000, pp. 145, 263, 372,

[25] W. Stevens, G. Riverin, V. Goutieres, Jean-Yves Fortin: *"Aluminium Melting and Dross Formation – a Historical and Modern Perspective of the situation"*. Light Metals 2003, Edited by Paul N. Crepeau, TMS, 2003, pp. 801 – 807

[26] D. E. Groteke, J. Fieber: *"A comparison of melt performance of stack melters versus traditional reverbs"*. 5th International AFS Conference on Molten Aluminium Processing Proceedings (USA), Nov. 1998, American Foundrymen's Society, Inc., pp. 368 – 376

[27] R. Tilak, J. Curiel: *"Aerospace Alloy Refining Efficiency Data for LARS™ (LARS™: Liquid Aluminum Refining System)"*. Light Metals 2003, Edited by Paul N. Crepeau, TMS, 2003, pp. 881 – 884

[28] W. Thiele: *"Die Oxidation von Aluminium- und Aluminiumlegierungs-schmelzen"*. Aluminium 38, Nr.11, 1962, pp. 780 – 786.

[29] S. Sibley, W. Simmons: *"Filtering liquid metals"*. WIRE INDUSTRY, March 1987

S. Sibley S, W. Simmons: *"Filtering Liquid Metals for Enhanced Quality and Productivity"*. Non Ferrous Metals World, (1), 1986 pp. 88-94.

[30] S. Lavoie, G. Dubé, C. Dubé: *"The Alcan Plasma Dross Process, a New Salt Free Dross Processing Technology"*. Second International Symposium – Recycling of Metals and Engineered Materials, Edited by Jan H.L. van Linden, Donald I. Stewart, jr. and Y. Sahai, The Minerals, Metals & Materials Society, 1990

[31] O. J. Siljan, G. Rian, D. T. Pettersen, A. Solheim, and C. Schoning: *"Refractories for molten aluminum contact--part I: thermodynamics and kinetics"*. Proceedings of the Unified International Technical Conference on Refractories (UNITECRALAFAR '01), Cancun, Mexico, November 2001. pp. 531-550

[32] Ole-J. Siljan, C. Schoning: *"Refractories for molten aluminum contact part II: Influence of pore size on aluminum penetration"*. Refractories Applications and News (2003), 8(1), pp. 21-29, 32.

[33] D. A. Weirauch Jr., G. E. Graddy Jr.. In: L. Hart (editor): *"Alumina chemicals: Science and technology handbook"*. Westerville: Amer. Ceram. Soc., Inc; 1990, p.489.

[34] T. H. Hall, G. Wilson. In: M. A. J. Rigaud (editor): *"Advances in refractories for the metallurgical industries"*. New York: Pergamon Press; 1988, p. 225.

[35] E.M. DeLiso, V.L. Hammersmith: *"Testing refractories for molten aluminum contact"*. American Ceramic Society Bulletin (1983), 62(7), pp. 804-808.

[36] G. Kaptay: *"On surface properties of molten aluminum alloys of oxidized surface"*. Materials Science Forum (1991), 77 (Solidif. Microgravity) pp. 315-330.

[37] Foundry Trade J. 175 (2001) Nr. 3579, pp. 15 – 16

[38] A. Moors: *"COSMA – Controlled Addition of Sodium Modifiers to Aluminium Alloys"*. Giesserei-Praxis (2001) Nr. 3, pp. 111 – 114

[39] P. Bakke, J. A. Laurin, A. Provost, D. O. Karlsen: *"Consistency of Inclusions in Pure Magnesium"*. Light Metals, 1997, pp. 1019 – 1026

[40] D.A. Weirauch Jr.: *"Technologically significant capillary phenomena in high-temperature materials processing. Examples drawn from the aluminum industry"*. Current Opinion in Solid State & Materials Science (2006), Volume Date 2005, 9(4-5), pp. 230-240.

[41] Stian Rørvik, Fundo Wheels AS, Høyanger, Norway (private communication)

[42] D. H. DeYoung, D. Apelian, R. Mutharasan: *"Method for Separation and Removal of Suspended Liquid Particles from Molten Metal and Associated Apparatus"*. US Patent 5,336,295 of Aug. 9, 1994

[43] T. Gudmundsson, G. Saevarsdottir, T. I. Sigfusson, D. G. McCartney: *"Chlorination of TiB_2 Grain Refined Aluminium Melts"*. Light Metals, 1997, pp. 851 – 855

[44] J.A. Eady, D.M. Smith, J.F Grandfield: *"Filtration of aluminum melts"*. Alum. Technol. '86, Proc. Int. Conf. (1986), pp. 93-100.

[45] Fielding, Roger A. P.; Kavanaugh, Carol F.: *"The role of grain refining, degassing and filtration in the production of quality ingot products"*. Light Metal Age (1996), 54(9,10), 46-59.

[46] Dubé and P. Waite: *"Processing of Molten Aluminum and Aluminum Alloys"*. International Conference on Recent Advances in the Science and Engineering of Light Metals, Japan, October 1991, pp. 1007 – 1014

[47] Celik and D. Doutre: *"Theoretical and Experimental Investigation of Furnace Chlorine Fluxing"*. Light Metals 1989, pp. 793 – 800

[48] D. D. Smith, L. S. Aubrey: *"Technical update on dual state ceramic foam filtration technology"*. ARABAL 99: Ninth International Arab Aluminium Conference and Exhibition, Kuweit, 27.-29. Nov. 1999

[49] *"More steps beyond rotary degassing"*. Aluminium Today (UK), 8, (6), 28-30, Dec. – Jan. 1996 – 1997

[50] S. Eketorp: *"Principles of Alloying, Refining and Heating of Metals"*. Proceedings International Seminar on Refining and Alloying of Liquid Aluminium and Ferro Alloys, Trondheim, 1985, p. 7.

[51] St. Kästner, J. Krüger, F. Patak: *„Raffination von Hüttenaluminium durch Spülgasbehandlung – Entfernung von Wasserstoff, Natrium und Lithium"*. From: Raffinationsverfahren in der Metallurgie; Published: GDMB – Gesellschaft für Bergbau, Metallurgie, Rohstoff- und Umwelttechnik Clausthal-Zellerfeld 1983, Verlag Chemie, Weinheim 1983, pp. 35 – 54

[52] J. Campbell, R.A. Harding: *"The Liquid Metal"*. TALAT Lecture 3202, IRC in Materials, The University of Birmingham, 1994

[53] M. Syvertsen: *"Removal of Hydrogen and Inclusions from Aluminum"*. Dr. ing. Thesis, Institut for Materialteknologi og Elektrokjemi, NTNU Trondheim, 2000, pp. xix – xx, 1 – 2

[54] G. K. Sigworth and T. A. Engh: *"Chemical and Kinetic Factors related to Hydrogen Removal from Aluminum"*. Metall. Mater. Trans. 28A,1997, pp. 1281 – 1288

[55] M. Bertherat, E. Blanquet, M. Allibert, P. Le Brun: *„Study of Aluminum Degassing by Hydrogen Analysis with Supersonic Expansion Mass Spectrometry"*. Light Metals 2003, Edited by Paul N. Crepeau, TMS, 2003, pp. 851 – 855

[56] G.K. Sigworth: *"Gas Fluxing of Molten Aluminum"*. Light Metals 1999, Edited by C. Edward Eckert, The Minerals, Metals & Materials Society, 1999, pp. 641 – 648

[57] M. C. Flemings: *"Solidification Processing"*. Mc Graw-Hill Book Company, 1974, p. 207.

[58] R. Wu et al.: *"Theoretical analysis and experimental study of spray degassing method"*. Materials Science and Engineering A, 2005, Volume 408, Issues 1-2, 5 November 2005, pp. 19 – 25

[59] A. I. Beljajew, E. A. Shemtschushina, L. A. Firsanova: *„Physikalische Chemie geschmolzener Salze"*. VEB-Verlag der Grundstoffindustrie, Leipzig 1964

[60] J. H. L. van Linden, D. L. Stewart: *„Molten Salt Flux Composition Effects in Aluminium Scrap Remelting"*. Light Metals 1988 (ed. L. G. Boxall) TMS, Warrendale 1988, pp. 391 – 398

[61] D. V. Neff, B. P. Cochran: *"Chlorination Technology in Aluminum Recycling"*. Light Metals, Light Metals (Warrendale, PA, United States) (1993), pp. 1053-1060

[62] D. V. Neff: *"The Use of Gas Injection Pumps in Secondary Aluminum Metal Refining"*. Proceedings, AIME, Recycle and Secondary Recovery of Metal, 1985, p. 73

[63] D. V. Neff: *"Environmentally Acceptable Chlorination Processes"*. 4th Australian Asian Pacific Course and Conference, Aluminium Cast House Technology: Theory & Practice, Edited by M. Nilmani, The Minerals, Metals & Materials Society, 1995, pp. 211 – 225

[64] J.C. Escobedo, A. Flores V., J.F. Hernández, D. Cortés, J.J. Velázquez: *"Recent Experiences with the use of SiO_2 for Removing of Magnesium from Molten Aluminum Alloys"*. Light Metals 2003, Edited by Paul N. Crepeau, TMS, 2003, pp. 885 – 891

[65] M. Garnier: *"Actual and Future Developments of Electromagnetic Processing of Materials"*. Proceedings of The Julian Szekely Memorial Symposium on Material Processing, H. Y. Sohn, J. W. Evans, D. Apelian, Eds., Minerals, Metals & Materials Society, 1997, pp. 313 – 322

[66] S. Ali, D. Apelian, R. Mutharasan: *"Refining of Aluminum and Steel Melts by the Use of Multi-Cellular Extruded Ceramic Filters"*. Canadian Metallurgical Quarterly, Vol. 24, No. 4, 1985, pp. 311 – 318

[67] Apelian, Diran; Choi, Kyung K.: *"Metal refining by filtration*". Foundry Processes: Their Chem. Phys., [Proc. Int. Symp.] (1988), Meeting Date 1986, pp. 467 – 493

[68] C. E. Eckert, R. E. Miller, D. Apelian, R. Mutharasan: *"Molten aluminum filtration: fundamentals and models"*. Light Metals 1984, 1984, pp. 1281 – 1304

[69] L. Maréchal, N. El-Kaddah, P.-Y. Menet: *„Influence of Convection on Agglomeration and Removal of Non-Metallic Inclusions in Molten Aluminum"*. Light Metals 1993, Edited by Subodh K. Das, The Minerals, Metals & Materials Society, 1992

[70] S. L. Soo: *"Fluid Dynamics of Multiphase Systems"*. Blaisdell Publishing Co, Massachusetts, 1967

[71] S. T. Johansen, S. Taniguchi: *"Prediction of Agglomeration and Break-up of Inclusions During Metal Refining"*. Light Metals, 1998, pp. 855 – 861

[72] M. Maniruzzaman, M. Makhlouf: *"Computer Simulation of Flotation Treatment Methods Used in Aluminum Alloy Processing"*. Light Metals, 1998, pp. 797 – 803

[73] M. Maniruzzaman, M. Makhlouf: *"Modeling of Flotation Process in Aluminum Melt Treatment"*. Proceedings of the Eighth International Symposium on Modeling of Casting and Welding Processes 1998, B. G. Thomas and C. Beckermann, Eds., TMS, 1998, pp. 705 – 712

[74] B. Gariepy, G. Dubé, C. Simoneau, G. Leblanc: *"The TAC process: A proven technology"*. Light Metals 1984, pp. 1267 – 1279, Warrendale, Pennsylvania

[75] T. R. A. Davey: *"Pyrometallurgical methods for refining metals"*. Techniques of materials preparation and handling part 2, ed. R. F. Bunshah, Chapter 12, Interscience, New York

[76] S. Nagata: *"Mixing, principles and applications"*. Wiley, New York, 1975

[77] K. Buxmann, G. B. Leconte: *„Verunreinigung und Reinigung von Aluminium in Giessereien"*. Verunreinigungen in Metallen, Deutsche Gesellschaft für Metallkunde e.V., 1977, pp. 109 – 127

[78] J. Szekely, N. J. Themelis: *"Rate phenomena in process metallurgy"*. Wiley-Interscience, New York, 1971

[79] J. Szekely, K. Nakanishi: *"Stirring and its effects on aluminium deoxidation in the ASEA-SKF furnace: Part II. Mathematical representations of the turbulent flow field and of tracer dispersion"*. Metall. Trans., 6B, 1975, pp. 245 – 256

[80] Y. Sundberg: *"Mechanical stirring power in molten metal in ladles obtained by induction stirring and gas blowing"*. Scand. J. Metallurgy, 7, 1978, pp. 81 – 87

[81] P. Cremer, J. Driole: *"Effects of the electromagnetic stirring on the removal of inclusions of oxide from liquid steel"*. Metall. Trans., 13B, 1982, pp. 45 – 52

[82] B. Pillin, P. Gillon, E. Beaugon: *"Method and Device for Separating Particles from an Electrically Conductive Liquid Flow Using Electromagnetic Forces"*. EP Patent 879087A1 of Nov 25, 1998

[83] P. Gillon, B. Pillin : *"Electromagnetic Separation of Particles from a Conducting Liquid Using a Strong DC Magnetic Field"*. Proceedings of Induction Heating Seminar HIS-98, Padua, Italy 1998

[84] B. Pillin: *"Utilisation Des Champs Magnétiques Intenses Pour la Separation d'Inclusions : Application aux Particules Solides Immergées Dans les Métaux Liquides"*. PhD EPM, CNRS-Grenoble, 1997, (French)

[85] A. G. Szekely: *"The removal of solid particles from molten aluminum in the spinning nozzle inert flotation process"*. Metallurgical and Materials Transactions B, Vol. 7, Nr. 2 / June, 1976, pp. 259 – 270

[86] F. Patak: *"Untersuchungen zur Natrium- und Lithium-Entfernung aus Hüttenaluminium"*. PhD, RWTH Aachen, 1983

[87] R. Kumar: *„Advances in Aluminium Alloy Melting Technology"*. Light Metal Age 1978, No. 2, pp. 5 – 14

[88] Michael F. Mattocks, R. A. Frank: *"Recent Quality and Efficiency Improvements through Advances in In-line Refining Technology"*. Aluminium Asia '98, 7-9 May 1998, 1998, pp. 1 – 14

[89] C. Tian, R. I. L. Guthrie: *"The Dynamic Process of Liquid Metal Filtration"*. Light Metals 1995, Edited by J. Evans, The Minerals, Metals & Materials Society, 1995, pp. 1263 – 1272

[90] P.D. Hess, E.L. Rooy: *"Minimize Air Pollution and Improve Metal Quality through Filtration in the Foundry"*. AFS Transactions, 1971, pp. 253 – 256

[91] D. Kocaefe, A. Murray-Chiasson, Y. Kocaefe, P. Waite: *"Investigation of Inclusion Re-Entrainment during Filtration"*. Light Metals 2003, Edited by Paul N. Crepeau, TMS, 2003, pp. 873 – 879

[92] X. Wang: *„Morphological Aspects of Inclusions in 3014 D & I Can Stock Alloy"*. Light Metals 1997, pp. 963 –972

[93] D. Apelian; Mutharasan, R; Romanowski, C. A.; Miller, R. E.; Eckert, C. E.: *"Commercially available porous media for molten metal treatment: a property evaluation"*. Light Metals (Warrendale, PA, United States) (1982), pp. 935 – 968

[94] J.E. Dore, J.E. Yarwood: *"Ceramic Foam Filter"*. U.S. Patent 3,962,081, June 8, 1976

[95] B. Hübschen: *"Metal Filtration - Modelling, Experiments and Calculations"*. Aachen University of Technology, Institute of Nonferrous Process Metallurgy, Presented at the 2nd International Melt Processing Technology Workshop, Dublin, 1-2 October 1998

[96] M.V. Brant, D.C. Bone, E.F. Emley: *"Fumeless In-Line Degassing and Cleaning of Liquid Aluminum"*. Journal of Metals, March 1971, pp. 48 – 53

[97] G. I. Eskin: *"Fine Filtration of Melt. The Usfirals Process"*. Proc. of Intern. Conf. High Temperature Capillarity, Slovakia, Inst. of Inorg. Chemistry of Slovak Academy of Science, 1994, pp. 321 – 329

[98] M. Zhou, D. Shu, K. Li, W.Y. Zhang, H.J. Ni, B.D. Sun, J. Wang: *„Deep Filtration of Molten Aluminum using Ceramic Foam Filters and Ceramic Particles with Active Coatings“*. Metallurgical and Materials Transactions A, Volume 34A, May 2003, pp. 1183 – 1191

[99] Ooaumi, Kenji; Nagakura, Yutaka; Masuda, Ryuhei; Yanagawa, Masahiro: *“Development of new filter for removal of non-metallic inclusions from the molten aluminum“*. KOBELCO Technology Review (2001), 24, pp. 32-36

[100] F. De Schutter, J. Verwimp, W. Engelen, S. Kuypers, M. Ryckeboer, W. Verberckt, P. Hermans, C. Castelijns: *„PROCIAS: A Joint Project on Process Control of Aluminium Melts“*. Light Metals 1999, Edited by C. Edward Eckert, The Minerals, Metals & Materials Society, 1999, pp. 849 – 854

[101] M. Otto: *“Analytische Chemie”*. VCH Verlagsgesellschaft mbH, D-69451 Weinheim, Germany, 1995, pp. 153 – 154

Chapter 2

PREVIOUS WORK - THERMODYNAMICS

2.1 Introduction

The problems industries are facing today are twofold: present technologies are restricted by tighter environmental, health and safety regulations as well as the economical margins. At the same time there is a strong drive from the downstream industries to meet demands from the expanding use of aluminium alloys for high end applications in castings, extrusion, rolling and so on. Optimization of todays refining techniques to achieve high removal rates with respect to H, alkali and inclusion removal is therefore indicated. The consumption of refining agents, which strongly depends on thermodynamics and kinetics, has to be optimized. Besides the cost of the refining agent and its environmental impact, any excess of it will be involved in collateral reactions. Reaction products may act as impurities which have to be removed later. All this leads to an increasing demand for the development of highly efficient, compact in-line

degassing and filtration systems with maximum operational flexibility combining previously separate treatment steps [1].

Today, powdery and granular refining agents are increasingly injected for both the removal of dissolved impurities and suspended particles, giving better pollution control than the gaseous chlorination processes. Granular fluxes are superior compared to powders with respect to particulate and fluoride emissions, also giving reduced addition rates. For the removal of suspended particles smaller than 30μm, where surface forces are believed to play a decisive role, “passive” filter materials prevail in industrial filtration technology with packed bed, rigid media and ceramic foam filters. A final break through of “sticky” filter material to increase surface forces and, hence, removal of suspended particles have not be reported, even though filter material based on or coated with chloride or fluoride salt fluxes has been in operation. Currently, research is carried out on adhesive coatings like NaBr or glassy enamels which are viscous at molten metal temperatures. For the removal of dissolved impurities such as alkali and magnesium it has been proposed to intercalate them temporarily into a host material, from which the elements could subsequently be recovered, mimicking what happens in the lithium ion battery [2].

However, refining aluminum with respect to dissolved elements and suspended particles still involves a multi-stage approach. Fluxes, both Ar-Cl_2 gases and salts, injected into molten metal readily float up, and the residence time is short. Thus, these fluxes do not effectively react with the molten metal [3].

Merging established fluxing techniques with known filtration technologies such as packed bed, rigid media or ceramic foam filters could circumvent such kinetic deficits as short contact times and small contact areas. A bed filter containing for example AlF_3 as a filter media could actively remove alkali from the melt and at the same time retain the reaction products. Some of these products such as NaF or KF act as surfactants [4]. By decreasing the surface tension at the melt/filter surface interface they may enhance alkali removal and particle capture. Based on the literature [5]-[10], ”active” filtration can be looked at as an enhanced removal of dissolved impurities/suspended particles in filters due to chemical reaction/adhesion, absorption and adsorption phenomena occuring at the filter media’s surface. In addition to alkali and Mg, AlF_3 is also reported to remove H, Sr and Sb.

Contact between a metal melt and the surface of a solid high melting substance or material plays a role in many physical phenomena and some important technological processes. They include the processes of crystal nucleation and growth from the metal melt, various metallurgical processes – melting, casting, moulding of steel and alloys, soldering and welding, processes of powder metallurgy mineral production by liquid-phase sintering or impregnation of a porous high-melting framework by a liquid-metal binder. Mutual interaction between a solid and a liquid via an interphase is also important in contact systems where for example metallic liquids act as transport media in heat exchangers, or nuclear fuel systems where the active substance is distributed as a stable, finely dispersed suspension in the liquid metal. Thus, the study of contact and capillary properties of metal melts, the processes of wetting solid bodies surfaces, and metal adhesion to the solid surface constitutes one of the most important aspects of modern metallurgy, physics and physical chemistry of solid substances and metallic liquids. Solid body wettability by molten metals at high temperatures poses a number of purely specific features and presents an independent problem [11]. This importance has been stressed recently by D.A. Weirauch Jr. [12] who identified areas for improved understanding of wetting, spreading, infiltration, and Marangoni flow behaviour by drawing examples from the aluminum industry. There, capillary phenomena are at play in all of the process steps.

In essence, this chapter aims to determine the physicochemical mechanisms in developments having efficient impurity removal in mind. Removal of dissolved impurities and suspended particles is treated separately, even though the removal of one type often causes the removal of the other also. Relevant fluxing techniques as well as recent and historical trends are presented in chapter 3.

The reader interested in fundamentals of fluid flow and mass transfer phenomena applicable to this work is recommended to study chemical engineering text books, for example [13], [14], [15]. Also one may refer to previous work by Engh [16], Frisvold [17] and Syvertsen [18].

2.2 Removal of Dissolved Impurities - Thermodynamics

When studying the literature a cursory glance at the Gibbs energy of formation, ΔG, of several sulfides, oxides, chlorides and fluorides in Fig. 2.1 [19] can give an idea about potential refining agents. The thermodynamic stability of a compound increases with an increasing negative value of the Gibbs energy of formation. For instance metal chlorides that have a standard Gibbs energy value more negative than $AlCl_3$ are more stable than $AlCl_3$. When Cl_2 is injected into aluminium containing various metallic elements, the chlorine will for kinetic reasons first react with Al and subsequently with these metallic impurities. The same applies to fluorides. Li, Na, K, Mg and Ba all form more stable chlorides and fluorides than aluminium and can, therefore, be removed by Cl_2, F_2, or SF_6 injection.

The equilibrium constant for reactions such as $Al + 3MeX = 3Me + AlX_3$, X = Cl or F, and Me = Li, Na, K and $Al + 1{,}5MeX_2 = 1{,}5Me + AlX_3$, X = Cl or F and Me = Ca, Mg, Ba, Sr is shown in Fig. 2.2 [19] for various metals. An equilibrium constant much greater than one implies that the reaction is shifted to the right, while a value much less than one indicates that at equilibrium the reaction is shifted to the left. Therefore, an alkali or alkali-earth chloride electrolyte has no tendency to react with aluminium. Corresponding metal-fluoride electrolytes are slightly more reactive, what turns them into effective additions to chloride salt based fluxes. There, they act as surfactants improving the stripping and removal of oxides from the melt. A chloride and fluoride electrolyte is, therefore, suitable for refining aluminium since it will promote the removal of alkali/alkali-earth metal impurities [20].

The application of F_2 gas would be advantageous for thermodynamic and physical-chemical reasons, since the same efficiency as for Cl_2 gas could be achieved already at a lower partial pressure. The generation and treatment of off-gases, and the generation of dross and the de-drossing would be influenced positively. But because of the higher toxicity compared to Cl_2 and the difficulty in producing it, the use of F_2 gas is abandoned [21]. AlF_3 in its solid state can be utilized instead. The holder of U.S. Patent 3,620,716 claims cost advantages of about 50 % of $KAlF_3$ over AlF_3 for Mg removal from aluminium melts. Potassium aluminum fluoride offers further advantages in decreased melt loss and greatly decreased fume generation during fluxing [22].

However, in the industrial production of aluminum metal it mainly serves as a component of the electrolyte that decreases the freezing point of the cryolite melt [23].

But even if thermochemical calculations tell whether a reaction may occur or not, kinetic considerations also have to be taken into account. They can give insight into the reaction to be expected. In pyrometallurgy with its various consecutive and parallel reactions it is of primary interest to determine the rate-limiting step of the overall reaction. Only by influencing this step can the rate of the total reaction be changed. Rate limiting, for example, might be diffusive mass transfer at the boundary layer, heat transfer (metal destillation), nucleation and growth or bubble growth respectively (degassing) [21]. Reference is made to chemical engineering text books [24] for mathematical tools and kinetic models.

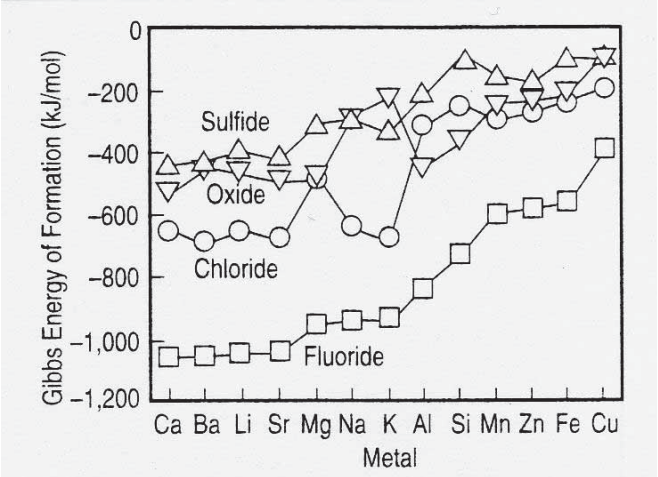

Fig. 2.1: Standard Gibbs energy of formation of several sulfides, oxides, chlorides, and fluorides. The data are given at 723°C per mole of S, O, Cl_2, and F_2, respectively [19].

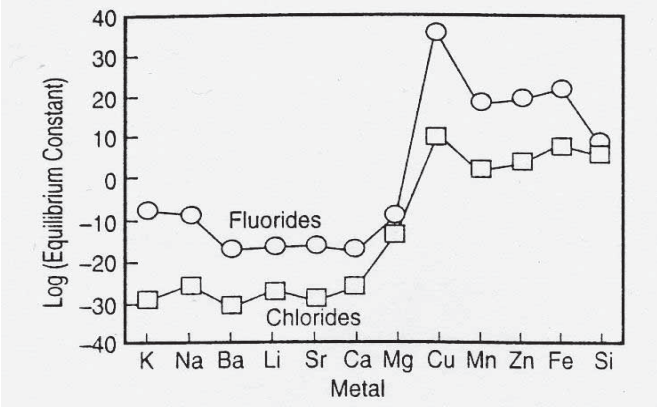

Fig. 2.2: Exchange equilibrium between Al and metal chlorides and fluorides at 723°C based on the reactions Al + 3MeX = AlX_3 + 3Me and Al + 1.5MeX2 = AlX_3 + 1.5Me.

From Fig. 2.1 and Fig. 2.2 it is apparent that the decision whether to use a chlorine or fluorine containing refining agent must be rather for practical (handling, price etc.) than for thermodynamic reasons. This is supported by the fact that the main kinetic factors (contact area and contact time) apply in both cases.

Chlorine gas and chloride salts are popular and approved industrial refining agents because of their low market price and good availability. Nevertheless, there are some drawbacks to deal with. In particular when treating Al-Mg alloys the use of these fluxes results in liquid reaction products which are more difficult to separate from a melt than solids [25]. This in fact may constrain the degree of melt cleanliness attainable. Again, some companies just do not like the handling of a gas despite the high removal rates with chlorine gas. Concerns are the elusive nature of chlorine gas affecting working environment for both workers and facilities. This may require precautions which are more elaborate than for solid refing agents or induce other additional costs (maintenance etc.). However, several authors [4], [25]-[27] claim the feasibility of employing “zero” emission chlorine gas fluxing units when properly designed. At the same time, Mg levels in Al-Mg alloys remain relatively unaltered.

As already mentioned, AlF_3 is an alternative source of fluorine. It does not contaminate the melt. Also, AlF_3 is not hygroscopic in contrast to $MgCl_2$ for example [28]. Furthermore, there is industrial evidence that spent AlF_3 may be returned to the pot-lines [10]. Industrially today, AlF_3 powder is added in a batch process either by stirring or injection. Alkali removal efficiencies in the order of 80% to 95% have been achieved. The process also has been proven to remove Al_4C_3 inclusions by a convection flotation mechanism [29]. Application of AlF_3 in industrial refining of liquid aluminium shows that it is economically advantageous versus chlorine gas and chloride salts in spite of its higher market price. Analysing the powder batch process with respect to kinetics one may find that AlF_3 is not utilized in an efficient way. Both contact time as well as contact area per kilogram melt exposed to AlF_3 should be considerably increased in a bed filter. A bed filter containing agglomerated AlF_3 as a filter media could actively remove alkali from the melt and at the same time retain the reaction products.

In the literature early reference is made to a process using fluorinated alumina pellets in a bed filter which will be referred to in section 3.3 [10], [30]. With the eutectic temperature for binary and ternary products with AlF_3 being relatively low [31], it is reasonable to expect that solid-liquid mixtures will be present at temperatures around 800°C. Precautions have to be taken to prevent a carry over of these mixtures into the melt. Thermodynamically some of the following reaction products can be expected to form: KF, NaF, LiF, CaF_2, MgF_2, Li_3AlF_6, Na_3AlF_6, $Na_5Al_3F_{14}$. Reported products of melt treatment operations [10], [32] regarding Na, Li, Ca are CaF_2, LiF, Na_3AlF_6, $Na_5Al_3F_{14}$, $Li_3Na_3Al_2F_{12}$. Some of these products such as CaF_2 [33], Na_3AlF_6, NaF or KF [34] act as surfactants. By decreasing the surface tension at the melt/filter surface interface they possibly enhance alkali and hydrogen removal and/or particle capture. The mechanisms and effects that apply have been reported by Silny and Utigard [34]. These facts indicate that a batch reactor could be replaced by a continuous one, simplifying proceedures and superseding the skimming procedure at the end of melt treatment.

As mentioned earlier in this text, an effective removal of dissolved alkali/alkaline earth impurities and Sr, often also Mg can be achieved only by the use of AlF_3 additions or reactive gases like Cl_2 or mixtures thereof with inert gases such as Ar

for instance [21]. In an extensive series of experiments in a 0.75 tonne furnace simulating industrial fluxing operations, D. Doutre and C. Celik [35] revealed a sequence of events as illustrated in Figure 2.3. The elements to be removed react indirectly with Cl_2 by forming first $AlCl_3$ (gaseous, T_S = 180°C) which is not thermodynamically stable in the presence of Mg or other alkali impurities. $AlCl_3$ then will convert for example Na to NaCl. All the chloride salts formed are less dense than liquid aluminum, and will float to, and accumulate at, the dross layer on top of the melt. Similarly they also coat the sidewalls of the vessel [36]. Additionally, flotation of the chlorides and also other inclusions present in the melt takes place [21]. If Mg is the most abundant of these species, as in Al-Mg alloys, $AlCl_3$ will react with dissolved Mg to form $MgCl_2$. $MgCl_2$ will form a thin molten film on the bubble surface. Both of these steps occur very rapidly. The $MgCl_2$ salt is then sheared off the bubbles surface to form a dispersion of minute magnesium chloride droplets within the melt. The majority of these are below the current detection limit for LiMCA equipment, i.e. 1-15μm, but account for a significant degree of alkali removal such as Ca. In this case the problem is a loss of Mg. A solution might be fluxing with a $MgCl_2$ containing salt instead [37].

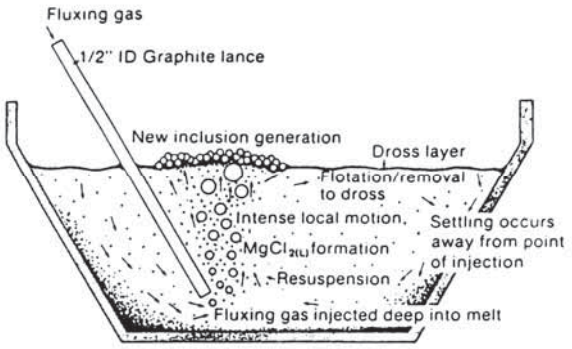

Fig. 2.3: Illustration of industrial furnace gas fluxing events (Al-Mg alloys) [35]

$MgCl_2$ is molten at aluminum refining temperatures and thermodynamically unstable in the presence of alkali impurities, and will react to form the insoluble chloride salts [38]. In turn these salts to some extent contaminate the aluminium melt. Figure 2.4 shows the stability of alkali and $MgCl_2$ salts relative to $AlCl_3$ (gas) [39]. In

essence, the lower the Cl_2 pressure required to form a salt, MCl, the more stable the salt is, and the easier it is to remove, M, by fluxing. It can be seen that $CaCl_2$ is the most stable, followed by Na, Li, Mg, and finally aluminium chlorides. Thus, when using Cl_2 as a fluxing agent, Ca will be the element removed first. If chlorine is used in amounts exceeding what is required for Li removal, Mg levels will start to be reduced. Finally, if the Mg level has been reduced to its thermodynamic minimum concentration, aluminium itself will be consumed. The given order of removal is only true from a thermodynamic point of view for equal concentrations of the named elements.

In general, in multicomponent refining processes, a great number of elements and simultaneous chemical reactions have to be considered. Computer-based equilibrium calculations for the refining of liquid Al indicate that the impurity elements Na, K, Li and Ca are removed simultaneously from Al by the refining agents AlF_3 and $MgCl_2$ [40]. The advantage of using a thermodynamic computer program in the calculation of the progress of aluminium refining is that the influence of temperature, amount of fluxing agents and alloy composition on the final metal composition can be studied. [41]

Table 2.1 gives the minimum realizable concentrations of solute elements when fluxing with reactive gases at 1000 K [16]. It should be noted, however, that these concentrations are determined solely by thermodynamic calculations, and that practically, the minimum concentration achievable will be somewhat higher due to kinetic constraints that become rate controlling at very low concentrations [38]. The bubble size here is of particular importance. Ideally, the Cl_2 carried in a gas bubble should be completely consumed when the gas bubble reaches the bath surface. Otherwise elementary Cl_2 will be released into the environment. This condition will be met by small bubles and for low contents of chlorine (<15vol%) [21]. Figure 2.5 shows the same type of information for the fluoride salt stability in liquid aluminium [39].

Table 2.1: Approximate minimum impurity levels attainable in aluminium by reactive gases (T = 1000 K) [39].

	Content remaining in p.p.m.	
Element	***chlorine***	***fluorine***
Be	65	85
Ca	3×10^{-5}	5.7×10^{-4}
Li	0.01	0.05
Mg	1.4	4.9
Na	3×10^{-5}	0.19

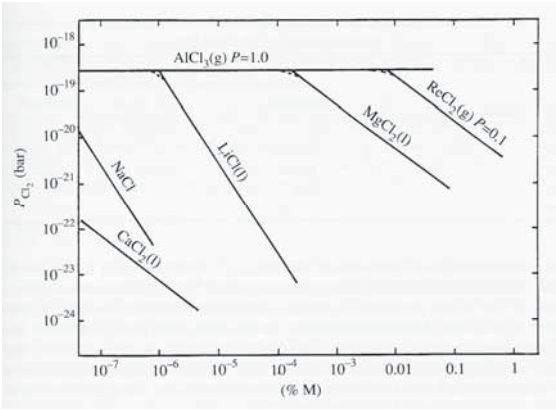

Fig. 2.4: Calculated equilibria for ternary Al-M-Cl systems at 1000 K [39]

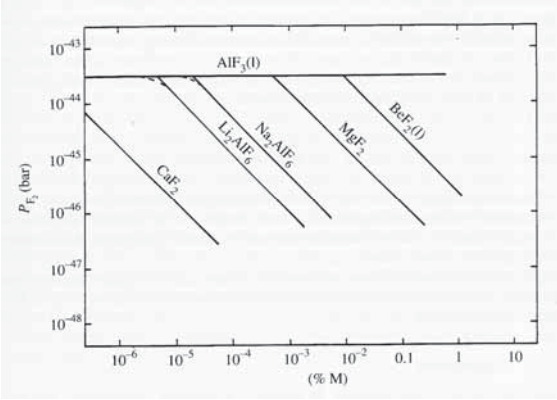

Fig. 2.5: Calculated equilibria for ternary Al-M-F systems at 1000 K [39]

On the basis of thermodynamic calculations Radin [42] explains the refining action of AlF_3 by the presence of the gaseous subfluoride AlF(g) which is formed in contact with aluminium abundant in the melt. The gaseous AlF(g) formed is volatile but may be dissolved as well in liquid halide salts present. The existence of this gaseous mono-fluoride was shown by Klemm and Voss [43] in 1943. AlF is only stable in the gas phase [22].

Generally, molten aluminium is more likely to form single valency bonds instead of three valency bonds in the presence of halide salts which can be explained by the low ionizing potential of the first valence electron of aluminium. The reaction of aluminium with halide salts may be described by Reaction 2.1:

$$1/k\ Al + 1/n\ MeY_n = 1/k\ AlY_k + 1/n\ Me \qquad (2.1)$$

where Me may be an alkali or earth alkali metal, Y can be fluorine or chlorine, n is the valence of the metal, k = 1 for the formation of the subfluoride or subchloride of aluminium, and k = 3 for the formation of aluminium fluoride or chloride. To asses the reactivity of halide salts in contact with molten aluminium one may compare the equilibrium pressures of the halide or subhalide gases (AlY_k) formed. For the pressures given in the same reference, which increase with increasing temperatures, for AlF_3 in equilibrium with molten Al is the highest. It must be mentioned that AlF_3 is more thermodynamically stable than the subfluoride AlF(g) at the considered temperatures. First, this means that an alkali or earth alkali metal will preferably react with the gaseous subfluoride rather than with the solid AlF_3. Second, due to the slow degradation, AlF_3 can steadily release AlF (g) over a longer period when in contact with the Al melt. According to Radin [42] the removal of for example Na may be described by the following two consecutive Reactions 2.2 and 2.3. Sodium in reaction 2.3 may be replaced by K, Ca, Mg, Li and Ba for example. However, NaF and LiF may react further forming more stable compounds such as Na_3AlF_6 (cryolite), $Na_5Al_3F_{14}$ (chiolyte) and Li_3AlF_6 when in contact with AlF_3.

$$2/3\ Al + 1/3\ AlF_3 = AlF\ (g) \qquad (2.2)$$

$$AlF\ (g) + Na = Al + NaF \qquad (2.3)$$

Refining operations are carried out at much lower temperatures than in the Hall-Heroult cell, which complicates the discussion of the chemistry.

In Radin's opinion the gaseous subfluorides and subchlorides also contribute to the removal of hydrogen from melts similarly to volatile chlorides or inert gases by diffusion into the gaseous phase. This view is shared by Pimenov [44] degassing melts when filtering out finely dispersed oxides in a bed of active lump fluxes. He points out that the separation of these suspended oxides, which act as nucleation sites for hydrogen, made it easier for the hydrogen to diffuse into the gaseous phase. This took place at a rate somewhat higher than achieved with bubble separation. Contrary to Radin, Morozov and Gokhshtein [5] explain the separation of the fluorine containing gas phase with the formation of complex compounds rather than with the reaction of fluorides with aluminum. The possibility that, when heated to melt temperature, vapours will form on the solid fluorine containing salts without any interaction with molten aluminum was confirmed by their tests. Kvande [45] assumed that the total pressure of the gaseous phase is given by the sum of these mechanisms: the pressure of the volatile species formed by the reaction of the liquid aluminium with the fluoride salt, and the vapour pressure over the fluoride salt in absence of the liquid aluminium. Kvande found that AlF (g) formed by reaction 2.2 is the major gaseous contribution in the AlF_3-Al system, whereas AlF_3 (g), being the main component of the vapour pressure over AlF_3 in absence of aluminium, constitutes only a minor amount. Adding NaF to the AlF_3-Al system, at 1027°C the main constituents of the vapour above the melt are $NaAlF_4$ (g) and AlF (g), both of about equal magnitude for AlF_3 contents > 50%. If the $NaAlF_4$ vapors are cooled slowly, a solid phase transformation occurs [46]:

$$5\ NaAlF_4\ (g) = Na_5Al_3F_{14}\ (s) + 2\ AlF_3\ (s) \qquad (2.4)$$

The refining effect of fluoride salts (AlF_3, NaF, KF, CaF_2) is associated with exchange reactions which involve both the melt (Al) as well as the salts themselve. The release of AlF (g), Na, K, Ca which are all more or less surface active is a result of these reactions. This will be treated further in section 2.2. These surface active substances gather at the melt/oxide interface both at the melt surface and in the bulk melt. This is accompanied by a thin layer of dry, dusty slag forming on the melt surface [5]. Such a dry oxide layer indicates a better separation of the two phases or a decreased wetting of melt and oxide, respectively. Then, the oxide can be picked up by the flux/filter more easily. As a side effect of the improved oxide removal, the rate of hydrogen diffusing out of the melt into the flux is much higher than it would be in the presence of a "wet" oxide layer.

According to some lab experience with AlF_3 the salt must not necessarily be in direct contact with the oxide. It may be as well immersed in the melt or coat the side walls of the vessel to achieve both the degassing and de-wetting effect. As a consequence, it must be the gaseous subfluoride AlF(g) that facilitates the latter two effects.

In 1973, Huggins evaluated lithium titanates as possible lithium host materials and studied the thermodynamic and kinetic properties of lithium insertion into several lithium titanium oxides. This kind of hosting also referred to as intercalation is the reversible insertion of a guest or chemical species into a solid compound or phase, that exists over a range of stoichiometry, usually without change of structure and minimal change in lattice parameter. It was found that it was possible to insert lithium into the structure to form $Li_{(2.3+\delta)}Ti_{3.4}O_8$ and to cycle it within the spinel phase region, $0 < \delta < 1$, with no noticable change in the lattice parameter [48]. Increase in lattice parameter actually is the reason for cathode swelling in the Hall-Heroult cell which is caused by the intercalation of sodium [49]. Hardeman and Fray [50] demonstrated that lithium could be removed from aluminum-lithium alloys and intercalated into lithium titanate pellets. It was shown that the lithium content of aluminum could be reduced significantly. The lithium in the pellets could be extracted by applying an anodic potential to the bed of pellets, held in a fused salt. Although measurements were performed on a single pellet, calculations showed that by using a packed bed of pellets, significant currents would be expected to flow, permitting rapid removal of the lithium [50]. All these operations would be silent, energy efficient, and pollution free. In 1995, Riley and Jong [51] extended this work to the removal of lithium from solid aluminum-lithium or aluminum-magnesium turnings and lithium titanate pellets held in a LiCl-KCl or $MgCl_2$ melt, respectively. Depending on the electrolyte, both lithium and magnesium could be removed from aluminum melts and the titanates discharged to produce clean metals. Overall, early estimates show that considering the price of chlorine and pollution abatement equipment, there would be significant economic benefits as well as environmental gains by purifying aluminum in a non-polluting way. The intercalation purification method has recently been extended to the removal of sodium and magnesium from molten aluminum using manganates as the host material [52]. It should be stressed that this process produces valuable metals rather than worthless salts with disposal problems and may be applicable to the refining of other metals and alloys.

2.3 Removal of Suspended Particles - Thermodynamics

In physico-chemical systems it is possible to distinguish clearly between the conditions governing mechanical equilibrium, and those relating to equilibrium in physico-chemical changes such as chemical reactions and phase changes. In the particular case of capillary systems, mechanical equilibrium is determined not only by those factors such as hydrostatic pressure and gravitational attraction common to all systems, but also by forces associated with surface tension. Among the physico-chemical changes which must be considered are modifications of the chemical composition at the boundaries between bulk phases, that is, adsorption (i.e. transition of some part of the substance into the surface or back but not through the interface) [11]. The term capillary system will be used to des cribe any system in which the surfaces separating the various bulk phases play a significant part in determining the physico-chemical state of the system. The surface energy depends not only on the composition of the surface layer, but also on the composition of the bulk phases. Therefore, one must distinguish between the contributions from the bulk phase and that which is truly a surface property. Also interactions between molecules on the surface and those in the bulk phases have to be taken into account [53].

Adsorption phenomena may be related to a geometrical surface by supposing that each of the two bulk phases it separates remains homogeneous up to this surface (Gibbs dividing surface). There are two cases in which the Gibbs model does give a complete description of the system. The first, and most important, is that in which the system is in equilibrium. The second is that of a freshly formed liquid surface, when the surface has the same composition as the underlying liquid [53]. Wether in equilibrium or not, there are interfaces and interfacial energies that may be attributed to such a system [11]. An “interface” is a boundary between phases. In most cases it is only a few molecular diameters thick. However, the rapid change in density and/or composition across the interface gives them their most important property, an excess free energy or lateral stress which is usually called interfacial energy, σ, or interfacial tension, γ, respectively [54]. The force acting upon the interface between two phases (liquid-liquid, liquid-solid, or solid-solid) is called interfacial tension. It is the result of the attraction of the molecules at the interface to the bulk of the two phases [55]. Surface tension in turn

refers to the interfacial tension of either a solid or liquid being in contact with a gaseous phase. In creating a surface, atoms or molecules must be transferred from minimum potential energy positions in the interior of the bulk phase to an interface with asymmetrical potential energy field. Since the surface species are in a state of higher Gibbs energy than those in the bulk, the tendency of the system is to reduce the number of atoms in the surface, *i.e.*, to minimize the surface area [55].

The work needed for reversible creation of additional surface of a liquid *L* in contact with a vapour *V*, identified by the term σ_{LV}, was defined by Gibbs [56] as:

$$\sigma_{LV} = \left(\frac{\partial G}{\partial \Omega} \right)_{T,v,n_i} \tag{2.5}$$

where G is the total free energy of the system, Ω the surface area, T temperature, v volume and n_i the number of moles of component i. However, this definition is not sufficient to describe the work needed for creation of a solid surface *S*.

For monoatomic solids, σ_{SV} is proportional to the difference in potential energy between an atom of the surface and an atom of the bulk solid. This difference does not remain constant when a solid creates new surface without increasing the number of surface atoms by purely elastic strain of the solid. Because surface atoms are bonded weakly compared to those in the bulk, the work needed to stretch the surface is less than for the bulk material. The extra stress due to the surface, called by Gibbs "surface tension", is denoted γ_{SV}. For solids, σ_{SV} and γ_{SV} are therefore different quantities. Moreover, σ_{SV} is always a positive quantity (breaking bonds needs work to be done) while γ_{SV} can be either positive or negative [57] since it also depends on the orientation along the face. For liquids, σ_{LV} and γ_{LV} are equal because a reversible stretching of a liquid surface is identical to a reversible creation of new surface. In both cases, the liquid can increase its surface area only by the addition of new atoms to the surface. [58].

Surface, σ_{SV}, and interfacial energies, σ_{SL}, are given in dimensions of energy per unit area [J/m^2] (or mJ/m$^{2)}$. For the reasons explained above these units will exclusively be used for S/V and S/L boundaries. For L/V surfaces, both the surface tension, γ_{LV}, and the surface energy, σ_{LV}, may be used interchangeably depending on

the context. γ_{LV} is measured as a force per length [N/m] (or mN/m). Note that , from a dimension point of view, an energy per unit area is aquivalent to a force per unit length and the values are numerically equal. [58]

The contact systems under consideration are usually characterized by developed interphase surfaces, a highly dispersed state of the solid phase, cavities, channels and spaces of small cross-section (capillaries) present in the solid phase. In such systems, the velocity and the direction, as well as the properties of the product obtained, depend on the state and properties of the interface, the degree of wettability of the solid phase by the liquid metal and the contact adhesion strength [11].

Several well-known formulae are considered [11]:

- capillary pressure

$$p = \frac{2\gamma_{LV} \cdot \cos\theta}{r}, \tag{2.6}$$

- the height of the liquid in the vertical capillary

$$H = \frac{2\gamma_{LV} \cos\theta}{rg\rho} \tag{2.7}$$

- the velocity of the movement of the liquid along the horizontal slot

$$L^2 = \frac{D\gamma_{LV} \cdot \cos\theta}{6\eta}\tau \tag{2.8}$$

- the adhesion strength of the liquid and the solid body (Dupré equation)

$$W_{SL} = \gamma_{SV} + \gamma_{LV} - \gamma_{SL} \tag{2.9}$$

where γ_{SV} is the surface tension at the interface of the solid and gaseous phases (Fig. 2.6 inclusion and purge gas), γ_{LV} is the surface tension at the interface of the liquid and gaseous phases (Fig. 2.6 melt and purge gas), γ_{SL} is the interfacial tension between the solid and one of the fluid phases (Fig. 2.6 inclusion and melt), θ the wetting angle of the solid substance wettability by the liquid, r the capillary radius, D the capillary slot width, η the dynamic viscosity of the liquid, g the acceleration of gravity, and τ the time.

Generally, wetting is governed by interfacial tensions as drawn in Figure 2.6. If it is assumed that the interfacial tensions can be taken as forces even for the solid-fluid interfaces, a force balance along the solid surface gives Young's equation [17], [54]:

$$\cos\theta = \frac{\gamma_{SV} - \gamma_{SL}}{\gamma_{LV}} \tag{2.10}$$

which is valid for a flat, undeformable, perfectly smooth and chemically homogeneous solid surface in contact with a non-reactive liquid in the presence of a vapour phase. Both the solid and the liquid surfaces are assumed free of any adsorbed species. If the liquid does not completely cover the solid, the liquid surface will intersect the solid surface at a "contact angle" θ. The equilibrium value of θ, used to define the wetting behaviour of the liquid, obeys this classical equation of Young [59] and [58].

Considering wetting two extreme cases may be distingiushed by the following expressions 2.11 and 2.12. When no value of θ can be found to satisfy Equation 2.10, and the liquid covers the whole area of the solid: the liquid is said to wet the solid perfectly;

$$\gamma_{SG} > \gamma_{SL} + \gamma_{LG} \tag{2.11}$$

or, alternativly,

$$\gamma_{SL} > \gamma_{SG} + \gamma_{LG} \tag{2.12}$$

in which case the liquid/solid surface is displaced completely by the gas/solid surface [53].

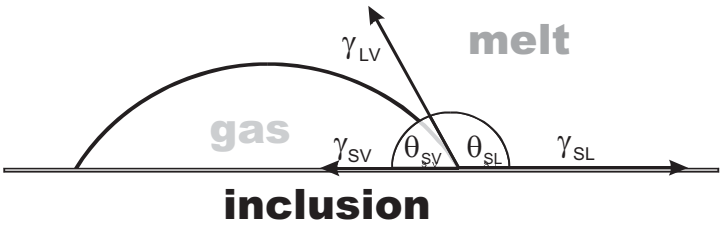

Fig. 2.6: Inclusion satisfying the wetting condition for removal by flotation (θ_{SL} melt – inclusion > 90°)

Real solid surfaces never satisfy completely the conditions for the Young equation to be valid, namely chemical homogenity and perfect smoothness. This may explain the considerable spread of experimental contact angle values, θ, reported for a given liquid/solid system [58].

Combining Equations 2.9 and 2.10, the following fundamental equation of wetting, known as the Young-Dupré equation [60], is obtained:

$$\cos\theta_{SL} = \frac{W_{SL}}{\gamma_{LV}} - 1 \tag{2.13}$$

The work of adhesion is equal to the decrease of free energy associated with the capillary process [53]. For example, liquid inclusions must physically wet the filter in order to lower their interfacial energy in the melt (increase the work of adhesion to the filter) [12].

Alternatively to Young's equation (2.10) the interfacial tension may be expressed as in Equation 2.14 [61]:

$$\gamma_{SL} = \gamma_S + \gamma_L - \phi(\gamma_S \gamma_L)^{0.5} \tag{2.14}$$

where γ_{SL} is the interfacial tension between a solid and a liquid phase (e.g., oxide and melt), γ_S and γ_L the surface tension of oxide and melt, respectively, and ϕ is the interaction coefficient which is given by the ratio ($W_a^{sl}/W_c^s\ W_c^l$) where W_a and W_c are the work of adhesion and cohesion, respectively.

According to Naidich [62] wetting phenomena should be discussed in terms of equilibrium systems and non-equilibrium systems. If the chemical potentials of all components are equal in both phases $\left(\mu_i^S = \mu_i^L\right)$ the system is in equilibrium. Equations 2.9 and 2.10 are valid for thermodynamic equilibrium. The interfacial energy σ_{sl} in equilibrium systems depends on nature and structure of the contacting phases and decreases as their properties become increasingly similar. Instantaneous adsorption is assumed and any non-equilibrium of the system is due to the kinetics of a simple adsorption process and is ignored. Factors determining the variation of tension under equilibrium conditions are adsorption and temperature change. For non-equilibrium systems one usually considers the case where the system is in thermal and mechanical equilibrium but not in chemical equilibrium. However, due to the tendency to attain chemical equilibrium the interfacial energy σ_{SL}, θ and W_a will change with time and depend on irriversible processes of chemical interaction at the interface, which are characteristic features of non-equilibrium systems. The action of these processes can

result in a substantial interfacial tension change. This may be expressed in terms of the Dupre equation [11]:

$$\gamma_{SL} = \gamma_{SV} + \gamma_{LV} - W_{SL} \tag{2.15}$$

From Equation 2.15 follows directly that a change in binding energy of the liquid and the solid, W_{SL}, results in a change of the interfacial tension σ_{SL}.

Eustathopoulos and co-workers [58] apply the term "reactive wetting" in the context of a system which is not in chemical equilibrium. They distinguish between the case of simple dissolution of the liquid in the solid and the case of formation at the interface of a 3D compound by reaction between the solid and the liquid. For dissolution two extreme cases may be considered. In the first one, dissolution of the solid into the liquid is assumed not to change significantly the surface and interfacial energies σ_{LV} and σ_{SL}. Therefore, dissolution modifies only the geometry at the triple line (Figure 2.7a). In the second case, the interfacial energies are modified due to dissolution of small quantities of tensio-active species of the solid, but the solid/liquid interface is assumed to remain nearly flat, i.e. the equilibrium contact angle is still given by the Young equation (Figure 2.7b). In case of formation of a 3D compound it has been observed that the reaction product may be either more wettable or less wettable than the solid subtrate.

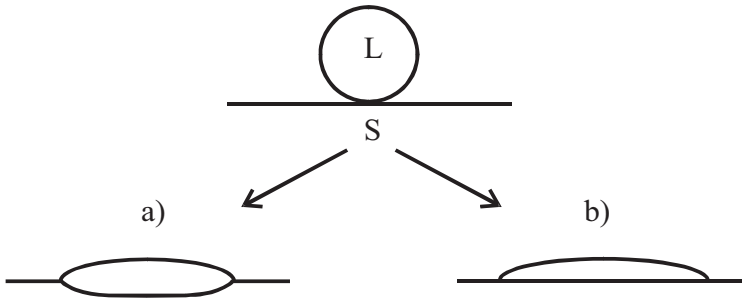

Fig. 2.7: Two extreme cases of dissolutive wetting. (a) Dissolution of the solid modifies the geometry at the triple line. (b) A slight dissolution is enough to modify the surface energies of the system while the S/L interface remains macroscopically planar. [58]

During the last few decades, the change in Gibbs energy, $\Delta G(t)$, of the system has been considered the driving force for reactive wetting. This was first proposed by Aksay et al. [63], both for dissolution reactions and for reactions with formation of a new phase at the interface. Accordingly, it has been concluded that the higher the reactivity in a system, the better the wettability. However, by varying the $\Delta G(t)$ term but keeping the surface energy term constant, Espie et al. [64] and Landry et al. [65] could show experimentally that wetting in reactive systems is governed by the final interfacial chemistry at the triple line rather than by the intensity of interfacial reactions. The model of Aksay et al. predicts that the $\theta(t)$ curve passes through a minimum before reaching the equilibrium contact angle. However, as a general rule, existing data for $\theta(t)$ in reactive couples show that θ decreases monotonically with time to a steady value.

The removal of non-metallic and intermetallic particulate suspensions is influenced by the wetting conditions between inclusion, melt and flux or filter [66]. The poor wetting of non-metallic inclusions by the Al melt ($\theta > 90°$) is a prerequisite for their removal from the melt by a third phase (gas bubbles, filter). In addition, such conditions favour the agglomeration of suspended particles. With a high degree of wettability (strong adhesion of the melt to the inclusions) adherence of suspended particles to the bubbles or the filter would be stopped or at least hampered [11]. Inclusion capture occurs when the de-wetted particles hit the filter material thereby being ejected by the melt due to the liquid metal's high surface tension and repulsive force, respectively. But there is little sign of adherence of the inclusions to the filter medium. To maintain the contact with the filter the forces of adhesion holding the particle in place must exceed the drag forces excerted on the captured particle by the flowing melt. One has to bear in mind that particle size, particle shape, and contact area affect adhesion. For example the contact area may be 1/10000 of the apparent area [17]. For this reason "active filtration" methods aim to increase wettability and forces of adhesion ensuring better and permanent particle capture in this range.

The drag force [67], F_D, is given in Equation 2.16,

$$F_D = C_D\left(\rho\upsilon^2/2\right)S_i \tag{2.16}$$

where C_D is the drag coefficient, S_i the projected surface area of an inclusion [m^2], υ the molten aluminum flow velocity [m/s] and ρ the molten aluminum density [kg/m^3]. The force, F_{SL}, necessary to separate the liquid from the solid body was given approximately by Ibe [68] and is given in Equation 2.17,

$$F_{SL} \approx 2 \cdot \frac{W_{SL}}{a} \Delta A \tag{2.17}$$

where a is the average distance between atoms for the two materials and ΔA is the contact area. From Equations 2.9 and 2.17 it is apparent that the force necessary to separate the solid and the liquid will increase when the solid – liquid interfacial tension , γ_{sl}, is reduced. Frisvold [17] calculated the force that holds a particle in place at the filter wall due to the surface tension of the melt. The force of adhesion for a particle of 10 μm is larger by a factor 10^4 compared to the drag force acting upon the particle. Industrial particle releases may be explained then by the considerable transit time of a particle through the melt boundary layer established in the viscous flow regime in such filters. Before adherence the particle is only loosely captured and may be re-entrained by virtue of changing flow conditions.

Wetting is closely related to the nature of the melt oxides. The wetting behaviour may be assesed in sessile drop experiments under carefully controlled conditions. The protective nature of the melt oxide that is present on the molten aluminium droplet has a large effect on the magnitude of the contact angle that is measured in these experiments [58], [69], [70]. As temperature is increased, the intervening oxide film is eventually penetrated and the molten aluminium wets the substrate with a contact angle less than 90°. The wetting transition temperature is strongly dependent on the details of the experiment (thickness of oxide film, temperature, local oxygen partial pressure) [71]. Unfortunately, many of the alloying elements of commercial aluminium alloys (Ca, Li, Mg, Zn) are volatile. They interact with the oxide layer breakdown in a poorly understood fashion making it difficult to isolate oxide film behaviour from the effect of alloying on wettability. The few wetting results that have been published for

multicomponent aluminium alloys have been conducted under ultra-high vacuum [72] - [74].

The laboratory measurement of the surface tension of liquid aluminium alloys is subject to some of the same shortcomings. Nakae [75] reviewed what is known about the surface tension of aluminium and binary alloys. One factor which distinguishes surface and interfacial properties from bulk properties (e.g., viscosity) is that small concentrations of surface active components (e.g. S, O in metals, CaF_2 in slags) can cause a dramatic change in both the surface (or interfacial) tension and its temperature dependency ($d\gamma / dT$)(). Surface activity in metals can be ranked in the hierarchy [61]:

1. Group VI elements > Group V > Group IV
2. Within any group the heavier elements are more surface active than lighter elements e.g. Te > Se > S ≈ O.

Na, Bi, Ba, Li, and Pb are known to be surface active. Dewing and Desclaux [76], Utigard and Toguri [77], proposed that surface active elements like sodium are adsorbed, and hence, concentrated on the molten aluminum surface. To calculate the excess surface concentration of these elements, Gibbs' adsorption equation [55] is often used

$$RT\Gamma^{xs} = -d\gamma / d\ln a_{solute} \qquad (2.18)$$

where γ is the surface tension of the liquid mixture, Γ^{xs} is the excess surface coverage and a_{solute} the activity of the surface active element, respectively. Only a very small amount of surface active atoms is needed to form a monolayer to cover the aluminum surface and to reduce the interfacial tension. The activity of such a metal (Me) is governed by the following reaction:

$$Al + 3/n\ MeX_n = 3/n\ Me + AlX_3 \qquad (2.19)$$

where X is a fluoride or chloride anion and n is an integer. The surface tension of liquid mixtures is generally not expected to be an additive quantity as given by the relation 2.20

$$\gamma = \chi_A\gamma_A + \chi_B\gamma_B \qquad (2.20)$$

where χ_A and χ_B are the mol fractions and γ_A and γ_B are the surface tension of the pure components, respectively. The commonly observed negative deviation from

relation 2.20 is explained by the surface enrichement of the component of lower surface tension. In this respect, Utigard and Toguri argue that the surface tension of liquids is a measure of the excess surface chemical potential of the surface atoms relative to the bulk atoms. [55]

It has also been shown that there is a large difference in the surface tension of an oxygen free surface and one that is oxygen saturated [78]-[81]. Consequently, those alloying elements that have a high affinity for oxygen (Be, Ca, La, Li, Mg, Zr) are surface active through their interaction with oxygen [71]. It should also be noted that it is the soluble O and not the combined O (e.g., oxides) which affects surface tension [61]. Mills and Keene [82] pointed out that certain elements such as Ca, Al and Mg react strongly with O and reduce the soluble O (denoted $\underline{O}$) to very low levels (e.g., a few ppm) and form stable metallic oxides. The total O is not a measure of the soluble O in such cases. Thus very low concentrations of these reactive elements (e.g., Ca) can have a marked effect on the process because of their effect on the surface active elements present. Data on the surface tension of commercial aluminium alloys is scarce [81].

Despite these shortcomings, carefully evaluated, labscale wetting or surface tension experiments can yield valuable information of chemical compatibility and the capillary tendencies of molten aluminium alloys with solids of interest [12].

The wetting of different ceramics by aluminium is summarized in Table 2.2 taken from the literature [58], [70]. Large obtuse contact angles are generally observed on all of the materials at low temperature. The value of 90° shown for aluminium oxide is the intrinsic angle (free of oxide film effects) that has been obtained by the experiments of many researchers [70]. The contact angles observed at high temperature reflect the influence of the ceramic substrate. The final equilibrium contact angle tends towards the value observed for the ceramic phase that is in chemical equilibrium with aluminium (Al_2O_3, AlN, Al_4C_3). The morphology of the reaction product exerts an influence on the final stable contact angle that is observed on those ceramics that react with aluminium [12].

Table 2.2: The wetting of ceramic materials by molten aluminium, after Li [70].

Material	Contact angle (°) at 700°C	Contact angle (°) at 1100°C	Reference
Al_2O_3	90	80	Li [65]
SiO_2	150	50	Li [65]
ZrO_2	150	87	Li [65]
AlN	160	50, 45	Li [65], Sobczak et al. [78]
BN	140	0 - 60	Eustathopoulos et al. [53]
Si_3N_4	160	60	Li [65]
Al_4C_3	-	54	Eustathopoulos et al. [53]
SiC	160	51, 43	Asthana & Tewari [79], Li [65]
TiB_2	140 - 160	0	Eustathopoulos et al. [53], Weirauch et al. [80]

The molten aluminium does not readily wet the filter material but rather flows in its own oxide skin. The presence of an oxide layer is likely because of the low partial pressure of oxygen required to form the oxide [86], [87]. This oxide skin may keep breaking up mechanically due to the tortuous flow and the surface roughness and/or by the chemical heterogenity on the surface of the flux/filter material changing contact angles all the time. For this reason we also speak of a dynamic nature of wetting [88]. A similar case concerns the (unwanted) wetting of refractories by aluminium alloys. The presence of an oxide film protects the refractories from the aggressive attack of molten aluminium. The degree of protection depends to a large extent upon the alloy and the nature of its oxide film [12]. A.M. Levin [89], who had studied the stability of refractories in liquid steel, formulated conditions for vigorous wetting of the solid phase by the liquid metal. He considered that it is necessary for the liquid and solid phases to be as far as possible from equilibrium contact conditions.

In metallic systems, wetting is easily achieved because of mutual solubilities or the formation of intermetallic compounds. On the other hand, wetting in metal-nonmetal systems is often poor for the basic reason that oxides are ionic or covalent in nature, and therefore, are not compatible with metallic species [90].

Several recent reviews [91], [92] give methods to enhance the wettability and work of adhesion in metal-nonmetal systems. Basically, wettability and work of adhesion between liquid aluminium and a flux or filter material may be increased both by increasing the overall surface energy of the latter, and using wetting agents such as alloying elements that can promote the wettability of the liquid aluminium with the flux or filter material by four mechanisms: 1) reducing the surface tension of the liquid

metal, 2) increasing the surface energy of the solid 3) decreasing the liquid metal – flux/filter interfacial energy, and 4) chemical reactions at the liquid metal – flux/filter interface. NaF, KF, LiF, CaF_2, BaF_2, Na_3AlF_6 and KNO_3 in the flux or filter material decrease the interfacial tension [34]. The same effect can be observed for increasing temperatures of the system. Mass transport taking place on the metal surface may as well change the interfacial tension [93]. A dramatic decrease in the interfacial tension has been reported [94], [95] for high mass transfer rates between metal and slag. Numerous alloying additions have positive effects on the wettability by reacting with a reactive flux/filter material such as AlF_3 (Na, K, Mg, Ca, Li), by modifying the characteristics of the oxide layer (Mg, Li) and by lowering the surface tension of aluminium (Li, Mg, Ca). The effect of the flux/filter – melt composition on the interfacial properties is the direct result of interaction between metal cations and halide anions at the flux/filter – melt interface. This also includes the formation of the surface active subfluorides by molten aluminium being in contact with AlF_3.

According to Kozakievitch and Olette [96] the change in the interfacial energies at constant temperature and pressure can be related to a change in the Gibbs free energy, ΔG, of the system. For a thin oxide layer of area S stripped away from the metal surface as illustrated in Figure 2.8,

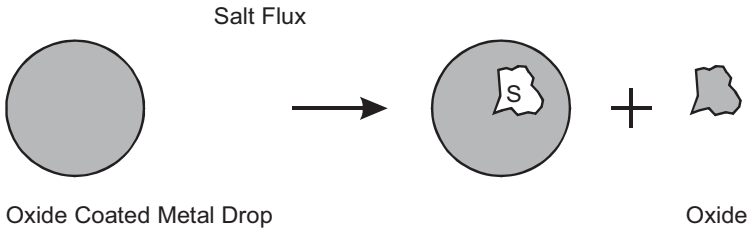

Fig. 2.8: Schematic of oxide film removal [93]

leaving an area of metal S in direct contact with the flux/filter, the change in the Gibbs free energy, $\Delta G_{Stripping}$, may be expressed as in Equation 2.21:

$$\Delta G_{Stripping} = S\left(\gamma_{metal/flux} + \gamma_{oxide/flux} - \gamma_{metal/oxide}\right) \tag{2.21}$$

Here $\gamma_{metal/flux}$, $\gamma_{oxide/flux}$, and $\gamma_{metal/oxide}$ stand for interfacial tension between molten metal and flux, interfacial tension between oxide and flux, and interfacial tension

between molten metal and oxide, respectively [93]. Equation 2.22 then gives Sully's wetting criterion which can be attained by applying Young's relation (Eq. 2.10 in terms of $\gamma_{metal/oxide} = \gamma_{oxide/flux} - \cos\theta_{metal/oxide} \cdot \gamma_{metal/flux}$) into Equation 2.21.

$$\Delta G_{Stripping} = S \cdot \gamma_{metal/flux}\left(1 + \cos\theta_{metal/oxide}\right) \tag{2.22}$$

θ in Equation 2.21 is the contact angle between metal and oxide when in contact with the flux/filter. A simple illustration of this which also satisfies Equation 2.23 and 2.24 is given in Figure 2.9. Larger contact angle, lower interfacial tension between metal and flux, and smaller area of oxide film being removed will promote oxide film removal [93]. However, it is seen that $\Delta G_{Stripping}$ in Equation 2.22 is positive for all values of $\theta_{metal/oxide}$ except for $\theta_{metal/oxide}=180°$.

In the process of interaction between flux, oxides and molten alloys, oxides are absorbed by the flux due to the absorption capability of the salt system. Because of the high chemical stability of aluminum oxides, there is no chemical interaction between flux and oxides. The physical interaction is determined by the interfacial tension, γ, at the boundaries between metal – flux ($\gamma_{metal/flux}$), metal – oxide ($\gamma_{metal/oxide}$), and oxide – flux ($\gamma_{oxide/flux}$). Any physical movement – stirring, plunging, gas purging, filtering – of the melt increases the kinetic energy of the oxide particles which may help them pass through the boundary layer. For removal of oxide film from the metal surface into the flux Sully et al. [66] suggested that the following interfacial tension criteria given by Equation 2.23 and 2.24 must be satisfied.

$$\gamma_{oxide/flux} < \gamma_{metal/flux} < \gamma_{metal/oxide} \tag{2.23}$$

$$\gamma_{oxide/flux} + \gamma_{metal/flux} < \gamma_{metal/oxide} \tag{2.24}$$

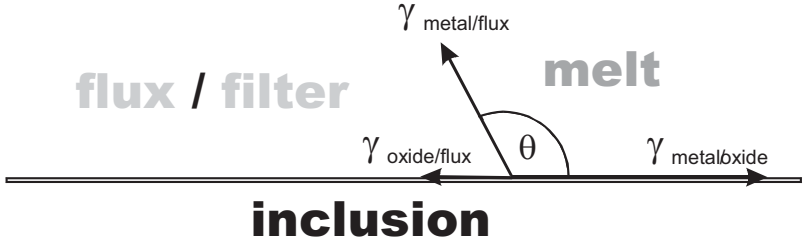

Fig. 2.9: Wetting conditions that favour oxide removal from the melt into the flux

Flux/filter should wet oxide better than it wets the aluminum alloy. For the flux/filter design, it is important to understand that the thermodynamic conditions of oxide removal also improve if the interfacial tension at the boundary metal – flux/filter is reduced (wetting angle $\theta < 90°$). This enables the melt also to enter and flow through very fine pores, thus depositing small inclusions [21]. However, filter materials which are non-wetting with respect to the metal have til now been found most efficient [99]. These findings are shared in [100] and [101] where solid inclusion separation is considered to require that both the inclusion and filter are non-wetted by the molten metal so the metal can withdraw from the filter leaving the inclusion behind.

Oosumi et al. [102] suggested to consider compounds (e.g. Na_3AlF_6+AlF_3, Na_3AlF_6+NaCl, $Na_2B_4O_7$, NaBr, Bi_2O_3) having melting points similar to the molten metal temperature when selecting an adhesive. Questions regarding the selection of flux materials for active filters are expatiated in the work of Kljagina and Spasskij [103] also. For the flux to remain in the solid state during filtration, the flux melting temperature is recommended to be at least 20 – 30°C higher than the temperature of the melt. According to their investigations, the following fluxes exhibit best wetting properties with respect to oxide inclusions: (1) eutectic mixture of 52.7 % CaF_2 and 47.3 % NaF (T_m = 810°C); (2) eutectic mixture of 51 % MgF_2 and 49 % NaF (T_m = 820°C); (3) borax (T_m = 741°C). Similar wetting conditions can be obtained by mixtures of (1) 66 % NaCl and 34 % NaF (T_m = 750°C), and (2) 60 % Na_3AlF_6 and 40 NaF (T_m = 890°C). With their relatively low surface tension, fluxes containing fluorides wet the high energy surfaces of both the molten aluminium and solid aluminium oxide film. In this way, a film of flux moves in between the metal and the oxide and separates the two. Grafas and Beljajew [104] confirmed the decrease in the metal/flux interfacial tension, $\gamma_{metal/flux}$, by fluorine additions to molten chloride fluxes (NaCL-KCl), but at the same time found $\gamma_{oxide/flux}$ to increase strongly with those additions. Therefore, they conclude that the way these molten fluorine containing chloride fluxes act, can not be explained by surface effects. Data on salt-metal interfacial energies between molten Al and a NaCl-KCl flux containing NaF, KF, LiF or Na_3AlF_6 can be found in [105].

The separation of the oxide from the metal involves both chemical dissolution and interfacial factors [106]. Marangoni interfacial motion due to non-uniform adsorption of sodium and potassium has been cited as a stripping force that separates the oxide layers from liquid aluminium [107]. Marangoni flow always occurs from a region of low surface tension to a region of high surface tension. Surface tension gradients can arise from (i) temperature differences along the interface which cause thermo-capillary flow; (ii) composition differences along the interface which cause diffuso-capillary flow; (iii) electrical potential differences along the interface which cause electro-capillary flow [61]. In fluxes with low aluminium oxide solubility, electrochemical attack of the interface may lead to film detachment [107]. Fluxes containing such fluorides as cryolite, sodium fluoride, or fluorspar do not dissolve appreciable aluminium oxide at normal foundry temperatures. Consequently, the solubility of alumina in fluorides is not a major factor in the fluxing process. The detached oxides are suspended in the molten flux and produce a gradual thickening. Even a thick flux is capable of stripping oxide. Lithium chloride can be added to increase the life of these cleaning fluxes, since this ingredient prevents flux thickening by dissolving suspended oxides into the flux [108]. On the other hand, experimental results regarding coalescence of aluminum droplets obtained by Peterson [28] and solubility data for aluminum oxide are in accordance, hence, suggesting the solubility of alumina being the determining factor.

To be effective, the flux must come into contact with the suspended oxides. A tortuous passage in addition to a large collision area favours the contact. One method of accomplishing this is by pouring molten aluminium into a salt melt or to stir or plunge a molten flux below the surface of the molten aluminium [108]. When molten aluminum droplets pass through a molten flux layer without stirring, the inclusions on the surface of the droplets can be removed. However, the inclusions inside the larger aluminum droplets may not come into contact with the molten flux. In this case as well as in the context of filtration, the probability of inclusions being at the melt/flux interface is higher for smaller droplets than for bigger droplets, and for smaller filter pores (voids) respectively. This is due to the shorter distance a randomly distributed inclusion has to cover for small cross sections to reach the interface [9]. Pouring the melt through a bed of lumps of salt flux or either inert filter grains or rigid filter media with coatings based

on salt fluxes disperses the melt into fine molten streams. Thus, the contact area increases which in turn increases the probability of contact. This is an advantage compared to the liquid flux applications. The salt fluxes form an adhesive layer on the filter surface. Compared to inert filter media the filtration efficiency is much higher, and therefore many more and also smaller inclusions are removed. BACO (British Aluminium Corporation) filtered molten aluminium with a packed bed of aluminium oxide spheres coated with flux, but the flux was run off easily. Therefore, research is being carried out on coatings applied to ceramic filters that are viscous at molten metal temperatures to help capture the non-metallic inclusions and which can resist corrosion of molten aluminium. Haim et al. [109] emphasize the fairly good wetting and adhesion of glass melts in contact with oxidized metal surfaces. Results indicate that enamels with high B_2O_3-P_2O_5-$AlPO_4$ content are resistant to the corrosion of molten aluminium [110].

2.4 Resume

Today, “passive” filter materials exist in industrial filtration technology like packed bed, rigid media and ceramic foam filters. The idea of “active filtration” is a consequence of limitations in filtration technology. Down to a particle size of about 30μm the capture mechanism is more or less mechanical, whereas surface forces are believed to play a decisive role in holding back the smaller particles. The surface forces are often not strong enough and the release of already captured particles can not be excluded. Therefore, filtration efficiencies are difficult to controll in the range of 1 - 30μm. To maintain the contact with the filter the forces of adhesion holding the particle in place must exceed the drag forces excerted on the captured particle by the flowing melt.

For this reason “active filtration” methods aim to increase wettability and forces of adhesion, ensuring better and permanent particle capture in this range. How to determine the different forces was discussed in chapter 2.3. This may help to select suitable materials. Adhesive coatings based on NaBr or glassy enamels are currently investigated to enhance surface forces.

A different way to look at “active” filtration is to employ chloride or fluoride salts or fused mixtures in a packed bed for fluxing out dissolved impurities and also suspended particles. The dissolved impurities chemically react at the filter surface and may be deposited instantly upon reaction or at sites downstream in the same filter. The wetting conditions may support the separation of the suspended particles out of the melt onto the filter surface with more success than in a “passive” filter.

From time to time such filter materials, originally for the removal of suspended particles, have been in operation. Even though the contact area in such a filter is much larger compared to other fluxing technologies, the operational flexibility is not sufficient for many applications. This may explain the advent of the rotary injection of powdery or granular refining agents. As with every salt fluxing practice the occurrence of liquid salts poses an other problem. In the future this problem might be solved by porous salt filter media presently developed by SELEE.

Bibliography

[1] D. D. Smith, L. S. Aubrey: *"Technical update on dual state ceramic foam filtration technology"*. ARABAL 99: Ninth International Arab Aluminium Conference and Exhibition, Kuweit, 27.-29. Nov. 1999.

[2] D.J. Fray: *"Aspects of Technology Transfer"*. Metallurgical and Materials Transactions B, Volume 31B, December 2000, pp. 1153 – 1162

[3] Yoshikazu Ohno: *"The latest Molten Metal Refining Processes in Cast Shop"*. Journal of Japan Institute of Light Metals, No.51, 2001, pp. 134-37, off print (Translated from Japanese)

[4] D. V. Neff: *"The Use of Gas Injection Pumps in Secondary Aluminum Metal Refining"*. Proceedings, AIME, Recycle and Secondary Recovery of Metal, 1985, p. 73

[5] Ya. I. Morozov, M. B. Gokhshtein: *"Mechanism of Degassing Aluminum Melts during Filtration through a Lump Active Filter"*. Tsvetnye Metally / Non-Ferrous Metals, UDC 669.715:046.54/55, pp. 64 – 65

[6] C. S. Sivaramakrishnan, R. K. Mahanty, R. Kumar: *"Special Ceramic Filter for Aluminium Alloys"*. Transactions of the Indian Ceramic Society, Volume 40 (4), July-August 1981, pp. 146 – 151

[7] J.-D. Bornand, K. Buxmann: *"DUFI: A Concept of Metal Filtration"*. Light Metals, 1986, pp. 1249 – 1260

[8] K. R. Butcher, D. D. Smith, L. Aubrey: *"Performance Evaluation of a Filtration Unit Developed to Remove Liquid Salts from Molten Aluminum"*. Selee technical papers (TEK99-11), Selee Corporation, 700 Shepherd Street, Hendersonville, NC 28792

[9] M. Zhou, D. Shu, K. Li, W. Y. Zhang, H. J. Ni, B. D. Sun, J. Wang : *"Deep Filtration of Molten Aluminum using Ceramic Foam Filters and Ceramic Particles with Active Coatings"*. Metallurgical and Materials Transactions A, Volume 34A, May 2003, pp. 1183 – 1191

[10] P. Achim, G. Dubé: *„Removal of Lithium in Commercial Metal"*. Light Metals 1982, 1982, pp. 903 – 918

[11] Ju.V. Naidich: *„The Wettability of Solids by Liquid Metals"*. Progress in Surface and Membrane Science, Vol. 14, Edited by D.A. Cadenhead and J.F. Danielli, Academic Press, 1981, pp. 354 – 375

[12] D.A. Weirauch Jr.: *„Technologically significant capillary phenomena in high-temperature materials processing. Examples drawn from the aluminum industry."* Current Opinion in Solid State & Materials Science. 2006

[13] E. Fitzer, W. Fritz, G. Emig: *"Einführung in die Chemische Reaktionstechnik"*. Vierte Auflage, Springer Verlag, 1995

[14] M. Baerns, H. Hofmann, A. Renken: *"Chemische Reaktionstechnik"*. Dritte Auflage, Georg Thieme Verlag, Stuttgart, 1999

[15] O. Levenspiel: *"Chemical Reaction Engineering"*. 3rd edition, Wiley & Sons, 1999

[16] T. Abel Engh: *"Principles of Metal Refining"*. Oxford University Press, 1992, pp. 2 – 3, 15, 77, 132, 345 – 347

[17] F. Frisvold: *"Filtration of Aluminium – Theory, Mechanisms, and Experiments"*. PhD Thesis, Norwegian University of Science and Technology, Trondheim, Norway, 1990

[18] M. Syvertsen: *"Removal of Hydrogen and Inclusions from Aluminum"*. Dr. ing. Thesis, Institut for Materialteknologi og Elektrokjemi, NTNU Trondheim, 2000, pp. xix – xx, 1 – 2

[19] T. A. Utigard: *"Thermodynamic considerations of aluminum refining and Fluxing"*. Proceedings of the International Symposium on Extraction, Refining and Fabrication of Light Metals (Ottawa, Canada: CIM, 1991), pp. 353 – 365

[20] T. A. Utigard, K. Friesen, R. R. Roy, J. Lim, A. Silny, and C. Dupuis: *"The Properties and Uses of Fluxes in Molten Aluminum Processing",* Journal of Metals, November 1998, pp. 38 – 43

[21] K. Krone: *"Aluminiumrecycling"*. Vereinigung Deutscher Schmelzhütten e.V., Düsseldorf, 2000, pp. 145, 263, 372

[22] P.D. Hess: *"Magnesium Removal from Aluminum Alloy Scrap".* U.S. Patent 3,620,716, Nov. 16, 1971

[23] J. Pinkas, H.W. Roesky: *„Review – Organoaluminum fluorides".* Journal of Flourine Chemistry, Vol.122, 2003, pp. 125 – 150

[24] O. Levenspiel: *"The Chemical Reactor Omnibook"*. 5th Ed., OSU Book Stores, Inc., Corvallis, Oregon 97339, July 1996

[25] D. V. Neff: *"Environmentally Acceptable Chlorination Processes"*. 4th Australian Asian Pacific Course and Conference, Aluminium Cast House Technology: Theory & Practice, Edited by M. Nilmani, The Minerals, Metals & Materials Society, 1995, pp. 211 – 225

[26] O. Hjelle, T.A. Engh, B. Rasch: *"Removal of Sodium from Aluminium-Magnesium Alloys by Purging with Argon and Cl_2"*. International Seminar on Refining and Alloying of Liquid Aluminium and Ferro-Alloys, August 26-28, 1985, Trondheim, Norway

[27] D. V. Neff, B. P. Cochran: *"Chlorination Technology in Aluminum Recycling"*. Light Metals, Light Metals (Warrendale, PA, United States) (1993), pp. 1053-1060

[28] R.D. Peterson: *"Effect of Salt Flux Additives on Aluminum Droplet Coalescence"*. Second International Symposium – Recycling of Metals and Engineered Materials, The Minerals, Metals & Materials Society, 1990, pp. 69 – 84

[29] R. I. L. Guthrie, M. Nilmani*: „Impurity Sources and Control – General Principles of Melt Treatment"*. Aluminum Melt Treatment & Casting, Edited by M. Nilmani, The Minerals, Metals & Materials Society, 1993

[30] L.D. Bylund: *"Treatment of Aluminum with Aluminum Fluoride Particles"*. 1967, U.S. Patent 3,305,351

[31] M.L. Saboungi, P.L. Lin, P. Cerisier, A.D. Pelton: *"Computer analysis of phase diagrams and thermodynamic properties of cryolite based systems: I. The AlF_3-LiF-NaF system"*. Metallurgical Transactions B, 11B, 1980, pp. 493 – 501

[32] G. Dubé, V. J. Newbury: *"TAC, a Novel Process for the Removal of Lithium"*. Light Metals 1983, p. 991

[33] P.N. Crepeau, M.L. Fenyes, J.L. Jeanneret: *"Solid Fluxing Practices for Aluminum Melting"*. Modern Casting, July 1992, pp. 28 – 30

[34] A. Silny, T.A. Utigard: *"Interfacial Tension between Aluminium, Aluminum Based Alloys and Chloride – Fluoride Melts"*. Light Metals 1997, pp. 871 – 878

[35] Celik and D. Doutre: *"Theoretical and Experimental Investigation of Furnace Chlorine Fluxing"*. Light Metals 1989, pp. 793 – 800

[36] B. Kulunk, R. I. L. Guthrie: *„On the Removal Kinetics of Calcium from Aluminium and Aluminium-Magnesium Alloys"*. Light Metals 1991, TMS, 1990, pp. 1057 – 1061

[37] G. Beland, C. Depuis, C. Leroy : *„Improving Fluxing of Aluminium Alloys“*. Light Metals, 1995, pp.1189 – 1195

[38] R. I. L. Guthrie, M. Nilmani: *„Impurity Sources and Control – General Principles of Melt Treatment“*. Aluminum Melt Treatment & Casting, Edited by M. Nilmani, The Minerals, Metals & Materials Society, 1993

[39] G. K. Sigworth, T. A. Engh: *”Refining of Liquid Aluminium – a Review of Important Chemical Factors”*. Scand. J. of Metallurgy, 11, 1982, pp. 143 – 149

[40] S. G. Hansen: *“Thermodynamics of Impurity elements Na, K, Li, Ca in Liquid Aluminum Alloys”*. PhD Thesis, NTNU, Trondheim, Norway, 2001, p. IV

[41] A. N. Waernes, S. G. Hansen, J. Kr Tuset, B. Rasch: *”Thermodynamic Computer Programs as an Aid in Refining of Aluminium”*. Light Metals 1999, 1999, pp. 861 – 876

[42] A.Ya. Radin: *“About the Applying Mechanisms when Fluxing during Melting of Aluminium”*. Trudy MATI, No. 56, 1963, pp. 45 – 70 (Russian)

[43] W. Klemm, E. Voss: *„Ein niederes Aluminiumfluorid“*. Zeitschrift für anorganische und allgemeine Chemie, Volume 251, 1943, pp. 233 – 240

[44] Yu.P. Pimenov, Tekhnologiya Legkikh Splavov (Byul. VILS), No. 2, 1969, pp. 66 – 68

[45] H. Kvande: *“Thermodynamics of the System NaF-AlF_3-Al_2O_3-Al studied by Vapour Pressure Measurements”*. PhD Thesis, Norwegian University of Science and Technology, Trondheim, Norway, 1979

[46] E.H. Howard: *“Some physical and chemical properties of a new sodium aluminum fluoride“*. Journal of the American Chemical Society, Vol. 76, 1954, p. 2041 – 2042

[47] R.A. Huggins: *“Solid Electrolyte Battery Materials”*. Technical Report No 1, ONR Contract N0014-67-A-0012-0075, Centre for Materials Research, Stanford, CA, 1973

[48] B.E. Liebert, W. Weppner, R.A. Huggins: Proc. Symp. on *„Electrode Materials and Processes for Energy Conversion and Storage”*. J.D.E. McIntyre et al., ed., The Electrochemical Society, Princeton, NJ, 1977, pp. 821 – 829

[49] K. Grjotheim, B.J. Welch: *“Aluminium Smelter Technology”*. Aluminium-Verlag, Düsseldorf, 1980

[50] R.W. Hardeman, D.J. Fray: *"Intercalation of lithium from aluminum-lithium alloys into lithium titanates"*. Materials Science and Technology (1988), 4(8), pp. 745 – 50

[51] W.D. Riley, B.W. Jong: *"Chloride-free processing of aluminum scrap to recover byproduct materials"*. Recycling of Metals and Engineered Materials, International Symposium, 3rd, Point Clear, Ala., Nov. 12-15, 1995 (1995), pp. 47 – 56

[52] A. Davidson, G.M. Kale, D.J. Fray, University of Leeds, Leeds, UK, unpublished work

[53] R. Defay, I. Prigogine, A. Bellemans: *"Surface Tension and Adsorption"*. Translated by D.H. Everett, Longmans, 1966, pp.XIV – XVI, 1, 16 – 19 (English edition)

[54] C.A. Miller, P. Neogi :*"Interfacial Phenomena – Equilibrium and Dynamic Effects"*. Surfactant Science Series, Vol. 17, 1985, pp. 1, 29 – 36, 55

[55] T. Utigard, J.M. Toguri: *"Surface Segregation and Surface Tension of Liquid Mixtures"*. Metallurgical Transactions B, Volume 18B, December 1987, 1987, pp. 695 – 702

[56] J.W. Gibbs: *„The Scientific papers of J. Williard Gibbs"*. Dover Publications, New York, 1961

[57] F.V. Nolfi, C.A. Johnson: *"The surface stress in copper"*. Acta Met., Vol. 20 (6), 1972, pp. 769 – 778

[58] N. Eustathopoulos, M.G. Nicholas, B. Drevet: *"Wettability at High Temperatures"*. Pergamon Materials Series, Edited by R.W. Cahn, 1999, pp. 1 – 3, 7, 22, 75 – 91, 254

[59] T. Young: *"An Essay on the Cohesion of Fluids"*. Philosophical Transactions of the Royal Society of London, Vol. 94, 1805, p. 65

[60] A. Dupré: *"Th*éorie *Mécanique de la Chaleur"*. Chapter IX, Actions moléculaires (suite), published by Gauthier-Villars, Paris, 1869

[61] K. C. Mills, E. D. Hondros, Zushu Li: *"Interfacial Phenomena in High Temperature Processes"*. Proceedings of the IV International Conference/High Temperature Capillarity, Journal of Materials Science, Vol. 40, 2005, pp. 2403 – 2409

[62] Yu.V. Naidich: *"Interfacial Surface Energies and Contact Angles of Wetting of Solids by Liquid in Equilibrium and Non-Equilibrium Systems"*. Russian Journal of Physical Chemistry, Vol. 42, Nr. 8, 1968, pp. 1023 – 1026

[63] I.A. Aksay, C.E. Hoge, J.A. Pask: *"Wetting under Chemical Equilibrium and Nonequilibrium Conditions"*. J. Phys. Chem., **78**, 1974, pp. 1178 – 1183

[64] L. Espie, B. Drevet, N. Eustathopoulos: *"Experimental study of the influence of interfacial energies and reactivity on wetting in metal/oxide systems"*. Metall. Trans. A, Vol. 25, 1994, p. 599 – 605

[65] K. Landry, C. Rado, R. Voitovich, N. Eustathopoulos: *"Mechanisms of a reactive wetting: The question of triple line configuration"*. Acta Mater., Vol. 45, 1997, p. 3079 – 3085

[66] A. H. Sully, H. K. Hardy, T. J. Heal: *"An Investigation of Thickening and Metal entrapment in a Light Alloy Melting Flux"*. Journal, Inst. Met. 82, 1953-54, pp. 49 – 58

[67] K. Uemura, M. Takahashi, S. Koyama, M. Nitta: *"Filtration Mechanism of Non-Metallic Inclusions in Steel by Ceramic Loop Filter"*. ISIJ International, Vol. 32, No. 1, 1992, pp. 150 – 156

[68] G. Ibe: *"Zur Thermodynamik und Kinetik der Phasengrenzflächen"*. Haftung als Basis für Stoffverbunde und Verbundwerkstoffe, edited by W. Brockmann, Deutsche Gesellschaft für Metallkunde, Oberursel, West Germany, 1983, pp. 281 – 301

[69] J.-G. Li, Rare metals, 1991; 10:255..

[70] J.-G. Li: *"Wetting of ceramic materials by liquid silicon, aluminum and metallic melts containing titanium and other reactive elements: a review"*. Ceramics International (1994), 20(6), pp. 391-412

[71] G. Kaptay: *"On surface properties of molten aluminum alloys of oxidized surface"*. Materials Science Forum, 1991, 77 (Solidif. Microgravity), pp. 315 – 330

[72] W. Kohler: *"Wettability of SiC by Pure Aluminium"*. Aluminium, 1975, 51, pp. 443 – 447

[73] Z. Lijun, W. Jimbo, Q. Jiting, N. Qiu, Q. Peixang, In: R. Lin, J. Arsenault, G. P. Martins, S. G. Fisherman: *"Interfaces in metal-ceramic composites"*. Warrendale, PA: TMS; 1990, p. 213

[74] K. Ogi, H. Miyahara, N. Mori, U.S./Japan cooperative science program on solidification processing for the 21st century; 1994

[75] H. Nakae: *"Wettability of liquid aluminum to nonmetallic materials"*. Keikinzoku (1989), 39(2), pp. 136 – 146

[76] E.W. Dewing, P. Desclaux: *"The Interfacial Tension Between Aluminum and Cryolite Melts Saturated with Alumina"*. Ibid., 8B, 1977, pp. 555 – 561

[77] T. Utigard, J.M. Toguri: *"Interfacial Tension of Aluminum in Cryolite Melts"*. Metall. Trans., 16B, 1985, pp. 333 – 338

[78] L. Goumiri, J. C. Joud: *"Auger electron spectroscopy study of aluminum-tin liquid system"*. Acta Metallurgica (1982), 30(7), pp. 1397 – 1405

[79] C. Garcia-Cordovilla, E. Louis, A. Pamies: *"The surface tension of liquid pure aluminum and aluminum-magnesium alloy"*. Journal of Materials Science (1986), 21(8), pp. 2787 - 2792.

[80] C. Garcia-Cordovilla, A. Pamies, E. Louis, In : F. Jeglitsch, editor. Eighth international light metals congress. Düsseldorf: Aluminium-Verlag; 1987, p. 493

[81] D. Emadi, J. E. Gruzleski, J. M. Togouri: *"The effect of Na and Sr modification on surface tension and volumetric shrinkage of A356 alloy and their influence on porosity formation"*. Metall Trans B, 1993, 24B, pp.1055 – 1063

[82] K. C. Mills, B. J. Keene: *"Factors affecting variable weld penetration"*. International Materials Reviews (1990), 35(4), pp. 185 – 216

[83] N. Sobczak, M. Ksiazek, W. Radziwill, L. Stobierski, B. Mikulowski: *"Wetting-bond strength relationship in Al-AlN system"*. Transactions of JWRI (2001), 30(Spec. Issue, High Temperature Capillarity), pp. 125 - 130

[84] R. Asthana, S. N. Tewari: *"Interfacial and capillary phenomena in solidification processing of metal-matrix composites"*. Composites Manufacturing (1993), 4(1), pp. 3 – 25

[85] D. A. Weirauch Jr., W. J. Krafick, G. Ackart, P. D. Ownby: *"The wettability of titanium diboride by molten aluminum drops"*. Journal of Materials Science (2005), 40(9/10), pp. 2301-2306

[86] S.M. Wolf, A.P. Levitt, J. Brown: "*Whisker-metal matrix bonding*". Chemical Engineering Progress (1966), 62(3), pp. 74 – 8

[87] D. Chatain, L. Coudurier, N. Eustathopoulos: *"Wetting and interfacial bonding in ionocovalent oxide-liquid metal systems"*. Revue de Physique Appliquee (1988), 23(6), pp. 1055 - 1064

[88] A. Mortensen, I. Jin: *"Solidification Processing of Metal Matrix Composites"*. International Materials Reviews, Vol. 37, No. 3 , 1992, pp. 101 – 128

[89] A. M. Levin, Sbornik trudov Dnepropetrovskogo metalurgicheskogo instituta, Dnepropetrovsk, vip. 28, 1952, p. 89

[90] C. Toy, W.D. Scott: *"Ceramic-Metal Composite Produced by Melt Infiltration"*. J. Am. Ceram. Soc., **73** (1), 1990, pp. 97 – 101

[91] A. Banerji, P.K. Rohatgi, W. Reif: *"Role of Wettability in the Preparation of Metal-Matrix Composites (a Review)"*. Metall., **38**, 1984, pp. 656 – 661

[92] F. Delannay, L. Froyen, A. Deruyttere: *"Review, the Wetting of Solids by Molten Metals and its Relation to the Preparation of Metal-Matrix Composites"*. J. Mater. Sci., **22**, 1987, pp. 1 – 16

[93] F.K. Ho, Y. Sahai: *"Interfacial Phenomena in Molten Aluminum and Salt Systems"*. Second International Symposium – Recycling of Metals and Engineered Materials, The Minerals, Metals & Materials Society, 1990, pp. 85 – 103

[94] M. Ferrari, L. Liggieri, F . Ravera, C. Amodio, R. Miller: *"Adsorption kinetics of alkylphosphine oxides at water/hexane interface. 1. Pendant drop experiments"*. Journal of Colloid and Interface Science (1997), 186(1), pp. 40 – 45

[95] P . V. Riboud, L. D. Lucas: *"Influence of mass transfer upon surface phenomena in iron and steelmaking"*. Canadian Metallurgical Quarterly (1981), 20(2), pp.199 – 208

[96] P. Kozakievitch, M. Olette: *"Rôle des phénomès superficiels dans le mécanisme d'élimination des inclusions solides"*. Rev. Metallurg., 68, 1971, pp. 635 – 646

[97] A. H. Sully, H. K. Hardy, T. J. Heal: *"An Investigation of Thickening and Metal entrapment in a Light Alloy Melting Flux"*. Journal, Inst. Met. 82, 1953-54, pp. 49 – 58

[98] M. H. Kogan: *"Design and Development of Fluxing Agents for the Aluminum Foundry Alloys"*. Proceedings 2nd International Conference on Molten Aluminum Processing, 1989, pp. 25.1 – 25.12

[99] D. Apelian, S. Luk, T. Piccone, R. Mutharasan: Steelmaking Proc AIME 1988;89:957

[100] J. R. Schmahl, L. S. Aubrey: *"Application of advanced reticulated ceramic foam filter technology to produce clean gray and nodular iron castings"*. Electric Furnace Conference Proceedings (1994), Volume Date 1993, 51, pp. 21-34.

[101] J. R. Schmahl, N. J. Davidson: *"Ceramic foam filter technology for aluminum foundries"*. Modern Casting (1993), 83(7), pp. 31 – 3

[102] K. Oosumi, Y. Nagakura, R. Masuda, Y. Watanabe, T. Ohzono: *"Development of new Filter for Removal of Non-Metallic Inclusions from the Molten Aluminum"*. Recycling of Metals and Engineered Materials, TMS, 2000, pp. 951 – 961

[103] N. S. Kljagina, A. G. Spasskij, 1960, referred to in V.P. Gudchenko: *"Investigation in Refining and Degassing Aluminium Alloys during Filtration"*. Trudy Mati, Nr. 63, 1965, pp. 5 – 9 (Russian)

[104] Grafas and Beljajew, 1959, referred to in A.Ya. Radin: *"About the Applying Mechanisms when Fluxing during Melting of Aluminium"*. Trudy MATI, No. 56, 1963, pp. 45 – 70 (Russian)

[105] L. Martin-Garin, A. Dinet, J. M. Hicter: *"Liquid-liquid interfacial tension measurements applied to molten aluminum-halide systems"*. Journal of Materials Science (1979), 14(10), pp. 2366 – 2372

[106] R. Roy, Y. Sahai, Mater Trans JIM, 1997 ; 38 ;571

[107] M. F. Jordan, D. R. Milner: *"The removal of oxide from aluminum by brazing fluxes"*. J. Inst. Metals (1956), 85(Pt. 2), pp. 33-40

[108] R. J. Kissling, J. F. Wallace: *"Fluxing – To Remove Oxide from Aluminium Alloys"*. Foundry, March 1963, pp. 76 – 81

[109] B.-Z. Haim, G. Grodentzik, Z. Rigbi: *"The Wetting of Metal Surfaces by a Glass Melt"*. Glass Technology, Vol. 23, No. 3, June 1982, pp. 156 - 157

[110] Z. Ming, L. Ke, S. Bao-de, S. Da, W. Jun: *„Anticorrosion Properties of Enamels with high B2O3-P2O5-AlPO4 Content in Molten Aluminum"*. Trans. Nonferrous Met. Soc. China,Vol. 12 No. 3, June 2002, pp. 470 – 474

[111] David V. Neff: *"Metallurgy and Melt Treatment of Aluminum-Silicon Alloys"*. 5th Australasian Asian Pacific Conference on Aluminium Cast House Technology, Edited by M. Nilmani, P. Whiteley, and J. Grandfield, The Minerals, Metals & Materials Society, 1997, pp. 155 – 177

[112] D. Apelian and S. Shivkumar: *"Molten Metal Filtration – Past, Present and Future Trends"*. 2nd International Conference on Molten Aluminium Processing Proceedings, Orlando, Florida, 6. – 7. November 1989

Chapter 3

PREVIOUS WORK - INDUSTRIAL WORK AND TRENDS

3.1 Metal / Flux

An early reference regarding the fluxing of aluminium [1] dates back to 1944. At that time, a process for "degassing" molten aluminum alloys was by pouring the latter into a molten salt containing $MgCl_2$ in excess of 50 percent.

In 1961 Foseco announced [2] a continuous method for treating large quantities of molten metal with a liquid flux to remove non-metallic inclusions called "Flux Washing". Metal and flux intimately mix by pouring the metal onto a horizontal plate submerged in the flux, which breaks up the metal flow and reduces the vertical momentum of the impinging stream. This technique has been in use in several companies all over the world. The so-called flux-washing process was first developed from a method which was intended to degas the metal. Suspended oxides are often also

the carriers of entrapped gas, therefore getting rid of the one problem, will also help to eliminate the other [3].

A more elaborate process of the previously mentioned "Flux Washing" was reported by Yudkin and Dubodelov [4] in 1974. There, in a closed system metal at sufficient superheat (720 – 730°C) is forced through an aperture subsequently deviding the thin metal streams into single droplets. In a sealed chamber the drops of metal fall onto a flux surface and sink to the bottom of the molten flux layer (75 – 80 mm thick) which rests on a head of metal. A batch of 120 kg needs about 2.6 min to pass through. The optimum refining period for metal circulating in the system was found to be 10iip – 12 min. Refining fluxes of two different compositions were employed: (1) a mixture of 30 % NaCl, 47 % KCl and 23 % Na_3AlF_6, and flux (2) consisting of 50 % NaCl, 10 % each KCl and Na_3AlF_6, and 30 % NaF. Inclusion (0.22 $\rightarrow$ 0.08 wt % Al_2O_3/melt) and hydrogen levels (0.49 $\rightarrow$ 0.22 cm^3 H_2/100g melt) in the melt were lowered substantially thereby increasing tensile strength (18.1 $\rightarrow$ 20.2 kg/mm^2) and elongation (0.8 $\rightarrow$ 2.3 %).

3.2 Metal / Gas Purging / Injection

One of the weak points of the filtration process in [5], [6] (see paragraph 3.3) was the necessity of having a continuous supply of smelter metal. Therefore, another simple and economical process for the elimination of lithium and other alkali metal contaminants from primary aluminium has been developed by Arvida Laboratories, Alcan International Limited. The treatment is done directly in the crucible, before furnace transfer, and does not require additional operations or holding capacity. In the process, aluminium fluoride powder is intimately mixed with the metal, using a specifically designed rotor. High alkali removal occurs through the formation of stable fluoride compounds. Removal rates depend on rotor speed and AlF_3 additions. The removal efficiency initially increases almost linearly with the amount of AlF_3 and reaches about 93% at a saturation level of almost 2.5 kg AlF_3/m.t. after 10 minutes at 760°C. Contradictory to the bed filter described in [5], [6] (see paragraph 3.3), the lithium removal rate is inversely proportional to metal temperature. An additional benefit is the reduction of Al_4C_3 inclusions from an average 14 ppm down to 4 ppm.

Routine production operations with the TAC system (Treatment of Aluminium in Crucibles) [7] began in Arvida during mid 1982 [8].

Introduced about 10 years ago, in 1993 so-called rotary flux injection machines became generally available. These machines combined rotary degassing with the ability to inject a measured amount of specially developed flux into the melt. They increased the efficiency of flux treatment by up to tenfolds in terms of flux usage, with significant improvements in oxide removal, the environment and reduction in treatment times. Since that time, new treatment technology has evolved with the introduction of combined melt treatments such as sodium modification and phosphorus refinement, calcium removal and grain refinement [9]. A further reference [10] confirms the claimed advantages and adds that the favoured injection regime is jetting rather than bubling.

In a patent specification for Na and Li removal from Al-Mg alloys by injecting AlF_3 with the help of a carrier gas, E. Maier [11] claims a low consumption of the refining agent. The reduction of the Na level from 29 ppm down to 2 ppm by mass requires an addition of 18g AlF_3 per tonne treated melt. However, stoichiometrically 33g of AlF_3 are required to remove 27ppm Na what corresponds to $27/23$ mole of Na according to the reaction $3\ \underline{Na} + AlF_3 = 3\ NaF + Al$.

A typical example of an injection process is Hydro's RAM – process (Removal of Alkali Metal) [12], [13] where the melt is fluxed by introducing AlF_3 together with argon through a spinning rotor head into the tapping crucible. A half-life period for Na of two minutes is attained and Na contents are typically reduced to 1-5 ppm. The process has caused a reduction of the amount of dross in the cast house of 23 %. In addition, the number of Al_4C_3 inclusions is halved by the treatment.

A completely new range of fluxes in granular form was launched by Foseco in 1995 [14]. Moving from a powder flux to a granular flux reduces the required amount by 50 % to 0.125 % of weight of the melt. Total chlorine savings account for 50% and are in accordance with the flux savings, furthermore the reductions for particulate and fluoride emissions exceed the flux savings and are 75 % and 85 %, respectively. As a logical supplement Foseco presented equipment for injection of its own granular fluxes in 1998 [15]. The agent is added using argon or nitrogen in an injection/stirring system

that achieved equivalent or better metal cleanliness compared to standard lance chlorine fluxing in research carrried out by Alcan. The study also concluded that emissions were reduced by factors of 10-25 compared with standard lance chlorine fluxing. This yields emission levels well below regulatory targets and negates the need for stack abatement equipment.

Near pollution-free demagging of aluminium is accomplished with the help of the gas injection pump. Demagging efficiencies with this device have been reported to be virtually 100 % when the molten metal bath temperature is kept at 760°C or slightly above [16], [17], [18]. Another benefit is the valuable by-product $MgCl_2$.

An alternative way of demagging by submerged injection of reactive SiO_2 particles, was presented by Escobedo et al. in 2003 [19]. The main attraction of such a process is the non-pollutant nature of the reagents employed. At a temperature of 750°C, a powder to gas flow rate of 18.5g SiO_2/min to 12 Nl N_2/min, and a particle size of –70+140 mesh, the magnesium content was reduced from 1.2 wt% to less than 0.1 wt% in about 40 minutes in a laboratory batch of 20 kg aluminium. The main reaction product produced by first order kinetics was the $MgAl_2O_4$ spinel. Kinetics generally improve with increasing temperature, decreasing particle size up to a certain value, and good contact/mixing provided. Argon is preferable to nitrogen as a carrier gas due to the possible formation of aluminium nitrides.

3.3 Active Filtration

In 1961 Spasskij et al. [20] studied the replacement of granulated refractory filter material by more chemically active materials such as fluorides. They are wetted by aluminium, what very much improves the removal of suspended particles. The fluorides are also more effective in absorbing aluminium oxide compared to the inert materials. A mixture of equal parts of calcium and magnesium fluoride produced a particularly effective filter material.

In the late 1960's tighter pollution control was demanded by the federal government of the USA. This induced rising costs during metal processing, especially when fluxing with chlorine or chloride bearing compounds, which made fume elimination increasingly more desirable. Alcoa's answer was the so-called Process 469

for continuous metal treatment without fume or furnace fluxing. This process simultaneously reduced hydrogen, inclusions, and undesirable trace elements to very low levels without fume. Argon gas containing 1-10% chlorine is bubbled countercurrent to metal flow through two types of packed refractory particle bed filters in series. The fluxing gas mixture de-wets inclusions and back-flushes the filter bed continuously. Chloride reaction products are simultaneously swept to the metal surface by the same purging action, thus extending the life of the filter bed appreciably. The reported life-time of the filter bed was between 3200-4550 tonnes of metal treated [21].

Foseco came up with a continuous method for removal of inclusions from molten metals in 1968. The method passed the molten metal through a bed of granular material consisting preferably of a mixture of 52% calcium fluoride and 48% magnesium fluoride. This mixture is made by first fusing the two components together and crushing and sieving the cold fused material afterwards. The granular material may have a grain size of 3 – 6mm, the particular choice of grain size depending on the metal to be treated, the treatment temperature and the flow rate of the molten metal required. Best results were obtained at molten metal temperatures of 720°C. The improved removal was believed to be due to an increased “wetting” action on the inclusions by the active granular materials [22].

M.V. Brant et al. presented a fumeless process for in-line degassing and cleaning of liquid aluminum in 1970. The metal first enters a degassing chamber for hydrogen removal where it is treated with nitrogen under a liquid flux cover. It then passes through a bed of flux-coated coarse refractory granules to remove oxide inclusions. The flux consisted of approximately eutectic composition of KCl and NaCl with a small addition of CaF_2. Finally, the melt takes an upward passage through coarse uncoated “dry” balls to strip out any residual flux carried over in the metal [23].

Based on U.S. Pat. No. 3,305,351 granted in 1967 [5] work started in Alcan in 1974 to develop a process for removing Li, and other alkali contaminants from smelter metal prior to furnace transfer. In the process, metal is transferred directly from tapping crucibles and passed through a bed of particles of material containing aluminum fluoride. The particles are made by treating alumina particles with hydrofluoric acid gas. To prevent a carry over of liquid reaction products into the melt, alumina balls wetted by molten fluoride salts form the layers downstream the AlF_3 particles. Removal

efficiencies as high as 90-95 percent can be achieved with increasing efficiencies for rising temperatures in the range of 700-900°C and efficiencies decreasing with filter aging. The removal efficiency was almost independent of the inlet concentration (it increased by 5% with an increase in c_{in} from 20 to 200 ppm of Na, Ca and Li). The consumption of AlF_3 is in the order of 0.8 kg AlF_3/m.t. Al for a Li filtration efficiency cut-off at 80 percent. No fumes or fluoride dust are generated during operation since the filter bed is always submerged in molten aluminum. Only combustion products may be found around the filter box during operation. An attractive feature of the process is that the bed materials can be readily recycled with recoveries of 85-90 percent for the active material [6].

Swiss Aluminium Ltd. was granted a patent [24] on a process for the removal of impurities from aluminium melts in 1979. A process is claimed where $AlCl_3$ (gas) is formed in the melt by supplying reactive chlorine diluted by argon into the melt. The gaseous aluminium chloride is “taken up” on a granular bed filter which contains one or more solid chlorides of the group of chlorides formed by alkali and alkaline earth elements. The melt passed through the filter should be between 690 and 750°C which is below the melting point of the solid chloride or chlorides. In order to prevent salt particles from being swept along by the flowing melt, it is useful to cover the filter with a second filter which physically holds back such particles.

In 1981, Sivaramakrishnan et al. [25] claimed the development of a special ceramic filter for aluminium alloys that is (1) reactive with the molten metal to cause grain refinement and (2) reactive to preferentially remove sodium, oxides etc. Oxides and sodium levels had been consistently reduced by more than 50 % with several values reaching up to 90 %. An effect of grain refinement was validated also. However, the composition of the filter media was not specified.

A deep bed filter made up of flux particles, employed at Péchiney in 1985, was reported to decrease reject rates in production of telephonic wire and foil stock [26].

The experience over 15 years with a petrol coke filter bed for the removal of alkali like sodium and lithium since the early 1970’s has been reported by Bornand and Buxmann [27] in1986. The mechanism of sodium removal is explained by sodium diffusing into the carbon lattice [28], [29]. For hydrogen removal the coke bed which is ballasted with corundum is flushed with argon counterflowing to the melt. Efficiencies

for a bed filled with 300kg of pure petrol coke increase with temperature, and are around 90 % and 80 % at 860°C for flow rates of 25t/h and 50t/h, respectively. A decline in the efficiency of the process of 5 % for approximately every 100 tons of transferred metal was ascertained as the petrol coke became saturated. A drawback of the process is the disposal of the contaminated petrol coke [6].

A similar process relying on a coke bed was patented by Nikitich and Yakovenko [30] in 1982. The filter bed should be maintained at a temperature between 900°C and 1400°C. The melt will not start oxidizing before a filter temperature of 1500°C is reached. The melt temperature prior to filtration should be maintained at 720°C to 730°C and will not change during filtration. Removal rates were in the range of 97% - 99% of the sodium. The removal mechanism is by burning the sodium at the melt – filter interface, thereby preventing saturation of the filter.

An approach to remove liquid salts originating by chlorine gas fluxing has been made by SELEE [31]. Salt filtration is achieved by the use of a microporous media designed to absorb the liquid salt.

Oosumi et al. [32] coated conventional filters with NaBr as an adhesive and published their results in 2000. The technology has made it possible to remove inclusions as small as 10-20 μm from the molten metal, which have been impossible to remove by the uncoated filter. An inclusion removal rate of up to 90 % has been attained. However, Br is a toxic substance.

Zhou et al. [33] showed in 2003 that enamels with high B_2O_3-P_2O_5-$AlPO_4$ content containing Na_3AlF_6 are resistant to the corrosion of molten aluminium, and at the same time can actively remove Al_2O_3 inclusions as small as 6 μm in size. The captured inclusions may be dissolved in the molten borophosphate enamel by converting them into AlO_4 which becomes a part of the enamels structure.

The most recent approach [34] dates from 2006 and describes a ceramic foam filter (CFF) coated with a salt flux that consists of equal parts of NaCl and KCl, 5% LaF_3 and 5% others not specified. Reported is the removal of virtually all inclusions larger than 6μm. This removal is associated with an increase in tensile strength and elongation of about 6% and 66.7%, respectively, compared to samples treated by an uncoated CFF.

Bibliography

[1] I.G. Farbenindustrie: *"Process for Degassing Molten Aluminum Alloys"*. Swiss Patent 231739, April 15th, 1944

[2] M.R. Reeve, G. Reeves: *"Flux Washing"*. Foseco developments, 7/12, 1961, pp.18– 26

[3] K. Strauss: *"Applied science in the casting of metals"*. Oxford : Pergamon Press, 1970

[4] S.A. Yudkin, V.I. Dubodelov: *"Drop Filtration of Aluminium Alloys through a Flux Layer"*. Translated from Liteinoe Proizvodstvo, (3), 1974, pp. 13 – 14

[5] L.D. Bylund: *"Treatment of Aluminum with Aluminum Fluoride Particles"*. 1967, U.S. Patent 3,305,351

[6] P. Achim, G. Dubé: *"Removal of Lithium in Commercial Metal"*. Light Metals, 1982, pp. 903 – 918

[7] B. Gariépy, G. Dubé, C. Simoneau, G. Leblanc: *"The TAC process: A proven technology"*. Light Metals, 1984, pp. 1267 – 1279

[8] A. Silny, T.A. Utigard: *"Interfacial Tension between Aluminium, Aluminum Based Alloys and Chloride – Fluoride Melts"*. Light Metals 1997, pp. 871 – 878

[9] *"More steps beyond rotary degassing"*. Aluminium Today (UK), 8, (6), 28-30, Dec. – Jan. 1996 – 1997

[10] P.Y. Li, J. Jia, J.J. Guo: *"Melt Treatment of A357 Alloy by Flux Injection"*. Materials Science Forum Vols. 331-337 (2000), pp. 283 – 288

[11] E. Meier: *"Procedure for Removal of Alkali and Earth Alkali Metals from Aluminium or Alloyed Aluminium Melts"*. Norwegian Patent Specification, No. 171799, 1988

[12] T. Leinum, B. Rasch: *„Crucible Fluxing of Potroom Metal in a Norsk Hydro Cast Shop – Effect on Dross Reduction and Increased Metal Recovery"*. Light Metals 2001, Edited by J. L. Anjier, The Minerals, Metals & Materials Society, 2001, pp.1049 – 1052

[13] B. Rasch, E. Myrbostad, K. Hafsås: *„Refining of Potroom Metal Using the Hydro RAM Crucible Fluxing Process"*. Light Metals 1998, Edited by Barry Welch, The Minerals, Metals & Materials Society, 1998, pp. 851 – 854

[14] S.R. Sibley: *"Granular Fluxes for Aluminium Alloys, Environmental and Technological Advances"*. Proceedings of the International Conference on Molten Aluminium Processing, Vol. 4th, 1995, pp. 417 – 430

[15] *"Tackling the Environmental Issues"*. Aluminium Castings, Aluminium, Vol. 74, 9/1998, pp. 660 – 664

[16] D. V. Neff: *"Environmentally Acceptable Chlorination Processes"*. 4th Australian Asian Pacific Course and Conference, Aluminium Cast House Technology: Theory & Practice, Edited by M. Nilmani, The Minerals, Metals & Materials Society, 1995, pp. 211 – 225

[17] Neff, David V.; Cochran, Brian P. *"Chlorination Technology in Aluminum Recycling"*. Light Metals (Warrendale, PA, United States) (1993), pp. 1053 – 1060

[18] D. V. Neff: *"The Use of Gas Injection Pumps in Secondary Aluminum Metal Refining"*. Proceedings, AIME, Recycle and Secondary Recovery of Metal, 1985, p. 73

[19] J.C. Escobedo, A. Flores V., J.F. Hernández, D. Cortés, J.J. Velázquez: *"Recent Experiences with the Use of SiO_2 for Removing of Magnesium from Molten Aluminum Alloys"*. Light Metals 2003, pp. 885 – 891

[20] A.G. Spasskij, M.V. Pikunov, A.V. Kurdyumov, E.A. Lebedev: *"Removing Films from Metals by Filtration"*. Russian Castings Production, 1961, pp. 546 – 549

[21] L.C. Blayden, K.J. Brondyke: *"Alcoa 469 Process"*. Journal of Metals, February 1974, pp. 25 - 28

[22] G. Snow: *"Method for the Removal of Inclusions from Molten Metals by Filtration"*. British Patent Number 1,148,344

[23] M. V. Brant, D. C. Bone, E. F. Emley : *"Fumeless In-Line Degassing and Cleaning of Liquid Aluminum"*. Journal of Metals, 23, March 1971, pp. 48 – 53

[24] R. Stary, A. Howald: *"Process for the Removal of Impurities from Aluminium Melts"*. British Patent 1.542.358, 1979

[25] C. S. Sivaramakrishnan, R. K. Mahanty, R. Kumar: *"Special Ceramic Filter for Aluminium Alloys"*. Transactions of the Indian Ceramic Society, Volume 40 (4), July-August 1981, pp. 146 – 151

[26] R. Figueres: *"Degassing and Filtering of Aluminum Alloys at Pechiney"*. International Seminar on Refining and Alloying of Liquid Aluminium and Ferro-Alloys, August 26-28, Trondheim, Norway, 1985, pp. 325 – 332

[27] J.-D. Bornand, K. Buxmann: *"DUFI – A Concept of Metal Filtration"*. Light Metals, 1986, pp. 1249 – 1260

[28] Krohn, Conrad; Soerlie, Morten; Oeye, Harald A.: *"Penetration of sodium and bath constituents into cathode carbon materials used in industrial cells"*. Light Metals (Warrendale, PA, United States) (1982), pp. 311 – 24

[29] Dewing, E.W.: *"The reaction of sodium with nongraphitic carbon: reactions occurring in the linings of aluminum reduction cells"*. Transactions of the American Institute of Mining, Metallurgical and Petroleum Engineers (1963), 227(6), pp. 1328 – 1334

[30] V.T. Nikitich, V.A. Yakovenko: *"Refining Aluminum Free of Sodium"*. Patent SU 1077943 A, Soviet Union, 1982

[31] K.R. Butcher, D.D. Smith, L.S. Aubrey: *"Performance Evaluation of a Filtration Unit Developed to Remove Liquid Salts from Molten Aluminum"*. SELEE Technical Papers, TEK99-11

[32] K. Oosumi, Y. Nagakura, R. Masuda, Y. Watanabe, T. Ohzono: *"Development of new Filter for Removal of Non-Metallic Inclusions from the Molten Aluminum"*. Recycling of Metals and Engineered Materials, TMS, 2000, pp. 951 – 961

[33] M. Zhou, D. Shu, K. Li, W.Y. Zhang, H.J. Ni, B.D. Sun, J. Wang: *„Deep Filtration of Molten Aluminum using Ceramic Foam Filters and Ceramic Particles with Active Coatings"*. Metallurgical and Materials Transactions A, Volume 34A, May 2003, pp. 1183 – 1191

[34] H. Ni et al.: *"Purifying effects and mechanism of a new composite filter"*. Materials Science and Engineering A, 2006, pp.1 – 6

Chapter 4

PRODUCTION OF FILTER GRAINS FROM AlF_3 POWDER

4.1 Introduction

AlF_3 powder can not be employed directly in a packed bed for filtration of aluminium. The melt can not penetrate the small interparticle voids. A grain size in the order of a few milimeters is necessary to form voids that are large enough to be penetrated by the molten aluminium. The procedure for producing the filter grains is given in detail for several reasons. The properties of the filter such as surface area and void fraction must be known accurately in order to precisely describe and study filter behaviour. Production of filter material based on powder has important industrial applications. Particles of sufficient size may be produced by agglomeration and subsequent sintering of the powder compact to give mechanical strength. An advantage of this procedure is that there is less surface exposed during sintering. The filter media is

finally obtained by crushing the sintered powder compact giving irregular shapes. In fact, these irregular shapes favour the capture of suspended particles compared to spheres. Irregular shapes also increase the tortuosity of the packed bed which may improve mass transfer and hence, removal of dissolved elements.

Powders exhibit a fluid-like character that allows shaping over a wide range of stresses. A variety of shaping processes prove to be applicable to powders, including die compaction, slip casting, tape casting, extrusion, injection molding, isostatic pressing, and rolling [1].

Applicable to all materials, sintering is a thermal treatment for bonding particles together into a coherent, predominantly solid structure via mass transport events (see Table 4.1 [1]) that occur largely at the atomic level. Two factors are important for mass transport in sintering: stress (or force) and mobility. The sintering stress is larger with smaller particles and higher surface areas, and the mobility increases with higher temperatures. Sintering lowers the surface energy by reducing surface area (i.e., the curvature of the neck surface [3]) with concomitant formation of cohesive interparticle bonds. Such bonding improves the strength, and other engineering properties of the compacted particles. Most materials exhibit sintering at temperatures between 0.5 – 0.8 times the absolute melting temperature. [1]

Table 4.1: Mass transport mechanisms [1].

Mass Transport Mechanisms	
Surface Transport	***Bulk Transport***
surface diffusion	plastic flow
evaporation - condensation	grain boundary diffusion
volume diffusion	volume diffusion

The sintering mechanism may be described by the path of mass flow as illustrated in Figure 4.1. Surface transport processes produce neck growth without a change in particle spacing (no shrinkage or densification) due to mass flow originating and terminating at the particle surface. Only bulk transport mechanisms are responsible for densification during sintering. For most inorganic powders, diffusion mechanisms are dominant, including flow over free surfaces, along grain boundaries, or through the

crystal lattice. Other mechanisms include vapour transport, plastic flow, viscous flow, and dislocation climb. For most materials, sintering usually occurs through the simultaneous action of several processes, although one is usually dominant. [1]

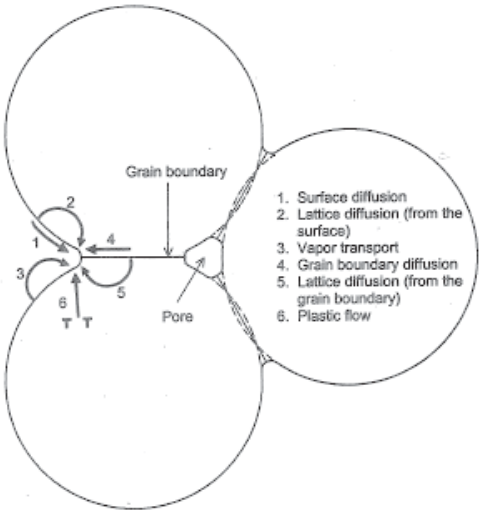

Fig. 4.1: Six distinct mechanisms can contribute to the sintering of a consolidated mass of crystalline particles: (1) surface difusion, (2) lattice diffusion from the surface, (3) vapour transport, (4) grain boundary diffusion, (5) lattice diffusion from the grain boundary, and (6) plastic flow. Only mechanisms 4 to 6 lead to densification, but all cause the necks to grow and so influence the rate of densification. [3]

The stages of sintering may be referred to geometric categories for the mass flow process as outlined in Table 4.2 [1].

The diagram in Figure 4.3 helps to relate the key sintering techniques. Basically, the techniques are divided in pressureless and pressure-assisted sintering processes. To understand the evolution of a final microstructure, attention must be given to particle size, initial density, and pore microstructure, heating rate, maximum temperature, hold time, and atmosphere. With such understanding it is possible to evaluate processing alternatives. Table 4.3 outlines some of the key processing changes and their effects. [1]

Table 4.2: Classic stages of sintering [1].

Stage	Process	Surface Area Loss	Densification	Coarsening
Adhesion	Contact formation	Minimal unless compacted at high pressures	None	None
Initial	Neck growth	Significant, up to 50% loss	Small at first	Minimal
Intermediate	Pore rounding and elongation	Near total loss of open porosity	Significant	Increase in grain size and pore size
Final	Pore closure, final densification	Negligible further loss	Slow and relatively minimal	Extensive grain and pore growth

An illustration of a typical sintering sequence is given in Figure 4.2. [1].

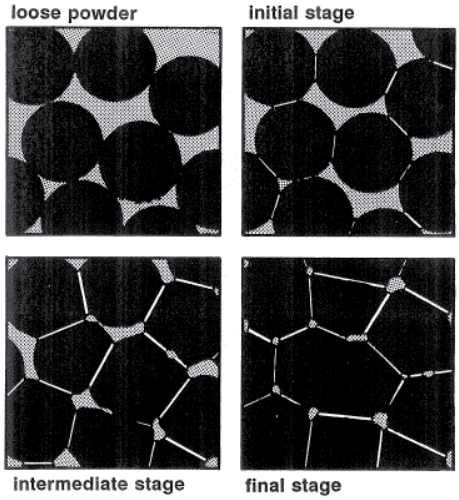

Fig. 4.2: Sintering stages start with a loose powder and subsequently sinter in each of the three stages. The initial open pore structure and high porosity are consumed by interparticle neck growth, grain growth, and pore shrinkage, with eventual formation of closed, spherical pores in the final stage. [1]

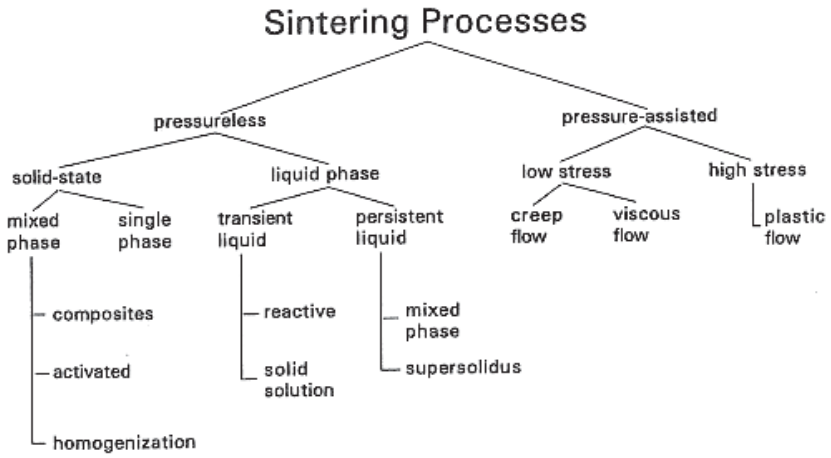

Fig. 4.3: Map to sintering processes and the subdivisions in terms of key processing parameters [1]

Table 4.3: Sintering processing effects [1].

Change to Aid Sintering	Effects
Decrease in particle size	Faster sintering
	Greater expense
	Higher impurity level
	Increased hazards
Increase in time	Greater expense
	Grain growth and coarsening
	Reduced productivity
Increase in temperature	Greater shrinkage
	Grain growth
	Greater expense
	Less precision
	Higher properties
	Furnace limitations
	Pore coarsening
Increase in green density	Less shrinkage
	Smaller pores
	Higher final density
	Uniform dimensions
	Density gradients
Increase in alloying/additives	Higher strength
	Homogeneity problems
	Higher sintering temperatures
Use of sintering aids	Faster sintering
	Lower sintering temperatures
	Embrittlement
	Distortion
	Grain growth control

4.2 Precursor

The raw material for the production of the "active" filter media is technically calcined AlF_3 powder of 94 % purity supplied by Sigma-Aldrich. It is formed when hydrogen fluoride is passed over red hot aluminium or aluminium oxide:

$$2Al + 6HF \rightarrow 2AlF_3 + 3H_2\,; \qquad Al_2O_3 + 6HF \rightarrow 2AlF_3 + 3H_2O\,.$$

AlF_3 plays an important role in the primary production of aluminium metal through a reaction with NaF forming cryolite used in the Hall-Heroult cell. It is a white powder which is insoluble in water, acids and bases, with melting point 1290°C and sublimation point 1272°C (ΔH_f = 1498 kJ mol^{-1}). It forms complex salts $M[AlF_4]$, $M_2[AlF_5]$ and $M_3[AlF_6]$ with alkali and other metal fluorides. [2] Its density is 2880 kg/m^3.

The equilibrium vapour pressure of AlF_3 was obtained using FactSage Thermochemical Software and Databases. The equilibrium constant, K, was calculated for temperatures in the range of 700°C to 1000°C. K is equal to the vapour pressure above solid AlF_3 ($a_{AlF_3} = 1$) according to Equation 4.2.

$$\frac{p_{AlF_3}}{a_{AlF_3}} = K \tag{4.1}$$

A semi-logarithmic plot of this vapour pressure versus the inverse temperature is shown in Figure 4.4.

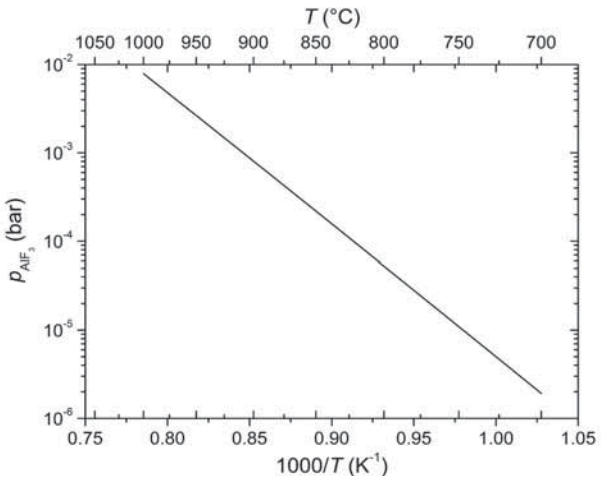

Fig. 4.4: Equilibrium vapour pressure of AlF_3

The particle size distribution of the AlF_3 powder (as received) given in Figure 4.5 was determined at SINTEF Materials Technology using a Coulter "LS Particle Size Analyzer". Figure 4.5 is summarized in Table 4.4. The mean particle size based on volume was found to be 63μm.

Table 4.4: Summary of particle size distribution of AlF_3 powder (as received)

Volume % <	*10*	*25*	*50*	*75*	*90*
Size μm	10.16	32.65	62.19	90.32	115.7

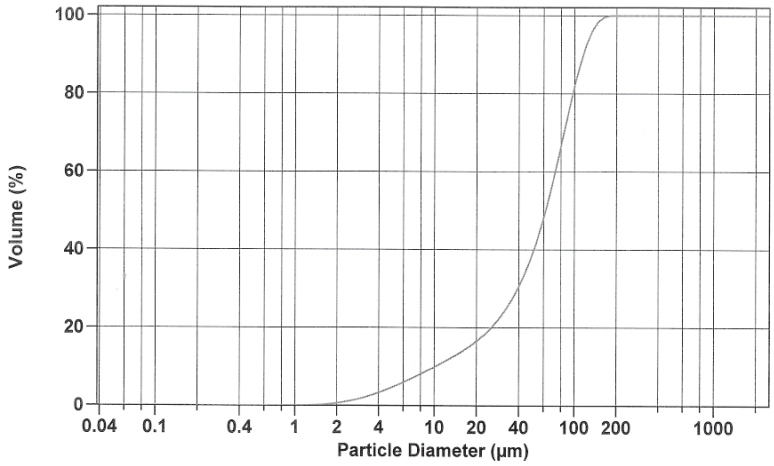

Fig. 4.5: Particle size distribution of AlF_3 powder (as received)

4.3 Green Powder Preparation

As outlined previously, the characteristics of the powder have a remarkable effect on subsequent processing, such as consolidation of the powder into a green body and firing. Hence, powder synthesis is very important to the overall fabrication. Desirable characteristics that a powder should possess are listed in Table 4.5. [3]

Powder synthesis methods may be divided into two categories: mechanical methods and chemical methods. Chemical methods include synthesis by solid-state or vapour-phase reactions, as well as from liquid liquid solutions. However, in this work an approach was chosen that commonly is referred to as mechanical comminution. This

is a process in which small particles are produced by reducing the size of larger ones by mechanical forces. It involves operations such as crushing, grinding, and milling. [3] Typically, machines such as jaw, gyratory, and cone crushers are used for coarse size reduction of the raw material, to produce particles in the size range of 0.1 – 1 mm [4], [5], [6]. The most common way to achieve further size reduction is by milling. A variety of mills may be used, including high-compression roller mills, jet mills (also referred to as fluid energy mills), and ball mills [6], [7].

Table 4.5: Desirable characteristics for advanced ceramics [3]

Powder characteristic	*Desired property*
particle size	fine (< ~ 1 μm)
particle size distribution	grain boundary diffusion
particle shape	spherical or equiaxial
state of agglomeration	no agglomeration or soft agglomerates
chemical composition	high purity
phase composition	single phase

4.4 Milling – Adjusting Particle Size Distribution

A lower sintering temperature is beneficial in some materials, especially those that evaporate or decompose at high temperatures like AlF_3. For small particle sizes the high surface area/volume ratio ensures that surface forces are relatively large , which promotes faster sintering. Surface diffusion and grain boundary diffusion are very sensitive to particle size. These interfacial diffusion processes are favored at smaller particle sizes due to the higher interface content per unit volume. Less sensitive is volume diffusion, and least sensitive is viscous flow. Evaporation-condensation is intermediate in sensitivity to particle size changes. An important consequence of the particle size effect on solid-state sintering is evident in examination of possible temperature reductions with smaller particles [1]. Hence, smaller particles may be able to compensate for the reduced mobility at lower temperatures due to an increased dominance of surface diffusion and grain boundary diffusion, and a decreased effect of evaporation-condensation, respectively.

The pre-cursor material had a mean particle size of 63µm. Further reduction in particle size was achieved by using a Comex jet mill of the JMX-200 type located at the department of geology and mining at NTNU. Comminution with jet mills is mainly based on the principle of introducing solid particles into high velocity gas or vapour streams, accelerating them and reducing their size by impact and attrition against other particles or targets [8]. The Comex jet mill used is a autogenous grinding unit where the material is comminuted by the repetitive collisions of the same kind of particles, so contamination is not a problem. The grinding principle of a jet mill is illustrated in Figure 4.6 [9].

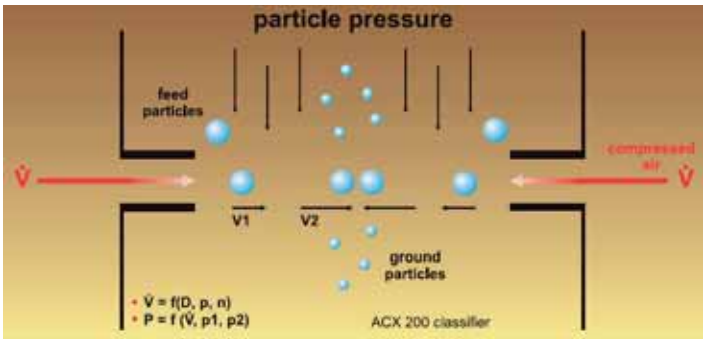

Fig. 4.6: Jet mill grinding principle [9]

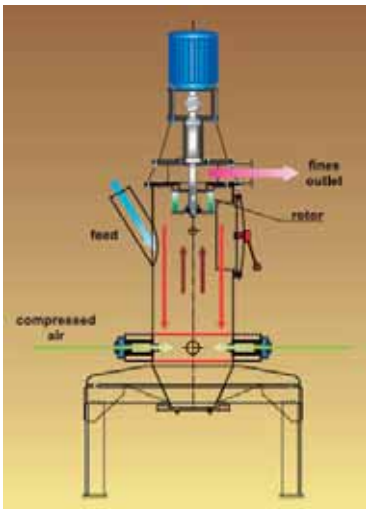

Fig. 4.7: Process design of Comex JMX-200 jet mill [9]

In Comex jet mills the feed material enters the mill chamber by gravitation, through a diagonal inlet pipe. Also feed material enters the grinding area where the air nozzles are located. The air nozzles inject the pure compressed air such that the material will be exposed to the air stream dragging the particles along with high velocities [9]. The air nozzles are aligned so that two or more gas jets are focused at a central point [8]. The accelerated particles collide at that point in the mill chamber being ground to finer sizes. The decompressed air lifts the ground particles to the upper part of the mill chamber, where the particles are trapped in an air classifier. There, size separation takes place. The fine particles leave the mill but the coarse particles fall back to the mill chamber [9]. The feed particles remain in the grinding zone until they are reduced to a sufficiently fine size. An advantage of jet mills combined with a particle classification device is their ability for rapid production of a powder with a narrow size distribution. Particle sizes obtained may be as small as ~ 1μm [3]. Monosized powders can be packed to high densities with minimal inhomogeneities, thereby supressing grain growth during sintering, unlike powders having a wide initial particle size distribution and a lower final density, respectively [10], [11]. The process design of this jet mill is outlined in Figure 4.7 [9].

The average particle size and the particle size distribution of the milled powder depend on a number of factors, including the size, size distribution, hardness and elasticity of the feed particles, the pressure at which the gas is injected, the dimensions of the milling chamber, and the use of particle classification in conjunction with the milling [3].

The mean particle size (63μm) and particle size distribution of the feed material (AlF_3 powder) was given in section 4.2. The throughput was in the order of 10 – 20 kg/h which is much below the capacity (40 – 500 kg/h) specified by the manufacturer [9]. This is due to the mechanical strength of the AlF_3 crystal structure. The jet mill was operated at a pressure of 6 bar and 7000 rpm for the air classifier. This was a compromise made between mean grain size to be expected and a throughput that was still reasonable. Running the jet mill for maximum fineness (2 μm) would have increased treatment times disproportionately. After milling, the particle size distribution of the AlF_3 powder (milled) was determined at SINTEF Materials Technology using the

Coulter “LS Particle Size Analyzer”. Figure 4.8 is summarized in Table 4.6. The mean particle size was found to be 6.6 µm.

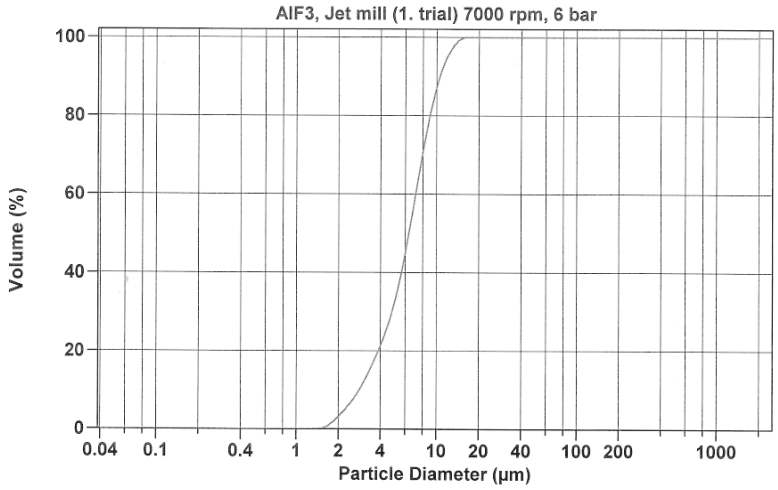

Fig. 4.8: Particle size distribution of AlF_3 powder (milled)

Table 4.6: Summary of particle size distribution of AlF_3 powder (milled)

Volume % <	*10*	*25*	*50*	*75*	*90*
Size µm	2.83	4.37	6.37	8.43	10.54

The milling reduced the mean particle size by a factor 10 compared to the feedstock. In addition, a particle size distribution was obtained that is much more narrow relative to the supplied AlF_3 powder.

4.5 Powder Consolidation

The flow chart in Figure 4.9 shows the process steps that are necessary prior to sintering of a powder compact. The consolidation of powders to produce a green body is commonly referred to as forming. The main forming methods include (1) dry or semidry pressing of the powder (e.g., in a die), (2) mixing of the powder with a fluid, as for example water, alcohol, or organic polymers, to produce a plastic mass that is shaped by pressing or deformation (referred to as plastic forming), and (3) casting from a concentrated suspension or slurry (e.g., slip casting, pressure casting and tape casting. [3]

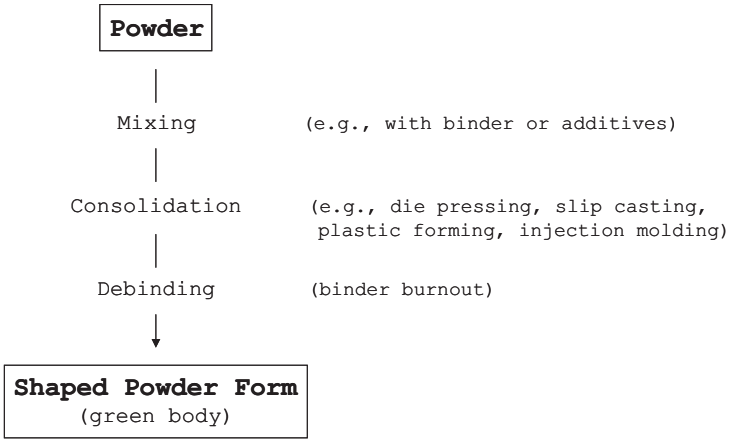

Fig. 4.9: Process steps necessary prior to sintering

The latter of the forming methods introduced, pressure casting to be more precise, was applied to the milled AlF_3 powder. This method is capable of producing a fairly homogeneous and dense particle packing in the green body. A homogeneous packing of the green body is important since deviations will lead to a heterogeneous microstructure during firing [3]. Also green density is an important factor in sintering. Higher green densities give more initial particle contacts, smaller initial pores, with less densification needed to obtain final density [1].

AlF_3 was dispersed in alcohol using a laboratory blender. Adherence occurs due to weak forces, including van der Waals forces and agglomeration forces from liquids [1]. The slurry obtained was composed of 3 parts AlF_3 powder and 1 part of liquid binder (by mass). Alcohol was used instead of water even though AlF_3 is insoluble in water. However, AlF_3 is not inert and halide oxides, AlOF, are known [2]. The suspension was then forced to settle with help of the filter press shown in Figure 4.10.

The filter press basically consists of a cylindrical chamber where top and bottom are inlet and outlet, respectively. The inlet may be locked. The outlet is open but covered with a filter cloth. A pressure in the range of 0.4 to 0.7 MPa was applied through a valve built in the lid of the filterpress. The alcohol is drained due to the overpressure. The AlF_3 powder remains in the filterpress as a dense “cake” on top of the cloth. The filter cake may be also called green body. Green density is an important

factor in sintering. A thickness of 20 – 30 mm was realized for filter cakes in this work. However, filter cakes could not be recovered in a single piece due to cracks remaining from the high pressure applied. The formation of cracks may be explained by the fact that the density of the cake is increasing with decreasing content of liquid. Hence, the pressure drop across and the forces acting upon the cake increase considerably. At a certain density the compressed air only may find its way out by forming channels finally tearing apart the filter cake. Subsequent drying for 24 hours at 105°C in a drying cupboard removes any remaining alcohol or binder, respectively. No loss in strength and no cracks were observed after drying. Prior to sintering the green powder compact shown in Figure 4.11 just holds together by forces of cohesion.

Fig. 4.10: Filter press used in making the AlF_3 filter grains

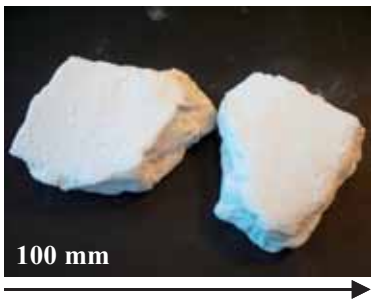

Fig. 4.11: Green powder compact prior to sintering

4.6 Sintering

Atom diffusion processes lead either to densification of the body (by transport matter from inside the grains into the pores) or coarsening of the microstructure (by rearrangement of matter between different parts of the pore surfaces without actually leading to a decrease in the pore volume). Coarsening reduces the driving force for densification. Whether densification or coarsening will dominate depends on the material and key processing parameters such as temperature, applied pressure, and gaseous atmosphere. [3]

As a practical guide, materials that exhibit weight loss during sintering (beyond adsorbed impurities) may give vapour transport. Higher temperatures give a higher vapour pressure and more vapour phase transport, since the flux depends on the evaporation rate. Evaporation – condensation dominates the sintering of low stability materials like NaCl, PbO, TiO_2, H_2O, Si_3N_4, BN, and ZrO_2 [1]. Also AlF_3 has a relatively high vapour pressure.

Introductory experiments were carried out to monitor sample weight and sample porosity as a function of time and temperature during sintering of AlF_3. Spherical samples had been made in a pelletizing drum from AlF_3 powder with a mean particle size of 63µm as given in paragraph 4.2. The porosity was obtained from volume and weight of the sample, and the density of AlF_3. This approach allowed the evaluation of the relative dominance of the vapour phase transport as well as the definition of a sintering cycle for the AlF_3 powder compacts.

A resistance heated tube furnace was used to carry out these experiments. The furnace allowed control over temperature and atmosphere. The holding temperatures of 700°C, 800°C, and 900°C were chosen regarding the temperature range for sintering which is typically between 0.5 and 0.8 times the melting temperature of the material. The temperatures correspond to different vapour pressures of AlF_3 which increase considerably above 800°C. The samples were exposed for 1 hour, 2 hours, 4 hours, and 8 hours at the aforementioned temperatures. The heating rates were low enough to avoid thermal shock and stress gradients that could have weakened the powder compact. Sintering is also highly dependent on the process atmosphere, with potential oxidation or reduction reactions dictated by the temperature and process gas purity [1]. Therefore,

30 liters of argon per hour were flushed through the furnace. The experimental conditions and results are summarized in Table 4.7.

The changes in mass (Δm.%) and porosity (%) during sintering are shown in Figure 4.12. (a) (b)

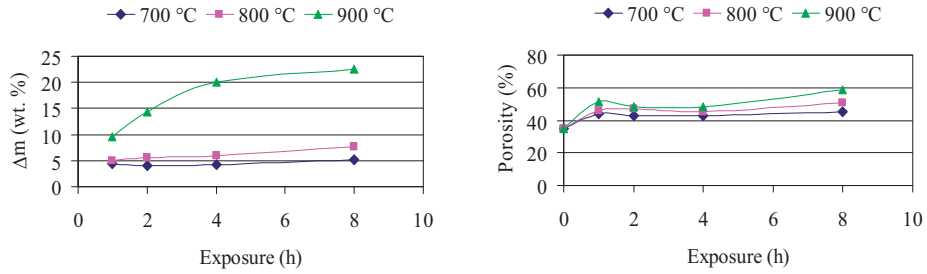

Fig. 4.12: Changes in mass (a) and porosity (b) during sintering

For the first hour exposed the samples at 900°C experienced a mass loss decreasing exponentially with time. The mass loss was twice as high at 900°C (9.5 m.%) compared to the temperatures in the range of 700°C (4.3 m.%) to 800°C (4.9 m.%). Between 1 hour and 8 hours exposure the mass loss is proportional to the exposure time for temperatures of 700°C and 800°C. The mass loss is 0.1 m.% and 0.4 m.% per hour for temperatures of 700°C and 800°C, respectively. The mass loss reaches 5.1 m.% and 7.6 m.% after 8 hours exposure. At 900°C the mass loss of the sample decreases exponentially with time also during 8 hours exposure and is 22.5 m.% after that period. The absence of densification and the actual increase in porosity in addition to the weight loss experienced point towards a considerable contribution of vapour transport during sintering of AlF_3, in particular at temperatures above 800°C. The conclusion drawn was that a temperature of 700°C and an exposure between 1 hour and 2 hours are sufficient to establish reasonable strength in a AlF_3 powder compact during sintering. It is believed that the sintering temperature could be reduced further by 50°C to 100°C.

A low vacuum furnace at the department was used for a small scale production of sintered filter cakes. The furnace chamber has a net volume of 190 liters. The furnace may be operated at temperatures up to 1700°C (by super cantal heating element) and internal pressures as low as 0.1 milibar. Argon was flushed through the furnace at a rate of 10 – 15 liters per hour. An image of the furnace is displayed in Figure 4.13.

Table 4.7: Summary of experimental conditions and results in sintering of AlF_3

Sample	Exposure (h)	Temperature (°C)	Mass (g)	Δ Mass %	Porosity (%)	∅ Porosity (%)
1	0 (green)	room	4.479	-	35.4	
2	0 (green)	room	3.204	-	37.2	
3	0 (green)	room	4.673	-	27.3	
4	0 (green)	room	4.567	-	36.9	
5	0 (green)	room	3.4	-	46.4	
6	0 (green)	room	3.029	-	44.5	34.9 ± 6.4
7	0 (green)	room	3.759	-	25.8	
8	0 (green)	room	2.675	-	32.3	
9	0 (green)	room	3.368	-	27.1	
10	0 (green)	room	4.231	-	33.5	
11	0 (green)	room	4.084	-	35.6	
12	0 (green)	room	3.298	-	37	
1	1	700	4.287	4.3	43.9	
2	2	700	3.072	4.1	42.5	
3	4	700	4.477	4.2	42.5	
4	8	700	4.332	5.1	45.3	
5	1	800	3.232	4.9	46	
6	2	800	2.862	5.5	47.2	-
7	4	800	3.538	5.9	45.2	
8	8	800	2.473	7.6	50.7	
9	1	900	3.047	9.5	51.3	
10	2	900	3.626	14.3	48.5	
11	4	900	3.266	20	48.3	
12	8	900	2.555	22.5	58.4	

Fig. 4.13: Low vacuum furnace

The plot in Figure 4.14 shows the temperature evolution versus time (h) in the low vacuum furnace both for the furnace chamber (dashed line) and the filter cakes to be sintered (solid line). During heating the temperature was ramped at 2.5°C per minute. The temperature in the furnace chamber was put on hold for two hours at 700°C. After the holding period the furnace was turned off and cooled naturally, the chamber being closed. Probably most of the sintering was performed in the range of 600°C to 700°C. The temperature of the cakes to be sintered reached 700°C only towards the end of the holding time. However, the reduced temperature seemed to give as good results as at 700°C. As suggested, a further temperature reduction (<700°C) may be therefore possible.

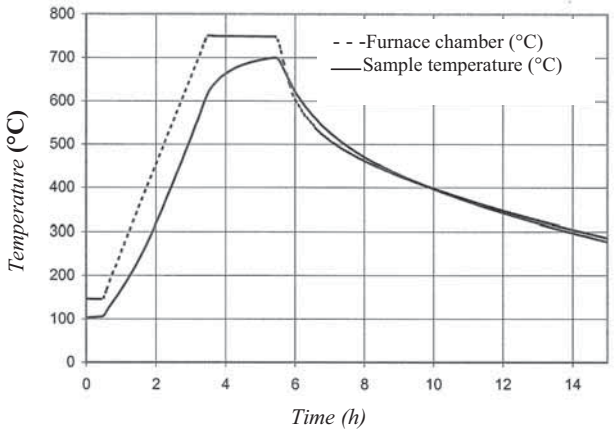

Fig. 4.14: Temperature evolution versus time during sintering in the low vacuum furnace both for the furnace chamber (dashed line) and the filter cakes (solid line)

4.7 Post processing - Comminution

The filter grains attained their final shape by comminution. Comminution of solids takes advantage of the brittle fracture behaviour of many raw materials. In practice, comminution machines and comminution processes are characterized according to (a) the size range of the grained product, and (b) the hardness and the fracture behaviour of the feed. The most important machines for crushing of (hard) lumps are jaw crushers and cone crushers. A jaw crusher, which may produce a top size < 12 mm, was used to reduce the sintered filter cakes to small pieces. Crushing of the sintered filter cakes gave irregular shapes, whose faces have the typical appearance of a brittle fracture surface, as shown in Figure 4.15.

A jaw crusher is basically built of a frame that holds a fixed (a) and an oscillating jaw (b). A gap opens and closes between the two jaws during operation. The lumps, A, enter upon opening and are crushed due to the pressure applied while the gap is closing. The product, P, may be released both when the gap closes or opens depending on gap length and size of the product. The functional principal is sketched in Figure 4.16. In the laboratory the jaw crusher was run at a gap length, s, of zero millimeter (close side setting). [12]

Fig. 4.15: Filter grains acquiring their irregular shape from crushing of sintered filter cakes.

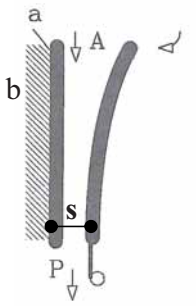

Fig. 4.16: Functional principle of a jaw crusher [12]

The product was screened after crushing. Screening or classification (separation based on the fall velocity in a fluid) means the separation of dispersed solids (usually > 1 mm for screening and < 1 mm for classification) [13] according to their grain size [12]. Therefore, a column of sieves was used having decreasing mesh sizes from top to bottom (9.52 mm, 6.68 mm, 4.76 mm, 3.36 mm, and 2.38 mm mesh size). Particles passing through the 2.38 mm grid were considered as fines. The fraction of fines was always less than 1/3 of the feed stock.

The intermediated separated size fractions were mixed to give a filter bed of AlF_3 grains with the following size fractions: - 3.36 + 2.38mm (25wt%), - 4.76 + 3.36mm (38wt%), - 6.68 + 4.76mm (37wt%). Only smaller size fractions were desired since they have a larger surface area per volume. Size fractions of - 2.38 mm (fines), - 9.52 + 6.68 mm, and + 9.52 mm were excluded from further investigations.

4.8 Characterization

4.8.1 Specific Surface Area

The knowledge of the filter's interfacial area is a prerequisite for characterization of the reaction kinetics and their subsequent modeling. Filter material should be characterized in terms of a specific surface area per mass [cm^2/g] or volume [cm^2/cm^3].

The filter grains are irregular in shape and they are assumed to be ordered randomly throughout the filter bed. In this case, a single section, if extensive enough to contain a statistically significant number of features, may be sufficient to obtain valid results [14]. This so-called statistico-geometrical approach as described by Underwood [14] allows us to determine the filter grain's interfacial area, and also the void fraction in a packed bed, from a two-dimensional image.

4.8.1.1 Metallography

The images were obtained applying a routine method used for metallographic examinations. A loose fill of filter grains was placed in a mould for metallographic sample preparation and cast in resin (Struers "EpoFix", 25 parts of resin + 3 parts of hardener). Subsequently, the mould was evacuated to release entrained air. After hardening (8h) the samples were bisected either horizontally or vertically. In addition, samples were cut from filter grains that had been used in filtration experiments where the melt remained in the filter bed and had solidified.

The specimens were ground mechanically by hand on a rotating disc using grinding paper of fineness 80, 120, 300, 500, 800 and 1000/1200 grit from coarse to fine. A step is regarded as finished when every stripe remaining from the step before has vanished. Ethanol instead of water was used as an agent for cooling, greasing and draining

Further preparation like polishing is necessary to obtain clear images. This was automated to some extent using Struers' "TegraSystem" which is a modular system for metallographic sample preparation. The system consists of a polishing machine (TegraPol – 31), an automatic sample mover to be mounted on the polishing machine

(TegraForce – 5), and a dosing system (TegraDoser – 5) for polishing suspensions/lubricants. The polishing went in 3 steps: (1) three minutes of fine grinding at a force of 30 N using Struers' "MD Largo" composite disk together with a diamond suspension (DP, A - 9μm grain size); (2) two and a half minutes of polishing at a force of 25 N using Struers' "MD Mol" polishing cloth together with a diamond suspension (DP, A - 3μm grain size); and (3) two minutes of final polishing at a force of 15 N using Struers' "MD Nap" polishing cloth together with a diamond suspension (DP, A - 1μm grain size). Struers' "DP – Suspension, A" is a water-free diamond suspension for preparation of water sensitive materials like AlF_3.

4.8.1.2 Image Analysis

The prepared samples were placed on an ordinary scanner to acquire images of the samples. Image analysis requires binary images to perform the measurements in mind. The transformation into a binary image was carried out using Adobe's Photoshop. An example of an image taken with a scanner and its transformation into a binary image are shown in Figure 4.17. Buoyancy effects caused by the metal melt or by infiltration of resin may give a reorientation of some of the particles but would not be expected to change the void volume fraction.

Twenty six cross sections of both types of samples with all together 1954 grains were examined. The following features have been determined with the Zeiss Kontron KS 300 image analysing system: frame area (total area of the image), field area (area covered by filter grains), field area percentage (area covered by filter grains in relation to the total area of the image), field count (number of grains per frame), and field perimeter (addition of perimeters of all the grains measured). The measurements are performed on a pixel basis. A pixel converts to a square of 42.3 x 42.3 (μm) taking the original size of the image into account. The data may be compared in Table 4.8. Frame area not covered by filter grains is considered as voids. The voids fraction, V_{V_0}, is easily obtained from the difference of hundred percent and the field area percentage. The mean voids fraction for all images was determined to be $V_{V_0} = 45 \pm 3.5\%$. The mean value for resin infiltrated samples (image 1 – 12) is $V_{V_0} = 44.7 \pm 3.1\%$, and $V_{V_0} = 45.3 \pm 4\%$ for

samples taken from grains where the melt had solidified in the filter bed (image 13.1 – 17.5).

(a) (b) (c)

Fig. 4.17: Two-dimensional image of a random cross-section through a packed bed of AlF_3 grains cast in metal (a) or resin (b), and the transformation of the latter into a binary image (c)

The surface area per unit volume (property in three-dimensional space), S_V, may be calculated by Equation 4.3 [14]

$$S_V = (4/\pi) L_A \tag{4.2}$$

which relates to a length of lineal elements per unit area, L_A, that can be measured on the two-dimensional section plane during image analysis. It is important to mention that Equation 4.3 is exact, in the sense that no simplifying assumptions are required as to size, shape, spacing, etc., of features in the image. There is the requirement, however, that the measurements be made randomly or with statistical uniformity and that the test sections be representative of the entire sample [14]. Here, L_A is a measure of the sum of perimeters determined for all grains in the two-dimensional image. It should be noted that the perimeter measured by the automatic image analyzer includes the part of the image frame intercepted by filter grains. This contribution equals the total frame perimeter multiplied by the field area percentage and must be substracted from the measured perimeter in order to obtain L_A [15]. The surface area of the AlF_3 filter grains S_V [m^2/m^3] (later called a^*) was determined with surface to volume 1140 ± 106 m^2/m^3.

The apparent density was estimated to be 850 kg/m^3 by determining the weight of a defined volume of filter grains using a measuring glass. The porosity of the filter

grains was derived from the same measurements taking the voids fraction in the packed bed (45%) and the bulk density of AlF_3 (2880 kg/m^3) into account in addition to the apparent density. The filter grains consist of 35% voids, what is the difference of 100 minus the product of bulk density, voids fraction in the packed bed and the inverse of the apparent density. The porosity of the filter grains must not be compared with the data given in paragraph 4.5 Figure 4.12b. The filter grains were made from AlF_3 powder which was an order of magnitude finer (6.6µm, see paragraph 4.3) and had been compacted at much higher pressures. The result is about 20 % less in porosity compared to the spherical samples characterized in paragraph 4.5.

Table 4.8: Image analysis data

Image	Frame area (μm^2)	Field area (μm^2)	Field area (%)	Field perimeter (μm)	Field count	L_A ($\mu m/\mu m^2$)	S_V (m^2/m^3)
1	748323534.3	438030518.7	58.53	820885.86	85	0.001011277	1287.597474
2	726403488.1	436259021.1	60.06	696091.46	63	0.000868667	1106.021417
3	750137977.3	416033528.7	55.46	816925.95	95	0.001008035	1283.470537
4	1108179116	595239300.2	53.71	1123905.2	116	0.000947684	1206.628832
5	1348220621	709620785.1	52.63	1540866.21	159	0.001085029	1381.501805
6	717918193.5	379780456.5	52.9	645366.69	63	0.000815783	1038.687524
7	623581472.5	374056193	59.99	679336.23	61	0.000985154	1254.33647
81	443455953.8	231609891.6	52.23	391655.31	33	0.000782949	996.8822455
82	214157956.1	107519168.4	50.21	200854.03	21	0.000800423	1019.130561
10.1	385399145.9	212889277.5	55.24	347942.66	31	0.000790162	1006.065194
10.2	319422491.1	179291662.3	56.13	315710.3	32	0.000862016	1097.552536
11	1456493123	782200294.6	53.7	1562136.64	152	0.001015827	1293.390667
12	1093872931	631835935.6	57.76	1103494.16	92	0.000936919	1192.922445
13.1	1361573060	809592300	59.46	1396328.16	130	0.000959357	1221.491788
13.2	1327198849	747364420.4	56.31	1244731.85	135	0.000874009	1112.822482
14.1	790612224.1	409629296.5	51.81	701131.27	76	0.000809981	1031.300264
14.2	492798425	275176207	55.84	495341.4	53	0.000894919	1139.446235
15.1	904968657.4	488256949.3	53.95	877090.08	83	0.000894046	1138.335199
15.2	602901474.7	301367530.7	49.99	565240.65	64	0.000848588	1080.455842
16.1	1014495523	527249580	51.97	1032590.84	115	0.000952092	1212.241694
16.2	570058982.7	326603319.3	57.29	569607.9	53	0.000902454	1149.040249
17.1	974012329.3	492132771.4	50.53	900768.67	98	0.000859978	1094.958177
17.2	482241015	243874381.1	50.57	486468.59	52	0.000897429	1142.641648
17.3	225391756	115752158.7	51.36	213596.74	27	0.000799037	1017.365538
17.4	357735153	218210927.9	61	322133.04	29	0.000766608	976.0757699
17.5	315770343	192293381.1	60.9	332326.81	36	0.000909503	1158.015143

Bibliography

[1] R. M. German: *„Sintering Theory and Practice"*. John Wiley & Sons, Inc., 1996, pp. vii, 1–2, 4, 7–8, 12–13, 17–19, 23–24, 27, 69, 79, 80, 82, 94, 96, 143–147, 150

[2] A. F. Holleman, E. Wiberg: *"Inorganic Chemistry"*. Academic Press, 2001, p. 1011

[3] M. N. Rahaman: *"Ceramic Processing and Sinetring"*. Second Edition, Marcel Dekker, Inc., 2003, pp. 49, 51 – 52, 55, 373

[4] R. H. Perry, D. W. Green, J. O. Maloney: *"J. O. Perry's Chemical Engineers' Handbook"*. 6th ed., McGraw-Hill, New York, 1984, Sec. 8

[5] G. C. Lowrinson: *"Crushing and Grinding"*. Butterworth, London, 1974

[6] J. K. Beddow: *"Particulate Science and Technology"*. Chemical Publishing Co., New York, 1980

[7] R. Polke, R. Stadler: *"In Concise Encyclopedia of Advanced Ceramic Materials"*. R. J. Brook ed., MIT Press, Cambridge, MA, 1991, pp. 187–193

[8] L. Özmerih: *"Optimization of a Fluidized Bed Opposed Jet Mill and Energy-Product Size Relations for Various Industrial Minerals in such Mills"*. Department of Geology and Mining, Norwegian University of Technology and Science, Trondheim, Norway, 1989

[9] www.comex-group.com, Comex AS, P.O. Box 53, 1309 Rud, Norway

[10] J. S. Chapell, T. A. Ring, J. D. Birchall: *"Particle Size Distribution Effects on Sintering Rates"*. J. Appl. Phys., Vol. 60, 1986, pp. 383 – 391

[11] E. A. Barringer, R. Brook, H. K. Bowen: *"The Sintering of Monodisperse TiO_2"*. Sintering and Heterogeneous Catalysis, G. C. Kuczynski, A. E. Miller, G. A. Sargent (Eds.), Plenum Press, New York, 1984, pp. 1 – 21

[12] H. Kellerwessel: *"Aufbereitung disperser Feststoffe: mineralische Rohstoffe, Sekundärrohstoffe, Abfälle"*. VDI Verlag GmbH, Düsseldorf, Germany, 1991, pp. 29, 30, 33, 35, 60, 61

[13] H. Schubert: *„Aufbereitung fester mineralischer Rohstoffe"*. Volume 1, 3rd Edition, VEB Deutscher Verlag für Grundstoffindustrie, Leipzig, Germany, p. 194

[14] E. E. Underwood: *"Quantitative Stereology"*. Addison-Wesley Publishing Company, 1970, pp. 2, 24 – 25

[15] Ø. Nielsen, L. Arnberg, A. Mo, H. Thevik: *„Experimental Determination of Mushy Zone Permeability in Aluminium-Copper Alloys with Equiaxed Microstructures"*. Metallurgical and Materials Transactions A, Volume 30 A, September 1999, pp. 2455 – 2462

Chapter 5

EXPERIMENTAL

This chapter presents the design of the experimental set-up and the experimental conditions. Further, chapter 5 comments on the experimental proceedure regarding melt preparation, sampling and subsequent analysis.

Batch experiments were carried out to get a first impression of how AlF_3 would behave in the environment of molten aluminium and the presence of alkali or magnesium. These experiments were later extended to study the fading of fluorine from AlF_3 when exposed to an aluminium melt.

However, the focus was on designing and building an AlF_3 filter on a laboratory scale that could be used to reveal the kinetics of the filter material. Changing one parameter at a time, pure aluminium melts as well as two different AlMg –alloys containing different levels of Na or Ca were filtered through a bed of the AlF_3 grains. Chemical reaction products produced when dissolved impurities go out of solution may be deposited instantly upon reaction or at sites downstream in the same filter. The deposits together with the release of fluorine as AlF (g) and AlF_3 (g) may cause a

deactivation of the AlF_3 filter grains. On the other hand, if surface active, the deposits may improve the capture of suspended particles in the melt.

A study of the removal of suspended particles did not give reproducible results. This may be explained by the design of the laboratory scale AlF_3 "active" filter as well as by the sampling technique. A filter outlet diameter of 2mm creates a thin stream of metal which has a large ratio of surface to volume and, therefore, is expected to generate an uncontrollable amount of oxide inclusions before and during sampling. Also, the melt sampled in crucibles could not be processed directly but was left to solidify and remelted later. Thus, a conclusion is that experiments should be carried out in an industrial setting to ensure proper sampling conditions for the study of the removal of suspended particles.

5.1 Batch Experiments

5.1.1 Introductory Experiments

Figure 2.1 shows that in the presence of fluorine alkali or Mg will form stable metal fluorides. The effect of molten aluminium and high temperature on the degradation of AlF_3 are illustrated by Equation 2.2 and Figure 4.4. A batch experiment was carried out to get an impression of the behaviour of the Al-F-Me system compared to the Al-O-Me system where Me may be an alkali metal or magnesium. Thus, 0.5 kg melt of a commercial Al7Si0.3Mg alloy was prepared. Alumina balls (industrial filter material) and AlF_3 pellets of equal size (∅ ~18mm) were placed in small graphite crucibles. The melt was poured into the crucibles which had been preheated together with the samples in a small resistance-heated furnace. The crucibles were put into the furnace heated to 780°C and covered with a thin insulating plate. The experimental set-up is sketched in Figure 5.1.

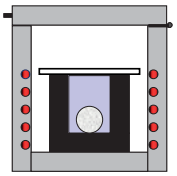

Fig. 5.1: Experimental set-up for introductory holding experiments in a batch

The mass of the samples was determined before the experiment as well as after 7 hours and 63 hours exposure, when recovered from the melt to record possible mass losses. A second sample was taken out of the furnace at these times but kept immersed in the melt for metallographic sample preparation and subsequent analysis by electron microprobe. The metal cylinders with the cast-in AlF_3 pellets were cut into halves to obtain a cross-section of the pellet. The halved cylinders were molded in resin. The specimen were ground with SiC papers up to a fineness of 2000 grit and polished on a hard and a soft cloth with diamond paste of grade 6 and 1µm, respectively. A prepared metallographic sample is shown in Figure 5.2. Chemical analysis by optical emission spectroscopy was carried out to record changes in the composition of the melt.

Fig. 5.2: Metallographic sample of the cross-section of a cast-in AlF_3 pellet

5.1.2 Time Dependence of Deactivating AlF_3 Pellets

The experiments described in the previous section indicated that after a certain time of exposure of AlF_3 to molten aluminium all fluorine will be lost from the filter material. For the reasons explained in chapter 2.1 it is believed that the contact with the molten aluminium alone is responsible for the fading of fluorine. The presence of alkali or magnesium does not seem to play a role. Therefore, samples of AlF_3 were exposed to pure molten aluminium for 10h, 20h, 40h, 50h, and 60h at 780°C furnace temperature. Metallographic samples have been prepared for a quantitative analysis of the fluorine concentration by electron microprobe mapping (for 10h and 50h exposure) as well as point measurements. Point measurements were taken from the surface towards the center of the sample at a step width of 2mm.

5.2 Filtration Experiments

5.2.1 Experimental Setup

The AlF_3 filter was designed and built with the following in mind: Design and dimensions had to be compatible with the facilities available in the laboratory; and an experimental run should last as long as possible to obtain data on how the efficiency of the filter changes with time. A technical drawing is presented in Figure 5.3.

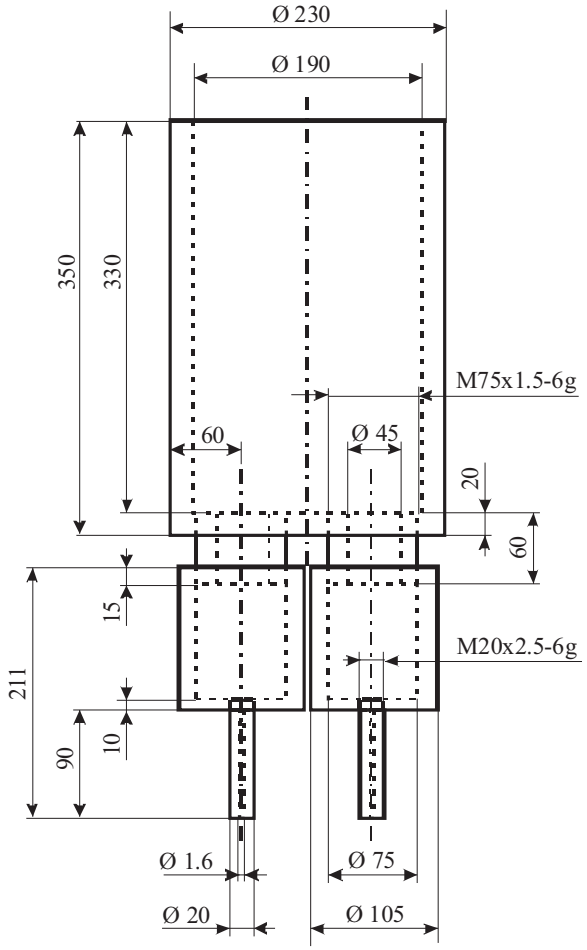

Fig. 5.3: Filter setup including reservoir, AlF_3 and Al_2O_3 filter unit, and outlet tubes

All the parts are machined from graphite. They have a “fibrefrax” coating outside to minimize high temperature oxidation of carbon and provide mechanical protection. Carbon may remove Na as reported in the literature [1]. To passivate the surface and minimize Na absorption by carbon the walls inside the filter units were coated with boron nitride (B_3N_2). Another experimental challenge was the loss of especially Na due to surface oxidation, which makes it difficult to evaluate accurately the contribution of AlF_3 to the Na removal. The solution was to employ a reference dummy filter. Therefore, the setup consists of two filter units fed with melt from a single reservoir. The filter unit contains AlF_3. The Al_2O_3 dummy filter provides similar flow conditions as in the AlF_3 - filter. This makes it possible to quantify the fraction of Na, Ca or Mg removed due to the AlF_3 filter media compared to the Al_2O_3 filter.

The complete filter setup in the cast shop as well as the AlF_3 and Al_2O_3 filter unit can be seen in Figure 5.4 and 5.5, respectively.

Fig. 5.4: Complete filter setup in the cast shop

Fig. 5.5: left – passive filter unit (Al_2O_3), right – active filter unit (AlF_3)

The filter set-up is placed in a furnace for preheating to prevent the melt from freezing upon filter priming. This furnace stands in front of a melting furnace with 150kg capacity (Al). Both furnaces are resistance heated. A steady supply of melt is ensured by tapping melt from the melting furnace into the reservoir which may contain 20kg of melt. After filtration the metal is collected in ingots underneath it. The whole setting is shown in Figure 5.6.

Fig. 5.6: Experimental setting consisting of furnace for melting and cylindrical furnace for preheating

The melt velocity is mainly controlled by the flow resistance in the outlet tube. The pressure drop over the filter and tube is equal to the metal head. The residence time, τ, of the melt in the filter was chosen to be 20 seconds what corresponds to a volume flow of $\dot{V} = 8.91 \cdot 10^{-6}\, m^3/s$ or a mass flow of $\dot{m} = 0.021 kg/s$. $\dot{V}$ and $\dot{m}$ are calculated as follows:

$$\dot{V} = \pi R^2 H_F \varepsilon / \tau \tag{5.1}$$

$$\dot{m} = \dot{V} \rho \tag{5.2}$$

where ρ is the density of molten aluminium at 750°C, R the radius, H_F the height, and ε the void fraction of the filter bed, respectively. The pressure drop, ΔP, is equal to the sum of the metallostatic pressure in the filter and outlet tube and given by Equation 5.3

$$\Delta P = (L + H_F) g \rho = H_M \cdot g \cdot \rho \tag{5.3}$$

where L is the length of the outlet tube, H_M the metal head, and g the gravitational acceleration. The inner diameter that will give the necessary flow resistance may be estimated by the Hagen – Poiseuille [2] law given by Equation 5.4

$$\dot{V} = \frac{\pi \cdot \Delta P \cdot R_0^4}{8 \cdot \mu \cdot L} \tag{5.4}$$

where μ is the dynamic viscosity of the melt and R_0 the inner diameter of the exit pipe. Strictly, ΔP in the Hagen – Poiseuille equation should be slightly less than given

by Equation 5.3. There is a slight pressure drop in the filter due to the metal flow. The parameters and their respective values employed in the calculation are summarized in Table 5.1. A radius of 0.8mm was calculated for R_0 according to the Hagen – Poiseuille equation. There was a variation of ± 0.1mm of the inner radius of the outlet tube which was due to machining tolerances in the workshop. However, the variations in melt flow velocity were larger than could be explained by these tolerances.

Table 5.1: Parameters and their respective values employed in the calculation

τ	$20s$
μ	$1.85 \cdot 10^{-3} Pa \cdot s$ [3]
ρ	$2350 kg/m^3$
g	$9.81 m/s^2$
ε	0.45
R	$0.0375m$
L	$0.1m$
H_F	$0.09m$
H_M	$0.455m$
R_0	$0.8mm$ *(calculated)*

5.2.2 Melting – Alloying – Sampling

The melt was prepared from pure russian Al 99.7 (~ 0.12wt% Fe) with additions of metallic Na (≈ 0.8g Na/kg Al) or Al10Ca master alloy (0.5g Al10Ca/ kg Al). The amount of Na and Ca added is in the range of concentrations typically met in the primary (Na) and secondary sector (Ca). Furthermore, aluminium alloys containing 0.2wt% Mg and 4.7wt% Mg were filtered to study the selective removal of Na from Al-Mg alloys. 0.1 grams of Na per kilogram Al were added to obtain Na levels experienced after alloying Mg in the industry. The complete analysis of the Al-Mg0.2 and the Al-Mg4.7 alloy is given in Table 5.2.

Table 5.2: Chemical composition of Al-Mg0.2 and Al-Mg4.7 alloy before adding Na or Ca

Alloy	**Element**								
	Mg	***Mn***	***Cu***	***Fe***	***Si***	***Ti***	***Na***	***Ca***	***Sr***
Al-Mg0.2	0.2159	0.7943	0.5989	0.4482	0.1919	0.0854	0.00019	0.0003	0.0002
Al-Mg4.7	4.6109	0.3435	0.0680	0.2653	0.1150	0.0204	0.00000	0.0000	0.0000

After melting the Na or Ca additions were submerged and stirred into the melt at a temperature of 800°C using a small perforated steel basket welded on a rod. The recovery of Na added was ≈ 0.2g Na/kg Al or 25%. The recovery of Ca added was ≈ 0.4g Al10Ca/ kg Al or 80%. The melt was tapped at a temperature of around 800°C. Figure 5.6 presents a typical example of the temperature evolution in the melt reservoir during the experiment. The temperature peaks are when melt is tapped from the melting furnace. The temperature drops with time and decreasing level of melt in the reservoir.

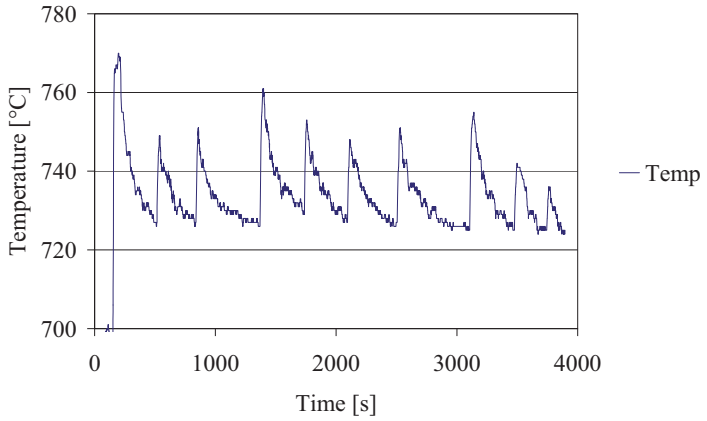

Fig. 5.6: Typical temperature evolution in the melt reservoir during the course of one experiment

Melt was sampled in crucibles held below the exit pipes two times during each filtration experiment. The melt flow velocity was determined from sampling time and sample mass. For chemical analysis disc samples have been taken at regular intervals from the melt reservoir and at the two filter outlets. Deposits at the filter grains that result from alkali or Mg reacting with AlF_3 will be called filter residues in the following. Filter residues and filter grains from the used AlF_3 filter and crushed alumina from the reference filter have been picked for further analysis. The residues as well as the alumina and AlF_3 grains were ground to fine powder in a mortar. Further, AlF_3 grains were molded in resin. The specimens were ground with SiC papers up to a fineness of 2000 grit and polished on a hard and a soft cloth with diamond paste of grade 6 and 1μm, respectively. Figure 5.7 shows some spent material from the AlF_3 filter. The metal runs off completely when the filter is drained. The residues may tend to flake off at room temperature.

Fig. 5.7: Spent filter material from the "active" AlF_3 filter

5.2.3 Analysis

The chemical analysis to quantify the effect of the AlF_3 filter on the level of alkali or Mg in the melt was carried out by optical emission spectroscopy. Two different ways of X-ray analysis have been used to look at the AlF_3 filter residue and exposed filter grains of both the AlF_3 filter and the Al_2O_3 filter. Ground filter residue and grains of both filters were subjected to a XRD analysis in a Philips PW 1730/10 to identify the various compounds present. The distribution of elements in the "active" filter media itself was determined by point measurements and mappings using a JXA-8900 EPMA

(electron probe microanalyzer). Temperature versus time was recorded once a second using the Campbell CR23X Scientific Micrologger together with a Type – K thermocouple.

5.2.4 Experimental Conditions

The concentrations of alkali and Mg, the melt temperature and the mass flow was varied in addition to the surface area of the filter. These data for the experiments performed are presented in chapter 6.

Bibliography

[1] J.-D. Bornand, K. Buxmann: *"DUFI: A Concept of Metal Filtration"*. Light Metals, 1986, pp. 1249 – 1260

[2] H. Netz: *"Formeln und Sätze der Physik"*. Hanser, Munich; Vienna, 1991, p. 57

[3] T. Iida, R. I. L. Guthrie: *"The Physical Properties of Liquid Metals"*. Clarendon Press, Oxford, 1988, pp. 150, 183

Chapter 6

RESULTS

6.1 Batch Experiments

6.1.1 Introductory Experiments

Table 6.1 lists the mass of the Al_2O_3 and AlF_3 pellets and shows how the mass of the AlF_3 pellets changes with time exposed to aluminium melt at 780°C furnace temperature. There was no measurable mass loss for the Al_2O_3 pellets. Figure 6.1 shows the changing mass of the AlF_3 pellets in mass percent versus time. The mass loss is proportional to the exposure time.

Table 6.1: Mass of Al_2O_3 and AlF_3 pellets in air dependent on time exposed to molten aluminium ($T_{Furnace}$ = 780°C)

Material	Mass (g) at time (t)		
	0h	***7h***	***63h***
Al_2O_3	12.38	± 0	± 0
Al_2O_3	14.14	± 0	± 0
Al_2O_3	16.32	± 0	± 0
Al_2O_3	15.16	± 0	± 0
AlF_3	5.18	5.09	-
AlF_3	4.87	-	-
AlF_3	4.96	-	4.24
AlF_3	4.91	-	-

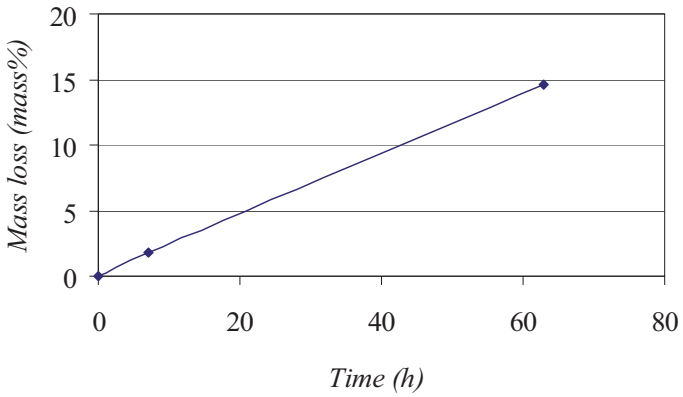

Fig. 6.1: Changing mass of the AlF_3 pellets in air in mass percent versus exposure time ($T_{Furnace}$ = 780°C)

The extraction of Mg from the bulk melt was followed up quantitatively by chemical analysis. The evolution of the Mg content with time for crucibles containing either Al_2O_3 or AlF_3 filter media is shown in Table 6.2. Figure 6.2 illustrates graphically the dependence of the Mg content on holding time and filter media. The content of Mg in the bulk melt decreases linearly with time for crucibles containing Al_2O_3. In contrast the level of Mg initially seems to drop exponentially with time in crucibles where AlF_3 had been immersed in the melt. The decrease in Mg initially exceeds the loss obtained

in the case of Al_2O_3. However, in both cases the concentration of magnesium seems to approach the same value at long times.

Table 6.2: Mg content in bulk melt depending on holding time and filter media ($T_{Furnace}$ = 780°C)

Time	wt% Mg	
	Al_2O_3	AlF_3
0h	0.38929	0.38929
7h	0.34827	0.21924
63h	0.03318	0.02275

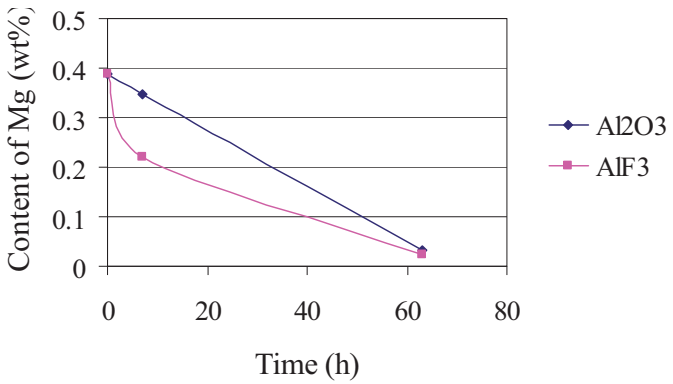

Fig. 6.2: Dependence of Mg content on holding time and filter media ($T_{Furnace}$ = 780°C)

The pictures in Figure 6.3 and 6.4 are taken by electron microprobe and show a qualitative mapping of the AlF_3/melt (top/bottom) interface with respect to F, Mg, O (6.3) and Al (6.4) concentration (area %) as well as possible compounds of these elements. A certain colour is assigned to each element as well as compound as can be seen in the scale bar. The brightness indicates the concentration of the single elements or compounds and increases with increasing concentration. Figure 6.3 shows the interface after 7h holding time. There is a large excess of F compared to the Mg present. Both elements accumulate at the interface forming a distinct layer of MgF_2. The accumulation of F and Mg proceedes, thus, after 63 hours this effect is even more

pronounced as shown in Figure 6.4. The formerly continuous layer is broken up and irregular in shape. Some MgF_2 can be even found in the bulk AlF_3. This may well be a result of sample preparation. In addition, almost all F has vanished.

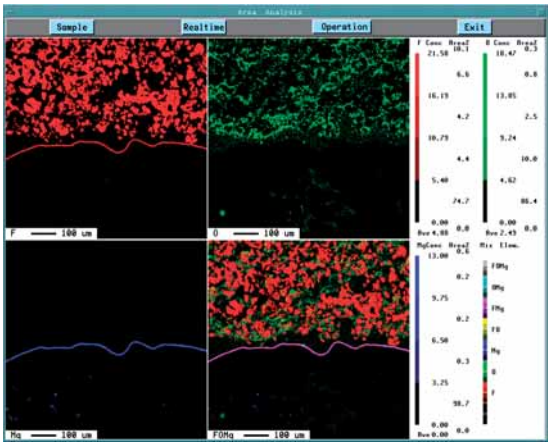

Fig. 6.3: Electron microprobe mapping of AlF_3/melt (top/bottom) interface with respect to F, Mg and O concentration after 7h holding time of Al7Si0.3Mg at 780°C

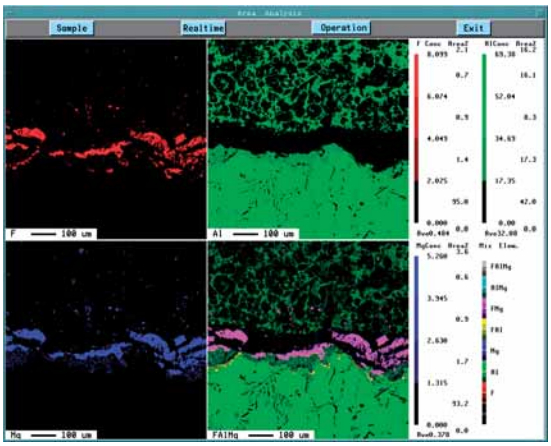

Fig. 6.4: Electron microprobe mapping of AlF_3/melt (top/bottom) interface with respect to F, Mg and Al concentration after 63h holding time of Al7Si0.3Mg at 780°C

6.1.2 Time Dependence of Deactivating AlF_3 Grains in Filter exposed to Aluminium Melt

Discrete (point) measurements performed at a step size of 2mm from the surface towards the center of the sample by electron microprobe (see paragraph 5.2.3 chapter 5) are summarized in Table 6.3. The analysis of a crystal surface is difficult due to its topography and the take off angle changes from point to point because of the facetted crystal surface. This gives different intensities for the same element and quantity. However, the ratio of two elements (const. quantity) should be independent of the take off angle. Therefore, Table 6.3 lists the ratio of F/Al and O/Al including standard deviation versus time. The ratios have been calculated from the mean value of the respective element given in mass percent. A mean value represents four single measurements taken across each sample from the surface towards the center. The F/Al ratios as well as the O/Al ratios change insignificantly during 50 hours of exposure. Between 50 hours and 60 hours of holding time the F/Al ratios and the O/Al ratios change dramatically and decrease or increase by 1400%, respectively. The results presented in Table 6.3 are plotted in Figure 6.5 to illustrate the behaviour of the F/Al and O/Al ratios in dependence of time. The presence of oxygen in the AlF_3 pellets at long times may be explained by the fact that the samples are not entirely covered by the aluminium melt (see Figure 5.2). The samples had contact either with the melt surface or the porous wall of the graphite crucible. This may have enabled the oxygen to diffuse into the AlF_3 pellet taking over sites left vacant by the fluorine released.

Table 6.3: F/Al and O/Al ratios including standard deviations at times of 10, 20, 40, 50, and 60 hours of exposure for AlF_3 grains ($T_{Furnace}$ = 780°C)

Time	Ratio	
	F/Al	***O/Al***
10h	16.2 ± 1.1	0.8 ± 0.5
20h	17.2 ± 1.2	0.9 ± 1
40h	13.7 ± 6.6	0.9 ± 0.7
50h	14.1 ± 3.4	1.0 ± 0.9
60h	0.4 ± 0.1	15.1 ± 6.4

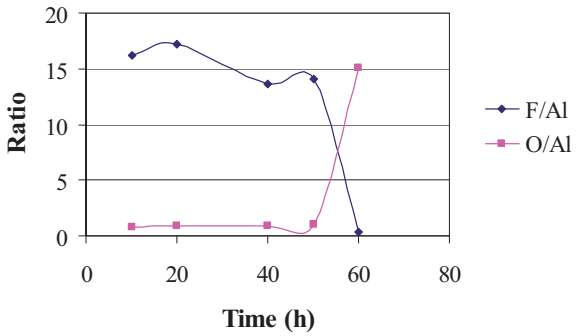

Fig. 6.5: F/Al and O/Al ratios in dependence on exposure time for AlF_3 grains in filter exposed to aluminium melt ($T_{Furnace}$ = 780°C)

Figure 6.6 shows an electron microprobe mapping with respect to the concentration of F across a sample from its centre to the left towards the surface at the right. The sample was exposed to molten aluminium at a furnace temperature of 780°C for 50 hours. A mapping of a sample taken after 10 hours looks the same as the mapping shown in Figure 6.6. The average concentration of F appears to be the same for both mappings and does not change across the sample. However, there are local concentration gradients which are shown by the changing colours in the scale bar.

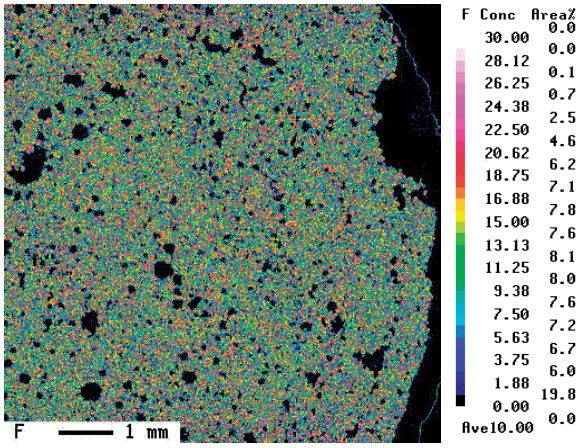

Fig. 6.6: Electron microprobe mapping with respect to the concentration of F across an AlF_3 sample exposed for 50h ($T_{Furnace}$ = 780°C) from its centre towards the surface (left to right)

6.2 Filtration Experiments

Table 6.4 gives a review of the experiments.

Table 6.4: Experimental conditions in AlF_3 filter

Exp. No	Addition	Height of filter bed [z]	Contact Area [$Aa_v z(1-\varepsilon)$]	Mass flow [time - s]	Re_p
1	Na	0.09m	0.248 m^2	18g/s (1200s), 17.1g/s (3300s)	18.8; 17.9
2	Na	0.09m	0.248 m^2	13.6g/s (700s)	14.2
3	Na	0.09m	0.248 m^2	18.3g/s (500s), 17.3g/s (2200s)	19.1; 18.1
4	Ca	0.09m	0.248 m^2	11g/s (700s), 10.2g/s (2500s)	11.5; 10.7
5	Ca	0.09m	0.248 m^2	14.4g/s (500s), 11.7g/s (2800s)	15.0; 12.2
6	Ca	0.09m	0.248 m^2	5g/s (1400s)	5.2
7	Ca	0.045m	0.124 m^2	20g/s (600s), 17g/s (3200s)	20.9; 17.8
8	Ca	0.045m	0.124 m^2	21.2g/s (400s), 23.2g/s (1800s)	22.1; 24.2
9	Ca	0.045m	0.124 m^2	21.3g/s (600s), 19.2g/s (1500s)	22.2; 20.1
10	Ca	0.0225m	0.062 m^2	20.8g/s (500s), 17g/s (1800s)	21.7; 17.8
11	Ca	0.0225m	0.062 m^2	13.6g/s (800s), 11.3g/s (2900s)	14.2; 11.8
12	Ca	0.0225m	0.062 m^2	9.7g/s (500s), 9.5g/s (2000s)	10.1; 9.9
13	Mg0.2Na	0.045m	0.124 m^2	10.3g/s (1100s)	10.8
14	Mg4.7Na	0.045m	0.124 m^2	9.4g/s (1500s), 10.1g/s (3300s)	9.8; 10.6

6.2.1 Evolution of Alkali and Mg in Molten Aluminium before and after Filtration

The graphs in Fig. 6.7a-c show the change with of the respective Na concentrations at the filter inlet and the outlet. The contact area is high 0.248m^2. Melt flow rates are between 18 and 14 g/s. Sodium inlet and Al_2O_3 outlet concentration drop roughly linearly with time. Outlet Al_2O_3 is somewhat lower than the inlet concentration of initially 200 to 250 ppm. Outlet Na from the AlF_3 filter is very low.

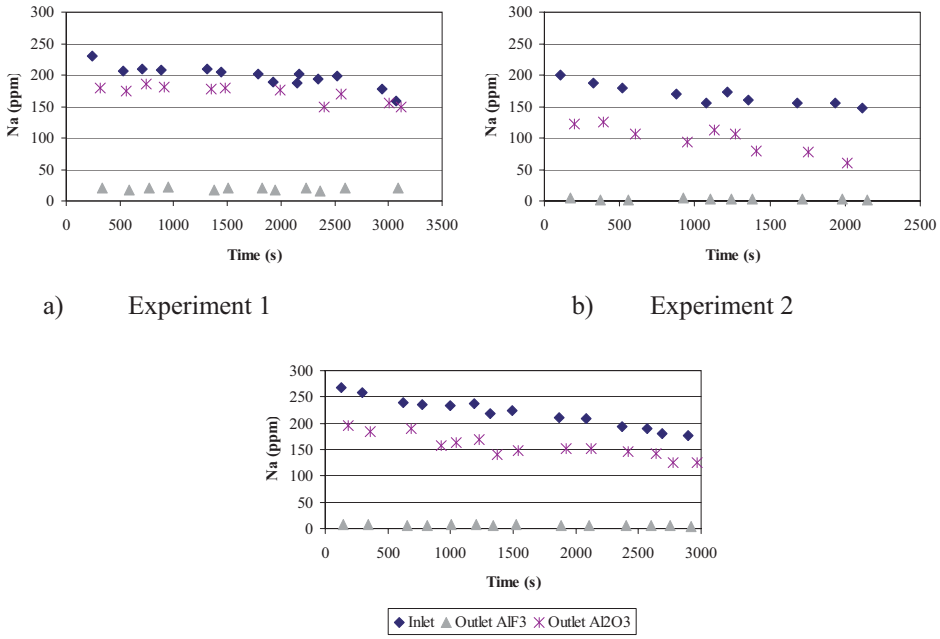

a) Experiment 1

b) Experiment 2

c) Experiment 3

Fig. 6.7a-c: Na – concentration – time curves for filtration experiments 1–3, flow rate 14 to 18 g/s, contact area 0.248m^2.

Figures 6.8a-c present the results for the same filter contact area as in Figure 6.7a-c but for a melt with Ca addition. Melt velocities are between 14 and 5 g/s. Calcium inlet and Al_2O_3 outlet concentration change very little with time. The contact area is high 0.248m^2. Outlet Al_2O_3 is somewhat lower than the inlet concentration of initially 30 to 40 ppm. Outlet Ca from the AlF_3 filter is very low, in the range 1 to 5 ppm.

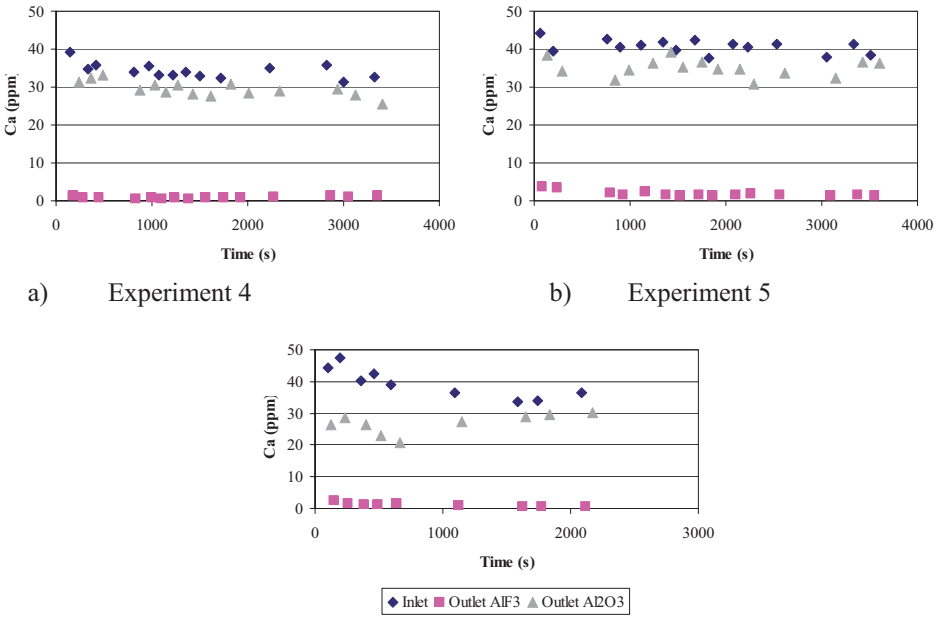

a) Experiment 4

b) Experiment 5

c) Experiment 6

Fig. 6.8a-c: Ca – concentration – time curves for filtration experiments 4–6, flow rate 5 to 14 g/s, contact area 0.248m^2.

The data plotted in Figure 6.9a-c are for high flow rates, 17 to 23 g/s. Calcium inlet and Al_2O_3 outlet concentration change very little with time. The contact area is lower 0.124m^2. Outlet Al_2O_3 is somewhat lower than the inlet concentration of initially 45 to 55 ppm. Outlet Ca from the AlF_3 filter is in the range 10 to 15 ppm.

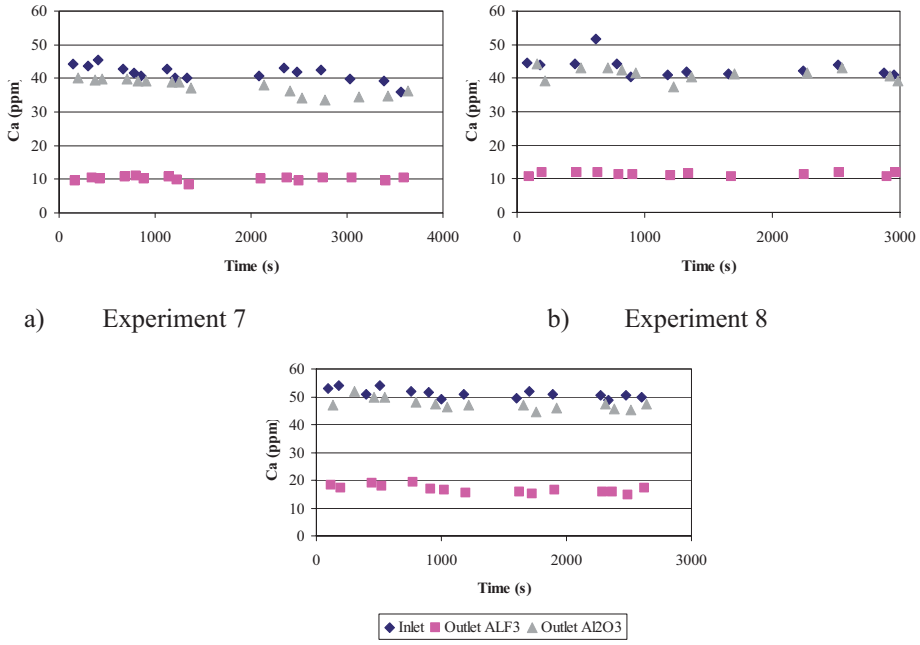

a) Experiment 7

b) Experiment 8

b) Experiment 9

Fig. 6.9a-c: Ca – concentration – time curves for filtration experiments 7–9, flow rate17 to 23 g/s, contact area 0.124m^2.

Ca – concentration – time curves at 0.062m^2 contact area and mass flow rates of 10 to 21 g/s are shown in Figure 6.10a-c. Calcium inlet and Al_2O_3 outlet concentration change very little with time. The contact area is low 0.062m^2. Outlet Al_2O_3 is somewhat lower than the inlet concentration of initially about 50 ppm. Outlet Ca from the AlF_3 filter is between 15ppm and 25 ppm.

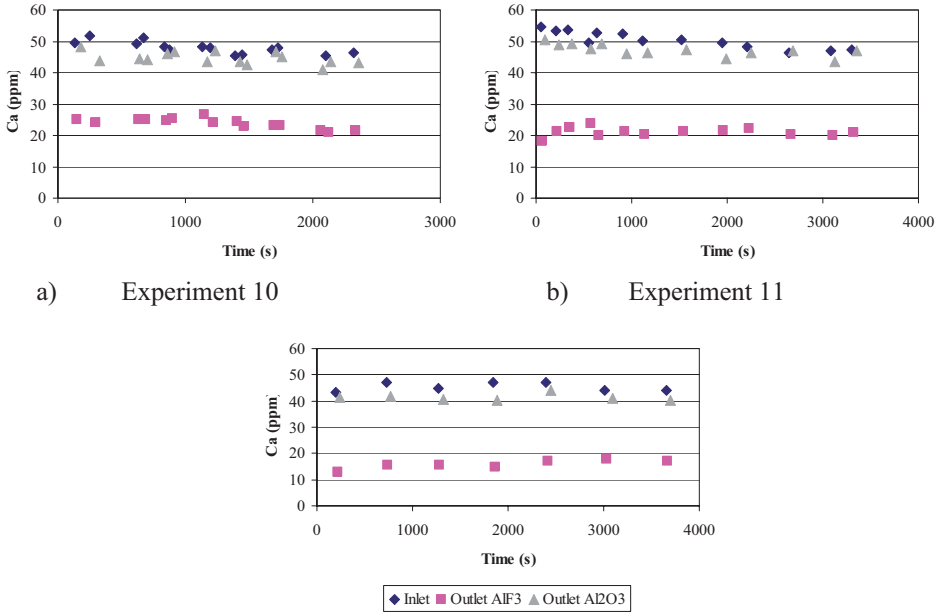

a) Experiment 10 b) Experiment 11

c) Experiment 12

Fig. 6.10a-c: Ca – concentration – time curves for filtration experiments 10–12, flow rate 10 to 20 g/s, contact area 0.062m^2

The Refining of an AlMg0.2 alloy at low input Na levels is shown in Figure 6.11a-b. The flow rate was 10 g/s and the contact area was 0.124m^2.

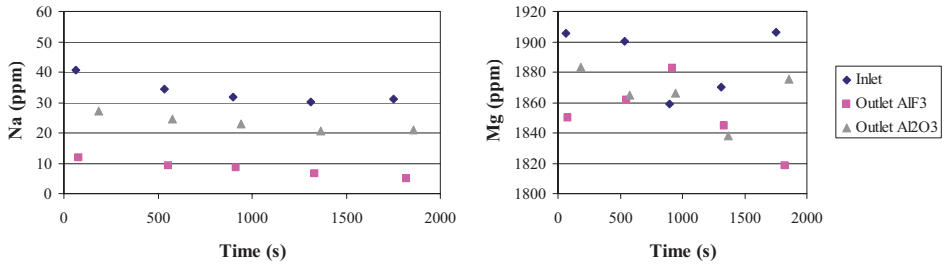

Fig. 6.11a-b: Concentration of Na (a) and Mg (b) with time for filtration experiment 13, flow rate 10 g/s, contact area 0.124m^2

Refining of an AlMg4.7 alloy with respect to low Na levels is shown in Figure 6.12a-b. Flow rates were between 9 to 10 g/s and the contact area was 0.124m^2.

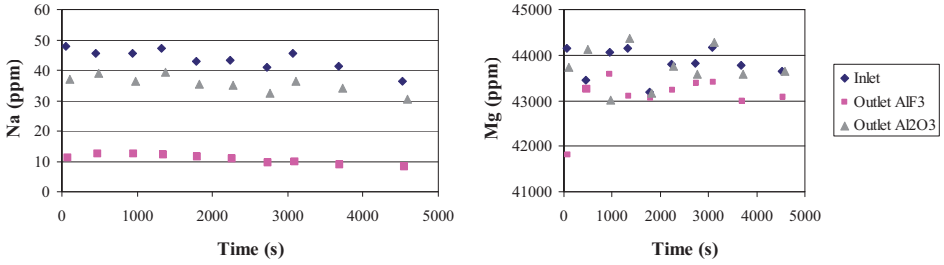

Fig. 6.12a-b: Concentration of Na (a) and Mg (b) with time for filtration experiment 14, flow rate 9 – 10 g/s, contact area 0.124m^2

In Figure 6.11a and 6.12a sodium inlet and Al_2O_3 outlet concentration drop linearly with time. Outlet Al_2O_3 is somewhat lower than the inlet concentration of initially 40 to 45 ppm. Outlet Na from the AlF_3 filter is about 10 ppm.

In Figure 6.11b and 6.12b magnesium inlet levels are high around 1900 and 44000 ppm, respectively. The scatter around these levels looks considerable but is actually less (≤ 1%) than for Na or Ca.

6.2.2. XRD Analysis of spent Al_2O_3, AlF_3 and Filter Residues

The XRD analysis gave graphs which are made up of superimposed single diffraction pattern characteristic of each compound identified. A diffraction pattern for a single compound shows the number of counts (y-axis) in relation to the angle of incidence “theta” (x-axis). The peaks of each pattern identified are designated by the compounds’ name and the colour assigned by the XRD analysis software.

Figures 6.13 – 15 show diffraction patterns obtained from spent Al_2O_3, AlF_3 and filter residues taken from the AlF_3 filter, respectively. The analysis of the alumina gave a composition of mainly Al_2O_3 containing traces of sodium aluminium oxide which is illustrated by Figure 6.13. Figure 6.14 shows the compounds identified in the AlF_3 filter grains which are named in the order of decreasing peak intensity: AlF_3, $Na_5Al_3F_{14}$, and Al_2O_3. AlF_3, BN (boron nitride), SiO_2, NaOCN (sodium cyanate), Al_2O_3 (corundum),

MgF_2, $FeBO_3$ (iron borate), Al3.8Mg3.15Fe1.05(Si1.75Al4.25O20) (Sapphirine 1Tc), $Na_5Al_3F_{14}$ (chiolite), and NaF is the respective order for the compounds identified in the residue shown in Figure 6.15.

The intensity of the peaks forming the different diffraction patterns of this XRD analysis can be regarded as a trend but not as a quantitative measure with respect to the concentration of each compound present in the filter residue and grains of the AlF_3 filter. This is because the equipment was calibrated only for the analysis of the Al_2O_3 grains. The Al_2O_3 filter grains contained 0.26 % sodium aluminium oxide which is in the lower range for such impurities typically found in industrial smelter alumina [1].

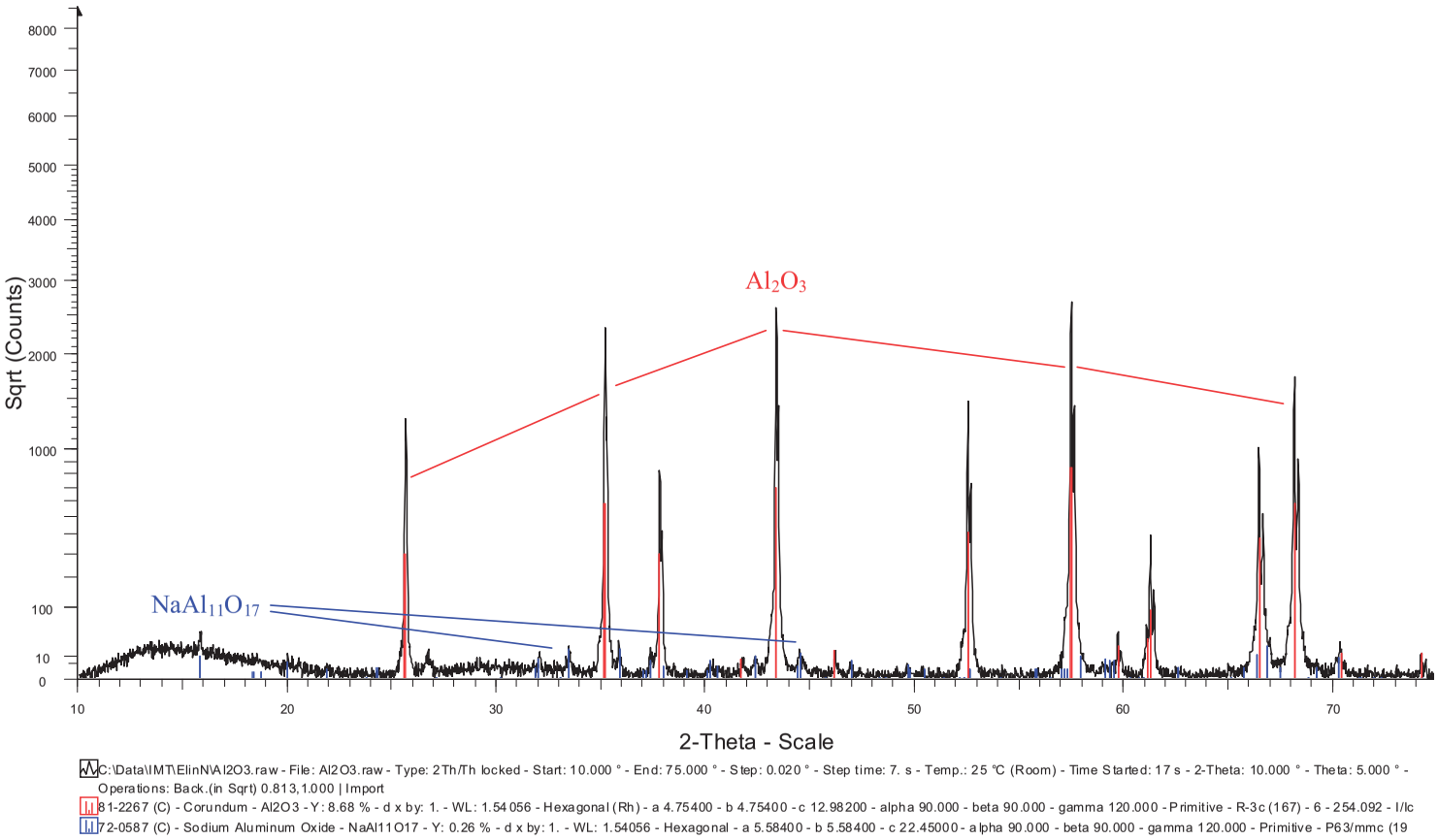

Fig. 6.13: XRD diffraction pattern of spent Al_2O_3 filter grains.

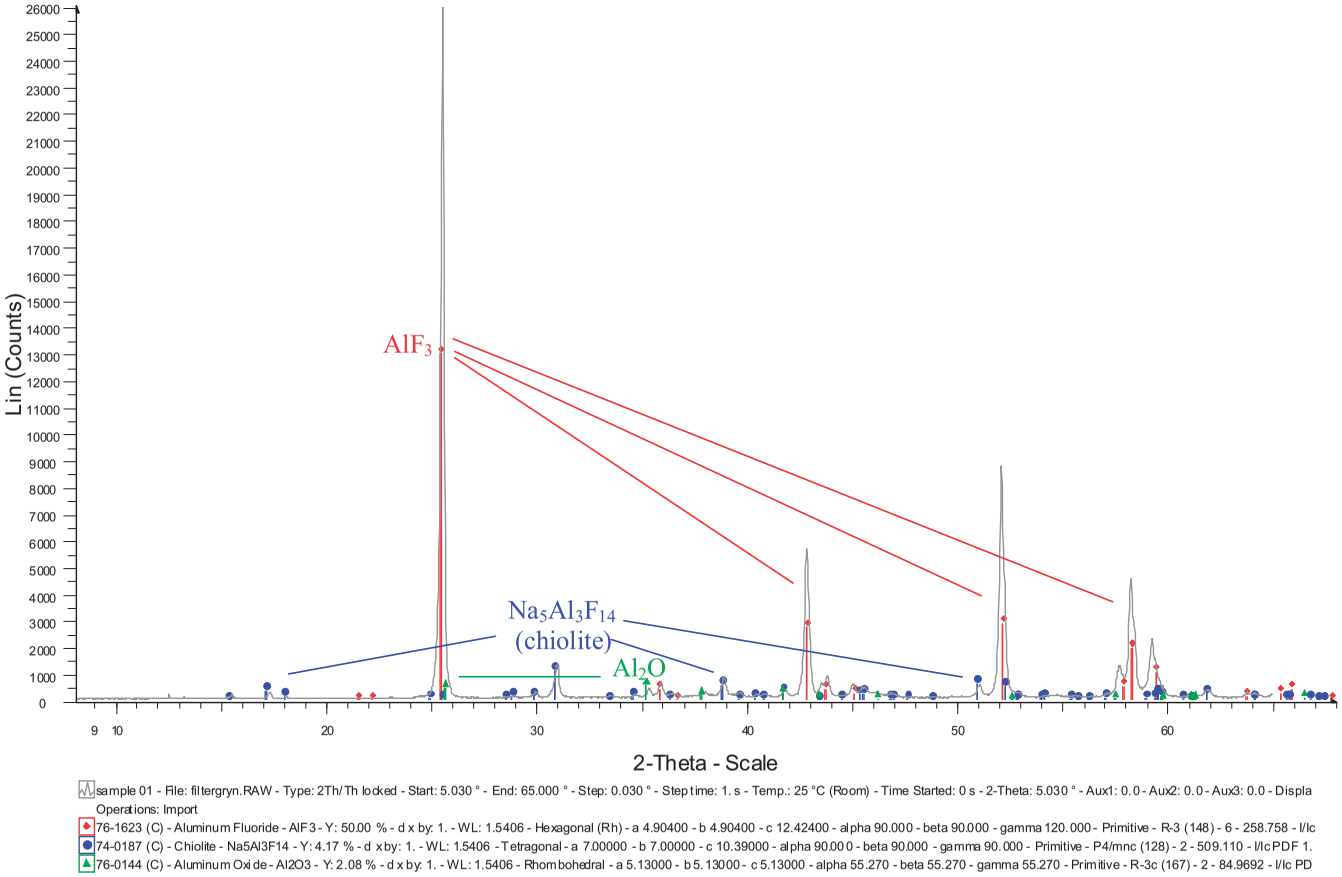

Fig. 6.14: XRD diffraction pattern of spent AlF_3 filter grains.

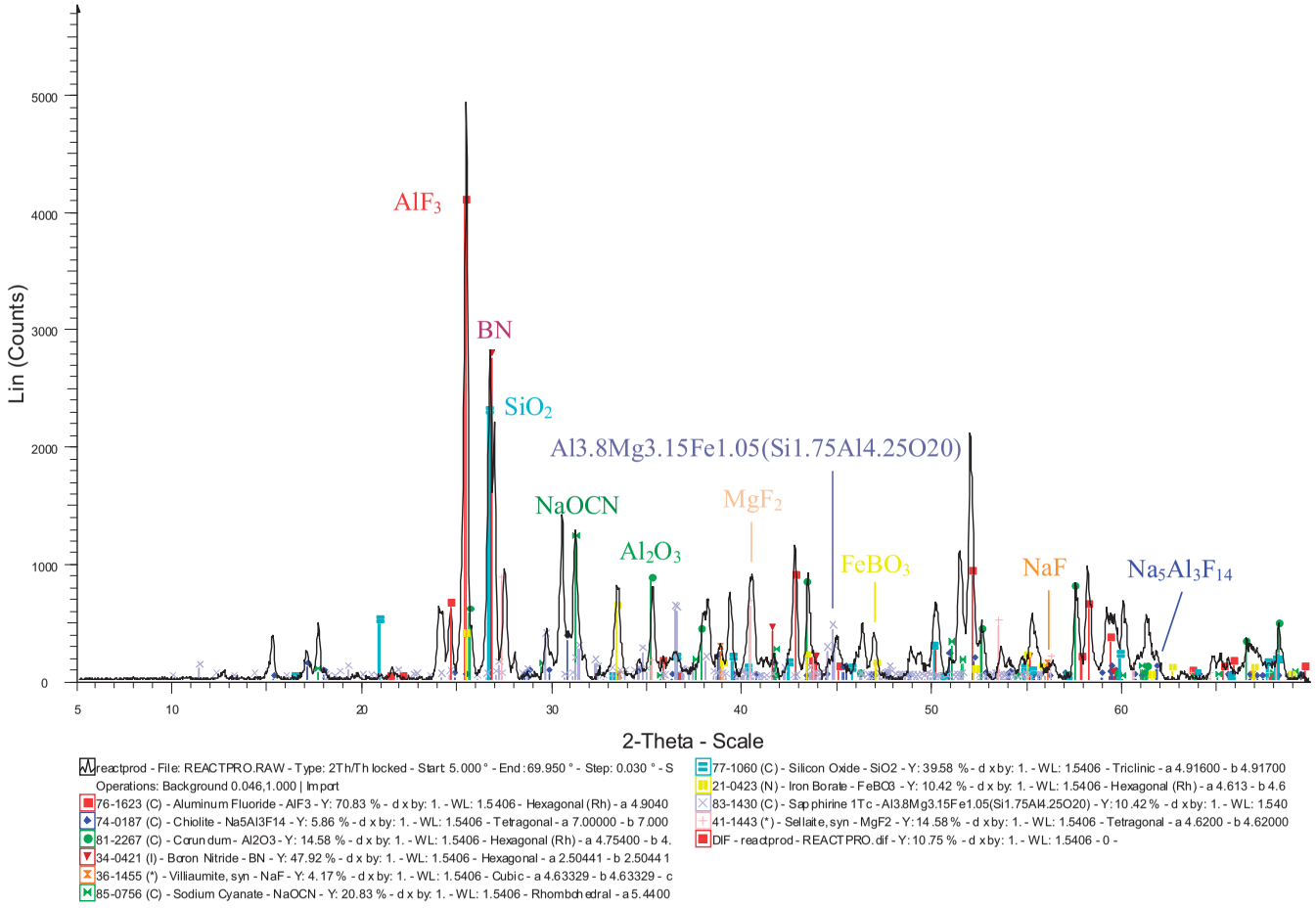

Fig. 6.15: XRD diffraction pattern of filter residues taken from the AlF_3 filter.

6.2.3 Electron Microprobe Measurements

The electron probe microanalyzer mappings in Figure 6.16 and 6.17 show a cross section of an AlF_3 filter grain that has been exposed to a melt bearing Na or Ca, respectively. The mappings cover the elements Al, F, Na, and Ca as well as possible combinations of these elements. However, this method does not give the stoichiometry. Mg is not included here the reason being that the mappings of the filter grains gave only poor evidence with respect to Mg and possible Mg containing compounds. Therefore, the reader may refer to paragraph 6.1.1 and 6.2.2 in this chapter. Figure 6.16 and 6.17 reveal the distribution of Na or Ca throughout the filter grain after being removed from the melt. Na and Ca in Figure 6.16 and 6.17, respectively, show different distribution patterns. The difference is both qualitative and quantitative. In contrast to Ca in Figure 6.17, where Ca barely has been detected, Na and its compounds cover a much larger surface area of the filter grains' cross section. Na in Figure 6.16 is enriched throughout the bulk AlF_3 and in a layer covering the surface of the filter grain. Parts of this layer were lost during sample preparation. In this layer, Na has been found as elemental Na and as part of fluorine bearing compounds (NaF and NaAl). The flake-like Na spots throughout the bulk AlF_3 and its surface belong to a (NaAlF) compound determined as $Na_5Al_3F_{14}$ (chiolite) previously. Figure 6.18a-c shows the variation in Na concentration detected at points in the bulk of the grains moving from top (a) to middle (b) and bottom (c) of the filter bed. Most of the Na is detected close to the inlet of the AlF_3 filter. The concentrations in the middle (b) and bottom (c) of the filter bed decrease slightly towards the outlet and are by far lower compared to the concentrations met close to the inlet of the AlF_3 filter. Ca (Fig. 6.17) could be detected only in a layer at the surface and in the bulk AlF_3 close to the surface of the filter grain. There is a steep gradient in concentration of Ca from the surface towards the centre. At the surface mainly elemental Ca can be found whereas in the bulk Ca is part of a fluorine bearing compound (FCa).

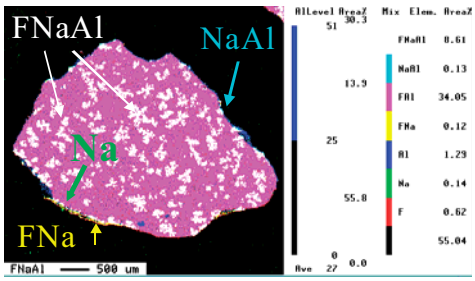

Fig. 6.16: Electron probe mapping tracing Na over the cross section of an AlF_3 filter grain

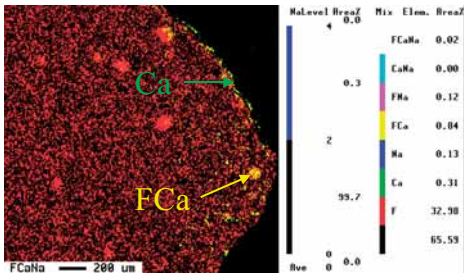

Fig. 6.17: Electron probe mapping tracing Ca over the cross section of an AlF_3 filter grain.

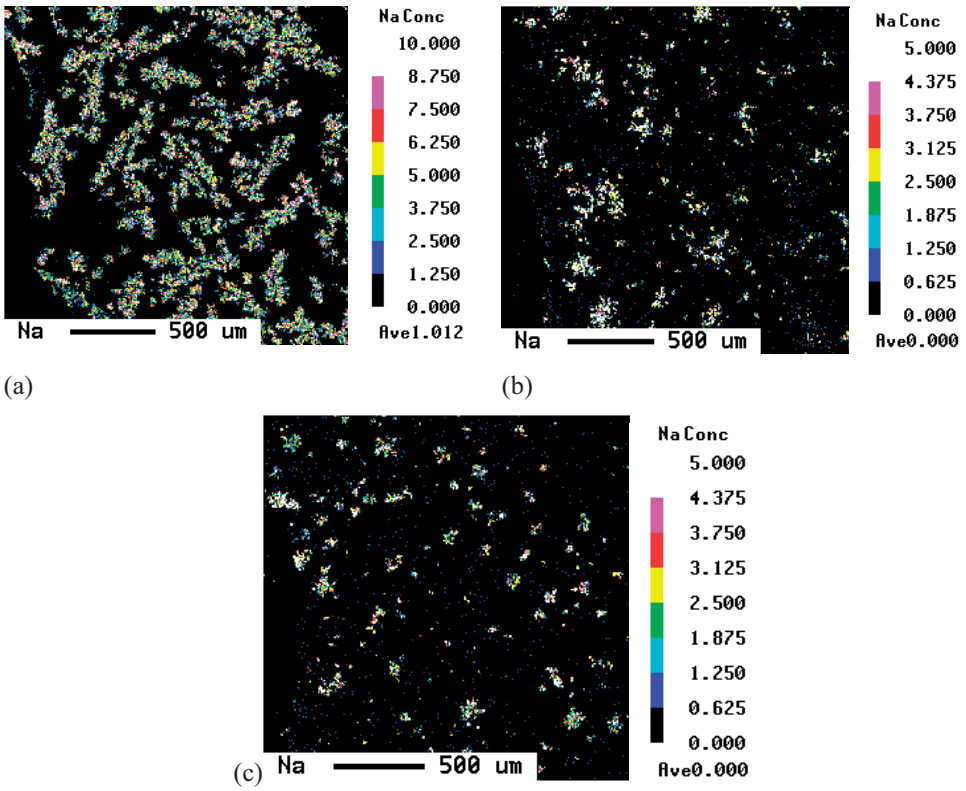

Fig. 6.18a-c: Electron probe mapping showing how Na levels vary in the filter bed moving from top (a) to middle (b) and bottom (c)

Mappings obtained for Ca as shown for Na in Figure 6.18a-c have been omitted. There was so little Ca detected already in the bulk grains at the inlet that the mappings were not illustrative.

Bibliography

[1] K. Grjotheim: *"Nature and Origin of Impurities in the Hall-Heroult Electrolyte and their Effect on Metal Purity"*. International Seminar on Refining and Alloying of Liquid Aluminium and Ferro-Alloys, August 26-28, 1985, Trondheim, Norway

Chapter 7

DISCUSSION AND CONCLUSIONS

The removal of dissolved elements Na, Ca or Mg in the "active" AlF_3 filter is controlled by thermodynamics and kinetics. The framework is the chemistry and thermodynamics of AlF_3 together with the fluid flow of molten aluminium in the filter. Therefore, the first two paragraphs are dedicated to theoretical considerations regarding the mass transfer coefficient as a function of the flow regime and phase diagrams / equilibria for the system under investigation. This will give the basis for the discussion of the results in the subsequent paragraphs. A model that can predict the results obtained experimentally will be derived from first principles at the end of the chapter.

7.1 Chemistry and Thermodynamics of AlF_3 in Molten Aluminium

7.1.1 Phase Diagrams

In the following, the phase diagrams for the systems under investigation, NaF – AlF_3, CaF_2 – AlF_3, and MgF_2 – AlF_3, show the formation of possible phases depending on composition and temperature of those systems. Figures 7.1 to 7.4 display the phase diagrams for the systems CaF_2 – AlF_3, and MgF_2 – AlF_3, NaF - MgF_2, and NaF – AlF_3, respectively.

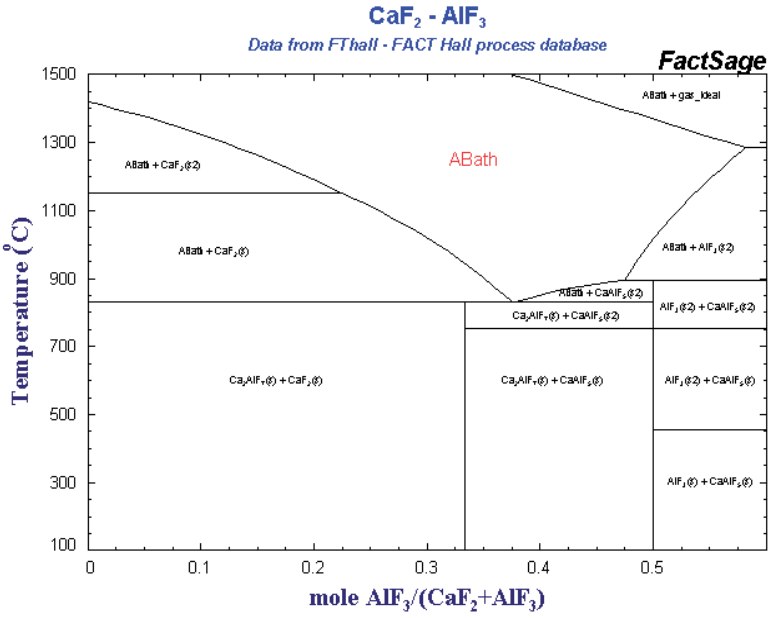

Fig. 7.1 Phase diagram for the CaF_2 – AlF_3 system [1]

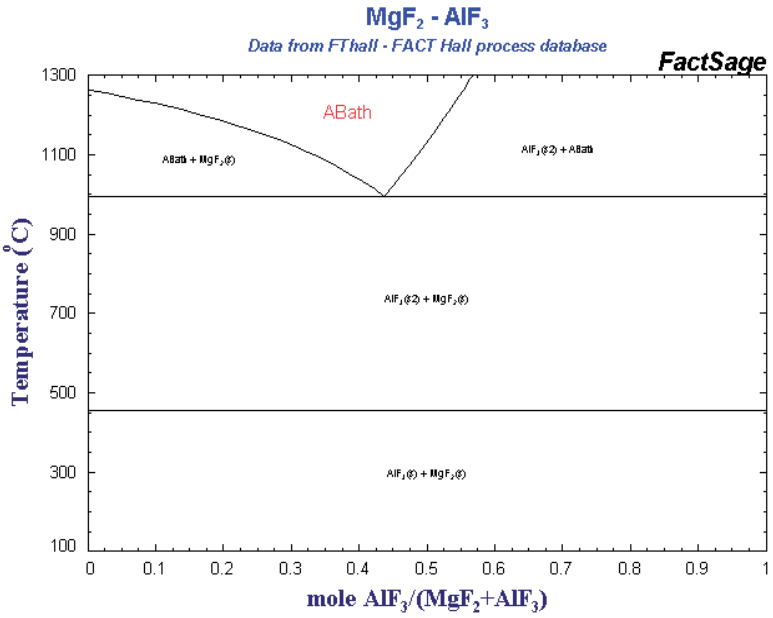

Fig. 7.2 Phase diagram for the MgF_2 – AlF_3 system [1]

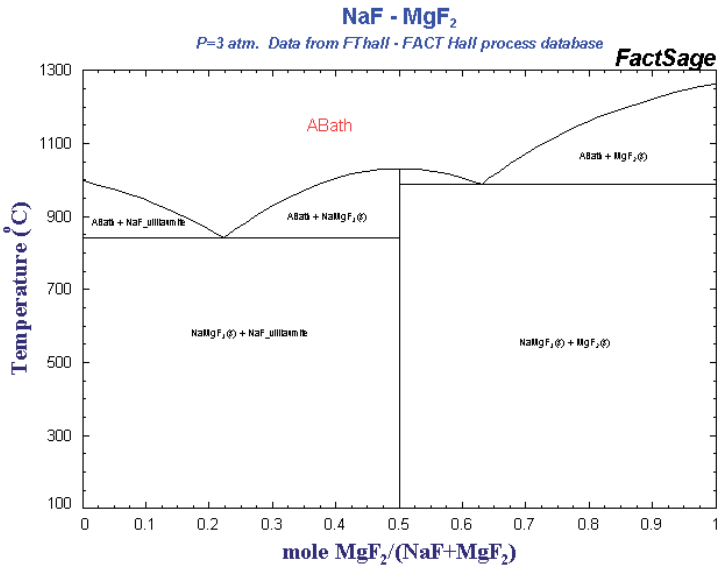

Fig. 7.3 Phase diagram for the MgF_2 – NaF system [1]

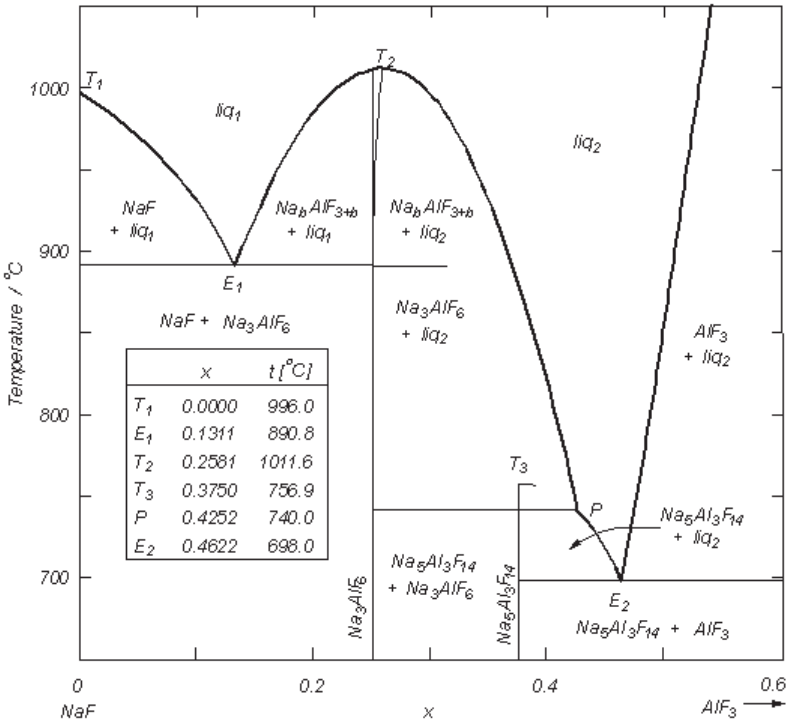

Fig. 7.4 Phase diagram for the NaF – AlF_3 system as given by Solheim and Sterten [2].

The evaporation of Na, Ca, and Mg is included due to their high vapour pressure compared to molten aluminium. Figure 7.5 shows the vapour pressure of pure Na, Mg, and Ca in dependence on temperature. Molten aluminium in comparison exhibits vapour pressures of 10^{-14} to 10^{-9} atm in the range of 550 to 800°C, respectively. Alkali metals and Mg can vaporize as follows [4]:

$$\underline{Na} \rightarrow Na\ (g);\ \underline{Ca} \rightarrow Ca\ (g);\ \underline{Mg} \rightarrow Mg\ (g)$$

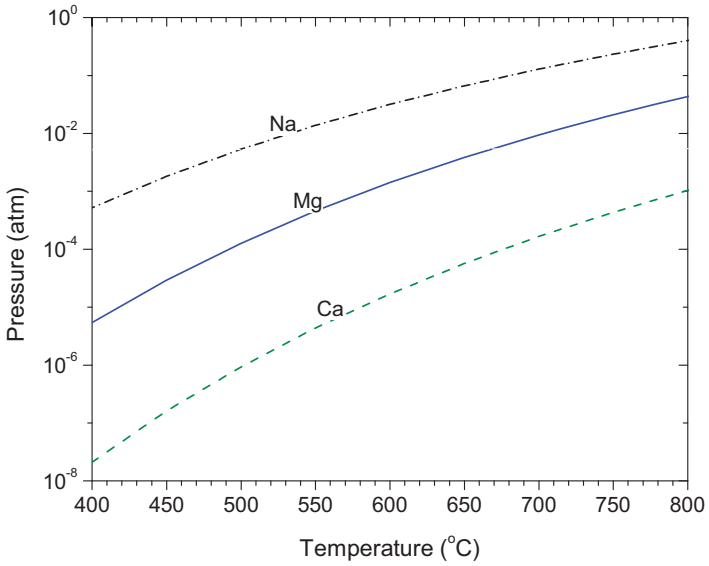

Fig. 7.5 Vapour pressure of pure elements calculated using Fact Sage [1]

According to Waernes et al. the overall reaction for sodium is the following [3].

$$AlF_3\ (g) + 3\underline{Na} = 3NaF\ (l) + Al\ (l)$$

According to the NaF-AlF_3 phase diagram, a liquid phase coexists with AlF_3 in the AlF_3 rich part at a temperature above 694°C. Chiolite ($Na_5Al_3F_{14}$) and AlF_3 are the stable products at equilibrium for the temperatures below 694°C [3].

7.1.2 Equilibrium Concentrations

The equilibrium concentrations for contents of Na and Ca in liquid aluminium in contact with NaF-AlF_3, CaF_2-AlF_3, and NaF-AlF_3-5%CaF_2 fluorides have been calculated using Fact Sage [1]. Those concentrations define the lowest level attainable by AlF_3 filtration. The results are presented in Figures 7.6 – 7.8.

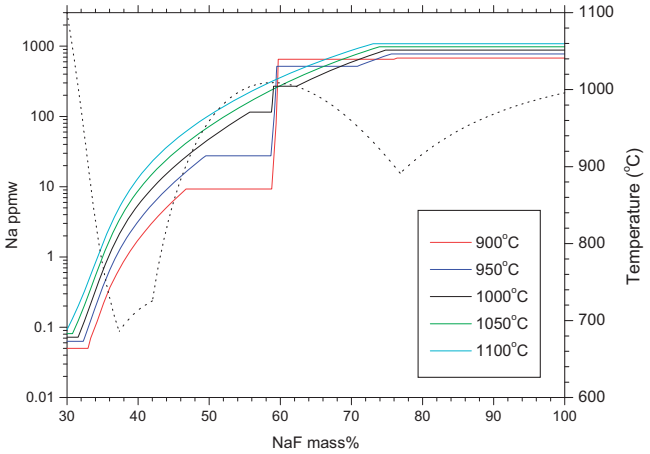

Fig. 7.6 Equilibrium Na contents in liquid Al in contact with molten NaF-AlF_3 fluorides [1].

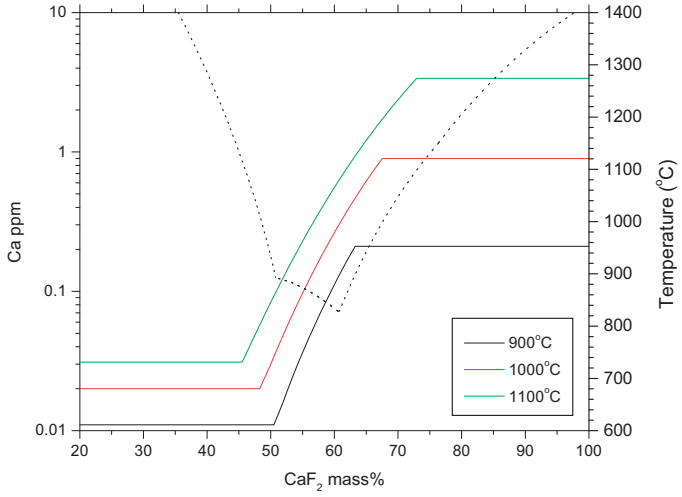

Fig. 7.7 Equilibrium Ca contents in liquid Al in contact with solid CaF_2-AlF_3 fluorides [1].

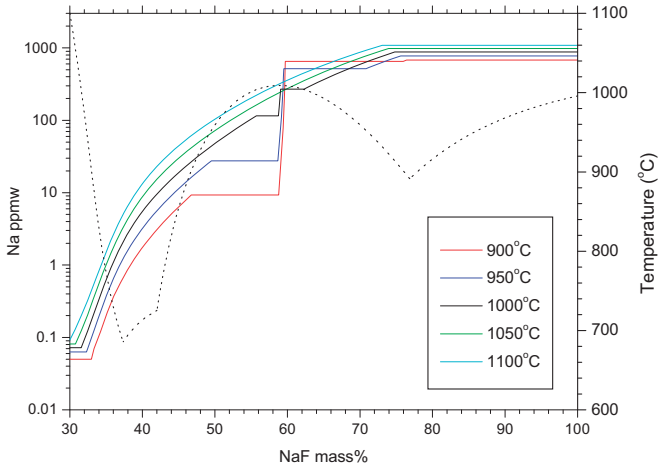

Fig. 7.8 Equilibrium Na contents in liquid Al in contact with molten NaF-AlF_3-5%CaF_2 fluorides [1].

It is seen from Figures 7.6 – 7.8 that at equilibrium with AlF_3, Na and Ca are far below the lower limit for their measurement in aluminium. The equilibrium concentrations for Na and Ca generally increase with increasing temperature as well as for increasing concentrations of NaF and CaF_2, respectively. However, the presence of small amounts of CaF_2 has virtually no effect on the equilibrium concentration of Na in liquid Al in contact with molten NaF-AlF_3-5%CaF_2 fluorides as shown by the calculations in Figure 7.8.

7.1.3 XRD Analysis of spent Al_2O_3, AlF_3 and Filter Residues in the AlF_3 Filter

A metallographic investigation of the exposed filter media and the filter residues by X-ray analysis can provide an insight into the behaviour of AlF_3 in a liquid metal environment, kind and distribution of reaction products and possibly the capture of suspended particles. The elements identified by the XRD in the AlF_3 grains and residue could be divided into two groups “a” (active = AlF_3, MgF_2, $Na_5Al_3F_{14}$, NaF) and “p” (passive = BN, SiO_2, NaOCN; Al_2O_3, $FeBO_3$, Al3.8Mg3.15Fe1.05(Si1.75Al4.25O20)). The active group contains compounds which are involved in reactions of the AlF_3 filter material with dissolved Na or Mg in the melt. The electron probe mappings can possibly

explain the higher levels in MgF_2 compared to NaF found in the residues by the XRD. Both MgF_2 and NaF form at the grains surface. But NaF is probably not stable and therefore reacts further to $Na_5Al_3F_{14}$. Chiolite then can be found throughout the filter grain as well as at the grain surface. According to the NaF-AlF_3 phase diagram, a liquid phase coexists with AlF_3 in the AlF_3 rich part, i.e. at a low concentration of NaF and a temperature above 694°C. Chiolite ($Na_5Al_3F_{14}$) is the stable product at equilibrium for the temperatures in the NaF-AlF_3 phase diagram. [3] The compounds in the passive group may be solids suspended in the melt and captured mechanically or due to adsorption and adhesion phenomena. NaOCN has probably formed in contact with air after the melt had drained off the filter bed.

The level of sodium aluminium oxide found by the XRD in the Al_2O_3 filter grains after filtration was 0.26%. This amount is in the lower range for such impurities typically found in industrial smelter alumina [7]. Sodium can dissolve in, or react with any alumina present [8]. The possible reaction is given by Motzfeldt [9]

$$3Na\ (g) + 2Al_2O_3\ (s) = 3NaAlO_2\ (s) + Al\ (l)$$

According to the results, the removal of Na by Al_2O_3 appears to be negligible in comparison to the amount removed by AlF_3.

7.1.4 Microprobe Measurements of spent Filter Grains

The distribution pattern for Na, Ca, and Mg was given in Figures 6.16, 6.17, and 6.3 – 4, respectively. Figure 6.16 may leave the impression that Na and/or its reaction products are transported away from the melt-filter interface much faster in comparison to Ca (Figure 6.17) and Mg (Figure 6.3 – 4). Therefore, one could expect different transport mechanisms in the grains for Na and Ca as well as Mg. One explanation could be the diffusion of the intermediate NaF into the bulk filter material to form the more stable $Na_5Al_3F_{14}$ (chiolite), thereby enhancing diffusion speed. This is in contrast to the much slower penetration of Ca and Mg which aparently form a stable product directly, possibly CaF_2 and MgF_2. However, according to the NaF-AlF_3 phase diagram, a liquid phase coexists with AlF_3 in the AlF_3 rich part, i.e. at a low concentration of NaF and a temperature above 694°C. Chiolite ($Na_5Al_3F_{14}$) is the stable product at equilibrium in the NaF-AlF_3 phase diagram [3].

The concentration of the fluorine remaining after the contact with the aluminium melt is the same throughout the filter and does not depend on the removal of Na and Ca. However, the concentration of those elements drops from the inlet towards the outlet of the filter as shown for Na in Fig. 6.18a-c. A large portion of the Na entering is removed already at the inlet. Such a distribution is typical for concentration dependent first order kinetics and is in line with Figure 7.10 which can be interpretet to say that about one half of the impurity load is removed in the first quarter of the filter going from inlet to outlet.

7.1.5 Deactivation of AlF_3 Pellets

7.1.5.1 Introductory Experiments

The mass loss proportional to time confirms that there is a steady release of one or more gaseous Al-F compounds when AlF_3 is in contact with molten aluminium. This shows already that AlF_3 is not only suitable for refining operations such as powder injection; AlF_3 is also useful for more continuous operations like filtration in a packed bed. There, the operational times are much longer. The vapour pressure may be high due to the elevated temperature.

Before running into laborious experiments the chemistry of AlF_3 reacting with an element dissolved in molten aluminium was studied. Magnesium as the element to be removed was chosen because of its good addition yield. This allows for better detection and makes magnesium suitable for long-lasting experiments compared to sodium or calcium. Even though the concentration of magnesium is similar at the beginning and end of the experiment for crucibles either containing Al_2O_3 or AlF_3, magnesium is lost at different rates as can be seen in Figure 6.2. This points to a difference in kinetics. In the case of AlF_3 extraction is mainly by chemical reaction to form MgF_2 particularly during the first seven hours. It looks like a first order reaction where rates are decreasing with decreasing concentration of magnesium in the aluminium melt. The low removal of magnesium towards the end of the experiment may be explained by the degradation of AlF_3 which is accompanied eventually by the loss of all fluorine originally contained in the AlF_3. Fluorine was present in excess of the stoichiometric amount necessary to form MgF_2. This may indicate a loss of F without being utilized. In turn, this could

confirm that the degradation of AlF_3 in molten aluminium is independent of the presence of dissolved alkali or magnesium. In the case of alumina, which is considered to be inert with respect to magnesium, magnesium is expected to be lost via surface oxidation of the melt. The formation and distribution of MgF_2 has been qualitatively shown in Figures 6.3 and 6.4. The fact that the product phase forms and deposits at the solid-liquid interface shows the potential of AlF_3 to be used as a filter material.

7.1.5.2 Time Dependence of Deactivating AlF_3 Pellets

The AlF_3 filter grains deactivate with time. It is believed that deactivation is caused due to the contact with the aluminium melt and the exposure to an elevated temperature. This process is slow compared to the removal of the elements disolved in the melt. It is in the order of magnitude of days (holding experiment) compared to the removal of the dissolved elements which can be measured in seconds. This allows for simplifications to be made in the treatment of the kinetics. [20] With respect to mass transfer this case may be treated as a heterogeneous reaction since mass is transported from one phase to a second phase. During heterogeneous reactions diffusion and reaction are separated. The reaction occurs at a reaction interface only (e.g. at the catalyst surface) and the mass transfer coefficient is not influenced by the chemical reaction [16].

As mentioned, over several days the concentration of AlF_3 does change as shown in Figures 6.3 and 6.4. However, the sampling frequency was not sufficient to indicate when the depletion for fluorine is complete and at which rate it proceeds. In 6.1.1 it was shown that after 63 hours all fluorine had vanished from the AlF_3 pellet. Electron microprobe mappings showed a decrease of fluorine concentration with a slight decrease of 17 percent between 10 hours and 50 hours. The remaining 83 percent have been lost during the last 10 hours of the experiment reaching zero percent after 60 hours. This result (Figure 6.6) agrees with the qualitative electron microprobe mappings in Figures 6.3 and 6.4. However, the result does not support that the change of mass is proportional to time as indicated in Figure 6.1. This may be explained by the fact that the point measurements in atomic percent do not properly reflect the stoichiometry of the AlF_3 pellet investigated. Increasing standard deviations of the F/Al ratios between 10 hours and 50 hours may indicate an increase in local concentration gradients, and

hence, a stronger decrease in the average fluorine concentration than suggested by the F/Al ratios in Table 6.3.

A second mechanism for deactivation not due to depletion of fluorine may be due to the adsorption of reaction product on the surface as well as the absorption inside the AlF_3 filter grains. This may hinder or eventually prevent the release of fluorine as well as the contact of the reactants. However, this mechanism is not indicated by the experimental data obtained.

7.2 Kinetics

To develop a mathematical model that can describe the removal of dissolved elements from an aluminium melt data regarding the thermodynamics and the kinetics of the considered system have to be supplied, i.e.

- the equilibrium behaviour, hence the lowest concentration attainable
- the removal rate which is controlled by the resistances at the melt/filter boundary layer and interface

There are two possible rate limiting steps to mass transport for reactions to remove unwanted dissolved elements. In the case of zero order reaction when the rate of the chemical reaction is controlling there is an excess of impurity (vs refining agent) at the reaction interface and the removal of the impurity will be independent of its concentration. In the case of a first order reaction when the rate of the chemical reaction is rapid compared with the rate of diffusion, the removal of the impurity will be dependent on its concentration. [24], [25]

7.2.1 Diffusion Model

First order kinetics controlled by the resistance in the melt boundary layer is assumed. A concentration gradient exists across this thin boundary layer at the melt/filter interface. Applying Fick's first law of diffussion, the flux of species, $\dot{n}_i$ [kmoles/sm^2], across the boundary layer is [24]

$$\dot{n}_i = \frac{D}{\delta}\left(c_i^* - c_i\right) = k_c\left(c_i^* - c_i\right) \tag{7.1}$$

where D is the diffusion coefficient, δ the boundary layer thickness, c_i^* and c_i are concentrations of the diffusion species at the interface and in the bulk, respectively. The term D/δ is used seldom; instead, the mass transfer coefficient, k_c, is used to represent D/δ. For a fluid phase δ is a function of the fluid's velocity along the interface, thereby decreasing with increasing velocity. Thus, k_c is a function of the fluid dynamic condition. c_i^* is difficult to determine experimentally. The equilibrium concentrations for Na and Ca in the presence of Al, AlF_3, NaF and CaF_2, respecively, are far below 1ppm as illustrated in Figures 7.6 and 7.7. Therefore, the concentrations of Na and Ca at the melt / filter interface can be considered to be zero and Equation 7.1 reduces to [24]

$$\dot{n}_i = -k_c c_i \tag{7.2}$$

Now, the amount of impurity being removed from the melt equals the amount of impurity being transferred to the filter. A mass balance for a differential slice of the packed bed in the vertical direction gives

$$-\dot{V}dc_i = k_c c_i A a_v (1-\varepsilon) dz \tag{7.3}$$

where $\dot{V}$ is the flow rate [m^3s^{-1}], A is the cross sectional area of the packed bed [m^2], a_v [m^2/m^3] the specific surface area of the filter grains given as surface to volume, ε the void fraction, and z the hight of the packed bed [m]. Integration over the height, of the packed bed yields*

$$c_i^{out} \Big/ c_i^{in} = \exp\left(-\frac{k_c A a_v (1-\varepsilon) H}{\dot{V}} \right) \tag{7.4}$$

c_i^{in} and $c_i^{out} = c_i(z = H)$ being the inlet and outlet concentrations, respectively of the element i. The exponent may be regarded as a dimensionless contact area, A^*. [6]

$$A^* = \frac{k_c A a_v (1-\varepsilon) H}{\dot{V}} \tag{7.5}$$

It should be pointed out that the integration should be along the flow path through the filter. Equation 7.6 gives the efficiency, E, as the ratio between the amount removed and the inlet concentration.

$$E = \frac{c_{in} - c_{out}}{c_{in}} = 1 - \frac{c_{out}}{c_{in}} \tag{7.6}$$

The efficiency, E, can be expressed in terms of the dimensionless contact area, A^*.

$$E = 1 - \exp(-A^*) \tag{7.7}$$

As an exponential function Equation 7.7 may be approximated by a power series expansion as follows [22].

$$e^{-A^*} \approx 1 - A^* + \frac{1}{2}(A^*)^2 - \frac{1}{6}(A^*)^3 + \ldots$$

For values of $A^* << 1$ the second term containing A^* can be neglected and the series reduces to $e^{-A^*} \approx 1 - A^*$ and $E \approx A^*$.

7.2.2 Mass Transfer as a Function of Velocity

The removal rate is controlled by the thickness of the boundary layer which in turn is governed by the velocity of flow past the filter grains [6]. For film resistance, the rate is rather temperature insensitive but is dependent on particle size and relative velocity between filter grains and melt [10].

Liquid-solid mass transfer coefficients are often expressed by the dimensionless Sherwood number, *Sh*, that [11] is a function of the dimensionless Peclet number, *Pe*, Schmidt number, *Sc*, and the void fraction, ε. The Peclet number is a measure of the ratio of transport by convective forces to transport by molecular diffusion [12]. This is expressed in Equation 7.8 as the product of dimensionless Reynolds number, *Re*, and Schmidt number, *Sc*,

$$Pe = \mathrm{Re}\, Sc \tag{7.8}$$

where

$$\mathrm{Re} = \mathrm{Re}_p = \frac{D_p u_0 \rho}{\mu} \tag{7.9}$$

with

$$u_0 = u\varepsilon = \frac{\dot{V}}{A} \tag{7.10}$$

and

$$Sc = \frac{\mu}{\rho D} \tag{7.11}$$

with D_p being the effective particle diameter [m], u_0 the superficial velocity of the melt [m/s], u the relative velocity of the melt vs. the particles in the filter bed [m/s], μ the viscosity [kg/ms], ρ the density of molten aluminium [kg/m^3], ε the void fraction

of the filter bed, and D the diffusion coefficient for mass diffusion of the solute element [m^2/s]. The Reynolds number gives an indication of the relative importance of inertial (convective transfer) and viscous (molecular transfer) forces, whereas the Sc number is the ratio of momentum diffusivity (kinematic viscosity $\upsilon = \mu/\rho$) to mass diffusity in the fluid system. [13] The superficial velocity is obtained by assuming that the same flow rate is passed through an empty column which means that the flow rate must be devided by the cross sectional area of the packed bed. Alternatively, when the relative velocity is known it may be multiplied with the void fraction to give the superficial velocity. In this work the superficial velocity by the void has been determined experimentally by measuring the mass flow rate of the melt. From the mass flow rate and the volume of voids in the packed bed one can calculate the residence time of the melt in the filter. Dividing the superficial velocity by the void fraction ε the relative velocity of the melt in the filter is obtained.

For a packed bed of nonspherical particles, the effective particle diameter D_p is defined as:

$$D_p = \frac{6}{a_v} \tag{7.12}$$

which is the diameter equivalent to a spherical particle having the same volume as the nonspherical particle [14]. The specific surface area of a particle, a_v [m^{-1}], is defined as

$$a_v = \frac{S_p}{V_p} \tag{7.13}$$

where S_p is the surface area of a particle [m^2] and V_p the volume of a particle [m^3]. For a spherical particle,

$$a_v = \frac{\pi D_p^2}{\frac{\pi D_p^3}{6}} = \frac{6}{D_p} \tag{7.14}$$

where D_p is the diameter in m. The specific surface area of a particle, a_v [m^{-1}], is related to the surface area per unit volume of packing, A_m [m^2/m^3] [13],

$$a_v = \frac{A_m}{1-\varepsilon} \tag{7.15}$$

According to Engh [6] [29] the mass diffusivity given by the diffusion coefficient D [m^2/s] can be calculated as follows:

$$D = \frac{kT}{2\pi\mu d}\left(\frac{m_1 + m_2}{2m_2}\right)^{\frac{1}{2}} \tag{7.16}$$

where k [1.38 10^{-23} J K^{-1}] is the Boltzmann constant, T [K] absolute temperature, μ [Nsm^{-2}] the viscosity of the solvent, d [m] 2 times the metallic radius of the solvent atom, m_1 the atomic weight of the solvent and m_2 the atomic weight of the solute, respectively.

$$\mu_{Al} = 1.3\times10^{-3}\, Ns/m^2;\ d = 286\times10^{-12}\, m;$$

$$m_{Al} = 26.98;\ m_{Na} = 22.99;\ m_{Ca} = 40.08;\ m_{Mg} = 24.31$$

At 1000 K Equation 7.16 gives the following diffusion coefficients for Na, Ca, and Mg:

D_{Na} = 6.16 10^{-9} m^2/ s ; D_{Ca} = 5.4 10^{-9} m^2/ s ; D_{Mg} = 6.07 10^{-9} m^2/ s .

As mentioned earlier, an expression for fluid flow that represents the ratio of total mass transfer by all mechanisms (including turbulence) to molecular mass transfer is the dimensionless Sherwood number [15]

$$Sh = \frac{k_c D_p}{D} \tag{7.17}$$

Now, particularly if Re_p > 10, the mean transfer coefficients that may be attained in packed beds can be calculated from [16]

$$Sh = C\,\mathrm{Re}_p^m\, Sc^n \tag{7.18}$$

where C and m depend on the porous medium and the range of Reynolds numbers investigated [17]. The factor C is determined experimentally. The exponent n of Sc is equal to 1/3 according to theoretical considerations [16]. However, experimental correlations have been compiled by Seguin et al [17] where Schmidt number exponent vary in a range of $Sc^{1/4}$ to $Sc^{0.58}$. The Sc number itself has an order of magnitude of Sc ≈ 1 in gas – solid systems and Sc >> 1 in liquid – solid systems, respectively [18]. 1000 is often referred to as a typical value for Sc in latter systems [15], [19], [20]. The Sc number decreases with increasing temperature. From Equations 7.11 and 7.16 it is seen that Sc is inversely proportional to the mass diffusivity which in turn increases with increasing temperature.

The following equation may be employed for engineering estimates [21]

$$j_M = \frac{k_c}{u_0} Sc^{2/3} = 1.17 \left(\frac{D_p G}{\mu} \right)^{-0.415} \qquad 10 < \mathrm{Re} < 2500 \tag{7.19}$$

where j_M is the Colburn j-factor for mass, k_c [ms^{-1}] the mass transfer coefficient, G the mass velocity [kgs^{-1}], and u_0 [ms^{-1}] the superficial velocity. The Reynolds number is based for convenience on the superficial velocity, but the average mass velocity is G/ε, and the local velocity at some points in the bed is even higher [19]. This kind of relation is based on empirical correlations and is also known as the Colburn analogy for heat and mass transfer [15]. Equation 7.19 is equivalent to the equation

$$Sh = 1.17\,\mathrm{Re}_p^{0.585}\, Sc^{1/3} \tag{7.20}$$

Equations 7.19 and 7.20 are recommended for spheres or roughly spherical solid particles that form a bed with about 40 to 45 percent voids [19].

To account for varying flow conditions the mass transfer coefficient k_c in Equation 7.5 has been replaced by an expression derived from Equations 7.17 and 7.20 to become a function of the flow conditions.

$$k_c = \frac{1.17\,\mathrm{Re}_p^{0.585}\, Sc^{1/3} D}{D_p} \tag{7.21}$$

7.3 Filtration Experiments

A study was carried out of the various parameters that effect the removal. The contact area has been varied while initial concentration of the element dissolved, melt temperature and residence time of the melt were attempted to be kept constant. However, fluctuations in melt temperature and residence time as well as initial concentration of the dissolved elements were inherent in the experimental procedure. The removal of dissolved elements seemed to be insensitive to temperature fluctuations of ± 15°C as the concentration – time curves show. The variations in initial concentration and residence time extended the range of investigated parameters that otherwise would have been necessary to cover with additional experiments.

The concentrations of Na, Ca, and Mg have been chosen in accordance with levels typically met in industrial operations. That gives a variation in concentration at the inlet which does not allow a direct comparison of the data obtained for the removal.

Also the selective removal of Na from the Al-Mg alloy may be not compared directly to the removal of Ca from pure Al even though the concentrations of Na and Ca are comparable. Since Mg is removed also, the interaction of Na and Mg has to be considered as well.

Comparing inlet and outlet concentrations of AlF_3 and Al_2O_3 filter units to determine the contribution of AlF_3 to the removal of alkali / Mg may be a problem. This is because the driving force for surface oxidation is much reduced in the AlF_3 filter due to the removal of those elements in this filter. In the Al_2O_3 filter in turn all incoming alkali / Mg will still be there when the melt exits this filter. Hence, the melt passed through the Al_2O_3 filter posesses a larger driving force for surface oxidation. Therefore, the contribution of AlF_3 to alkali / Mg removal requires a correction that takes surface oxidation into account. This is especially true for sodium which exhibits the highest vapour pressure of the elements studied. However, in practice a correction for surface oxidation is not important for several reasons.

For experiments 1-3 (Na) and 4-6 (Ca) exit levels have been low such that the contribution of surface oxidation can be neglected. Secondly, the procedure of calculating the removal efficiencies, which was applied to all experiments, already includes a reasonable estimate of surface oxidation to the removal of the considered elements in the AlF_3 filter. Each case will be illustrated by a numerical example given in Tables 7.1 and 7.2, respectively.

Table 7.1 compares the removal efficiencies determined for experiments 1-3 (Na) and 4-6 (Ca) either neglecting the contribution of surface oxidation to the removal or taking into account its estimate by defining the removal in the AlF_3 filter as the difference of the outlet concentration of the Al_2O_3 filter and the AlF_3 filter. The removal efficiencies taking into account surface oxidation are insignificantly lower compared to the removal efficiencies neglecting surface oxidation. The difference is within the narrow standard deviations. This shows that surface oxidation can be neglected for exit levels that are low compared to the levels at the inlet. To show the impact of surface oxidation on the removal efficiency in the presence of higher exit levels in comparison to the case that neglects surface oxidation experiments 7 – 12 (Ca) and 13 – 14 (Mg-Na) have been included.

A correction for surface oxidation may be based on the fact that the losses are proportional to the concentration of the element lost. On average about 27.6% (±12.9%), 10.5% (±8.8%), and 22.6% (±6.5%) have been lost of the inlet concentration upon exiting the Al_2O_3 filter and sampling for chemical analysis via surface oxidation during experiments 1-3 (Na), 4-12 (Ca), and 13-14 (Mg-Na), respectively. As a consequence, the surcharge of the former losses to every outlet concentration determined for the AlF_3 filter should account for the reduced effect of surface oxidation. In Table 7.2 this case of calculating the removal efficiency as the difference of the inlet concentration and the corrected outlet concentration of the AlF_3 filter is compared to the procedure that was the base for calculating the removal efficiencies throughout this work. This was the difference of both the outlet concentration of the Al_2O_3 filter and the AlF_3 filter. The difference in removal efficiency between the two cases is within the standard deviation of each experiment.

Table 7.1 Removal efficiencies for experiments 1 - 14

	E (outlet$_{Al2O3}$ - outlet$_{AlF3}$)		**E (inlet - outlet$_{AlF3}$)**	
Experiment	*E %*	*STD E %*	*E %*	*STD E %*
1	88.6	1.1	90.1	1.3
2	96.7	1.1	98.2	0.5
3	96.1	0.4	97.2	0.2
4	97.0	1.0	97.4	0.8
5	94.5	2.0	95.3	1.7
6	95.3	2.7	97.1	1.3
7	73.1	2.2	75.7	2.0
8	72.5	1.7	73.7	1.6
9	64.7	2.3	67.3	2.4
10	46.2	3.3	49.9	2.9
11	55.4	3.5	58.1	3.7
12	61.7	3.8	64.9	3.7
13	65.5	7.2	76.1	5.1
14	70.1	2.6	75.6	2.3

Table 7.2 Comparison of removal efficiencies for experiments 1 - 14 taking into account losses due to surface oxidation

	E (outlet$_{Al2O3}$ - outlet$_{AlF3}$)		E (inlet - outlet$_{AlF3, corrected}$)	
Experiment	*E %*	*STD E %*	*E %*	*STD E %*
1	88.6	1.1	86.4	1.8
2	96.7	1.1	97.5	0.7
3	96.1	0.4	96.1	0.3
4	97.0	1.0	97.1	0.9
5	94.5	2.0	94.8	1.9
6	95.3	2.7	96.7	1.5
7	73.1	2.2	72.8	2.3
8	72.5	1.7	70.6	1.8
9	64.7	2.3	63.5	2.7
10	46.2	3.3	44.0	3.2
11	55.4	3.5	53.2	4.1
12	61.7	3.8	60.8	4.1
13	65.5	7.2	69.1	6.6
14	70.1	2.6	68.4	3.0

The data leaves the impression that filter ageing does not have an effect over the course of one experiment since the exit levels remain more or less constant. Referring to paragraph 7.1.5, the assumption of no filter ageing should be allowed since the supply of fluorine does not cease noticeably in the time frame of an experimental run (~1h). Also deposition of the reaction product at the surface of the filter grain or the absorption throughout should be low.

7.3.1 Dependence of Efficiency on Residence Time and Contact Area

For experiment 1–3 shown in Figure 6.7a-c the amount of Na removed increased with increasing Na concentration at the inlet. Removal was from 6% to 59% for the conventional filter and from 87.5% to 99% for the AlF_3 filter. Variations in melt flow velocity seem to have little effect on Na removal. Probably, little or no Na or Ca is removed in the conventional filter. Removal is by free surface oxidation only at the outlet stream and during sampling due to a large ratio of surface to volume of the melt exposed. The contribution of free surface oxidation to the removal of Na in the AlF_3

filter is low compared to the Al_2O_3 filter due to a much lower Na concentration in the melt leaving the AlF_3 filter. The driving force for removal at the free surface is much reduced.

For Figure 6.8a-c (experiment 4–6) Ca removal was from 5% to 47% for the conventional filter and from 91% to 99% for the AlF_3 filter. Due to the low output values in the AlF_3 filter, losses or removal due to free surface oxidation are hardly an issue. Melt flow velocities differ from the values in the previous series by a factor 3.5 as well as they vary within this series by a factor 3. Again, these variations seem to have little effect on the removal rates. The removal efficiencies for experiments 4 – 6 are in line with the efficiencies determined for experiments 1 – 3.

Removal of Ca for the AlF_3 filter in Figure 6.9a-c is from 66% to 78% with efficiencies decreasing with increasing inlet concentrations for Ca. The net removal seems to be independent of the inlet concentration as Figures 6.9a-b are compared to Figure 6.9c.

The graphs in Figure 6.10a-c show the removal of Ca in the AlF_3 filter increasing from 50% (experiment 10) over 60% (experiment 11) to 70% (experiment 12). With melt mass flows being between 20 and 10g/s and a contact area of $0.062m^2$, this increase may be explained by a decrease in melt flow velocity which eventually doubles the contact time. A comparison of the removal pattern given in experiment 7 and experiment 10 yields a similiar observation. Using only half the contact area causes the efficiency to decrease by approximately 20%. The same observation with respect to contact area can be made comparing experiments 4-6 and experiments 7-9. This shows that the influence of the velocity is not as straightforward as it is in case with contact area. An increase in velocity reduces the contact time but at the same time mass transfer is improved for the reasons explained in 7.2.2.

The outcome of filtration experiments to study the selective removal of Na from Al-Mg alloys has been plotted in Figures 6.11a – 12b. The removal of Na from the alloy with low Mg content (0.2wt%) and $0.124m^2$ contact area at a melt velocity of 10g/s was in the order of 65% in the AlF_3 filter and 30% after the Al_2O_3 filter which is shown in Figure 6.11a. The loss in Mg which is shown in Figure 6.11b was 1.1 % in the AlF_3 filter (excluding surface evaporation from Al_2O_3 filter) and 1.4 % after the Al_2O_3 filter. The graph in Figure 6.12a shows the removal of Na from the alloy with high Mg

content (4.7 wt%) and 0.124m^2 contact area at melt velocities between 9 and 10g/s increasing from 68% to 72% in the AlF_3 filter but remaining unchanged at 18% after the Al_2O_3 filter with Na concentrations decreasing at the inlet. The loss in Mg for experiment 14 which is shown in Figure 6.12b was 1.5 % for the AlF_3 filter (excluding surface evaporation from Al_2O_3 filter). The amount of Mg lost after the Al_2O_3 filter was 0.5 % or 242ppm (vs. 26ppm in experiment 13). The removal of Na in an AlF_3 filter with 0.124m^2 contact area seems comparable to the removal of Ca from a pure aluminium melt at the same contact area with respect to amount originally contained vs. amount removed. Also the removal efficiencies obtained for Na seem not to be affected by the considerable increase in Mg concentration going from low Mg content to high Mg content in the Al-Mg alloy. Mg in turn needs about 75 times the concentration of Na to achieve the same net removal as has been achieved for Na in the AlF_3 filter when both elements are present in the aluminium melt at low Mg content.

The variation of the removal efficiency for Na and Ca in dependence of residence time and contact area in the AlF_3 filter is illustrated in Figures 7.9 – 12. Figure 7.9 shows that for a "small" contact area the removal efficiency is increasing with increasing residence time. An increase of ~50% in removal efficiency obtained for a 100% rise of the residence time points to first order kinetics.

Figure 7.10 shows the removal efficiency versus the contact area for experiments 1 – 14 including all cases of "small", "intermediate", and "large" contact area. The removal efficiency increases with increasing contact area such that doubling the contact area causes the original efficiency to rise by ~ 50%. To illustrate that for a case of 100ppm of impurity entering the AlF_3 filter, removal would increase from 50ppm to ~ 75ppm, doubling the contact area again would further increase the removal to approach 100ppm. Figure 7.10 can be also read in the way of tracking the evolution of the removal efficiency from inlet to outlet in a filter having a "large" contact area. This picture together with the demonstrated example let the concentration dependence, and hence, first order kinetics of the removal become apparent also from the point of contact area. The larger error bars in Figure 7.10 for experiments at "small" contact area (~ 0.062m^2) in comparison to experiments at "intermediate" contact area (~ 0.124m^2) and "large" contact area (~ 0.248m^2) reflect the sensitivity of the removal efficiency to fluctuations in melt velocity during those experiments (10 – 12).

Figures 7.11 – 12 show that for "intermediate" contact area and "large" contact area the removal efficiency becomes independent of the residence time and hence, velocity.

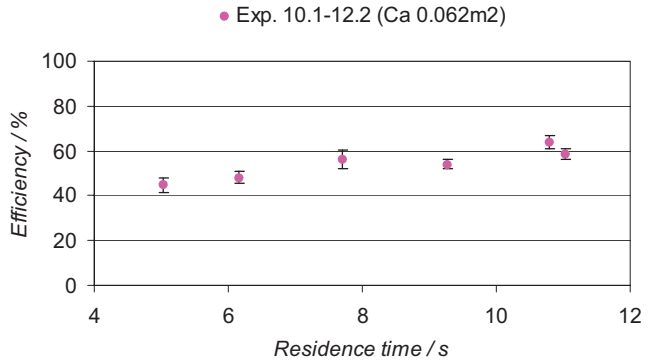

Fig. 7.9 Removal efficiency for Ca in dependence of residence time for experiments with "small" contact area (~ 0.062 m^2).

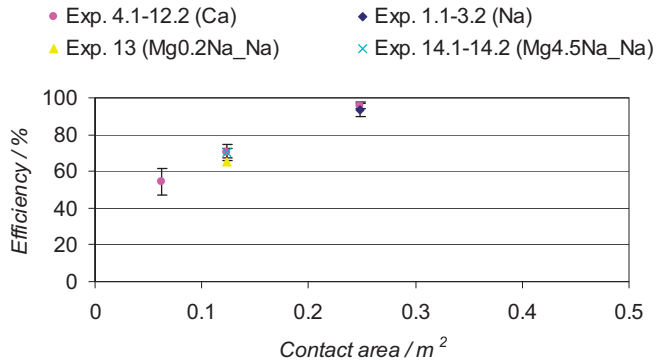

Fig. 7.10 Removal efficiency vs contact area for experiments 1 – 14

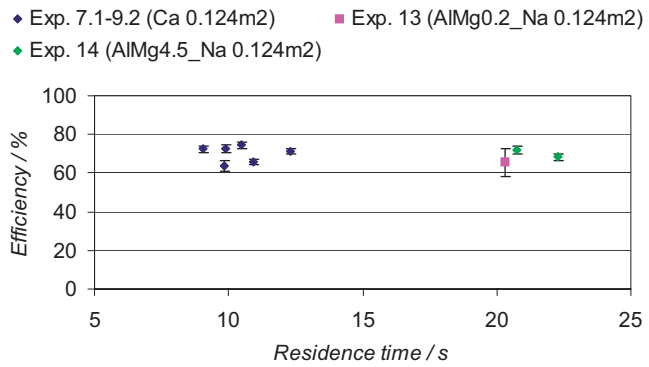

Fig. 7.11 Removal efficiency for Ca in dependence of residence time for experiments with "intermediate" contact area (~ 0.124m^2)

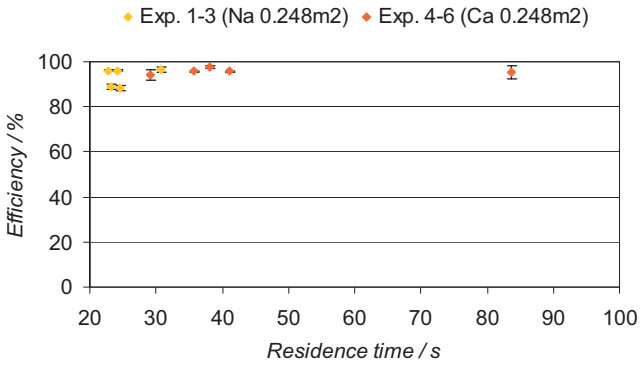

Fig. 7.12 Removal efficiency for Ca in dependence of residence time for experiments with "large" contact area (~ 0.248m^2)

7.3.2 Comparison of Experiments with Fluid Flow Calculations

Given the knowledge of mass transfer coefficients, bed characteristics, and flow rate Equation 7.4 may be used to predict filtration efficiency. Yet unknown, the mass transfer coefficient k_c has to be determined experimentally or from the theory of diffusional exchange between flowing fluids and surfaces. Figure 7.13 shows a plot of Equation 7.21 (lines) for Na as well as for Ca together with the experimental data (dots) as mass transfer coefficient versus superficial velocity to compare expected and actual flow conditions. Both for experimental and empirical values the mass transfer increase

with an increase in melt velocity. According to Equations 7.19 and/or Equations 7.20 $k_c \sim u_0^{0.585}$.

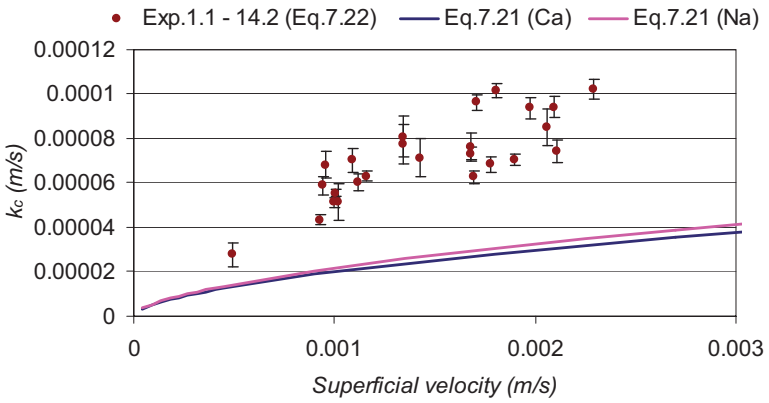

Fig. 7.13 Empirical (lines acc. to Eq. 7.21) and averaged (dots acc. to Eq. 7.22) experimental mass transfer coefficients vs superficial velocity for every flow rate determined

Equation 7.22 has been used to calculate a value of k_c for every measurement.

$$k_c = \frac{-\ln(c/c_0)\dot{V}}{Aa_v(1-\varepsilon)z} \tag{7.22}$$

Average values of $\bar{k}_c$ have been calculated for every mass flow rate rate determined (1 or 2 for each experiment) including the standard deviation to represent the experimental data in Figure 7.13. The standard deviation Δk_c for every flow rate determined is between 3% and 20% with an average of 7%.

The k_c-values that have been determined experimentally are larger by a factor ~3 compared to the predictions based on Equation 7.21. The high k_c values relative to the theory may be due to the morphology of the investigated packed bed which is determined by the shape of the filter grains. The surface area of the grains is larger due to the jagged " coast of Norway " effect in comparison to spherical particles. The jagged grains also give an increased tortuosity compared to spheres. This changes the flow pattern in a way that the melt has to travel a longer distance. Both increased surface area and tortuosity are expected to increase mass transfer. Figure 7.14 has been included to illustrate the morphology of the jagged grains. However, the main explanation for the

factor 3 may well be the value of the diffusion coefficient D_{Ca} which could be erroneus up to a factor of 10. Since $k_C \propto D^{2/3}$ this could explain the factor 3.

Fig 7.14 Morphology of jagged filter grains

Figure 7.15 shows the results of filtration experiments 1 – 14 in terms of filtration efficiency E versus dimensionless contact area A^* to be compared with the model expression for first order kinetics which is equivalent to Equation 7.7. The actual mass transfer coefficients are still unknown. Figure 7.15 already gives insight into the kinetics of the investigated AlF_3 filter for both the removal of Na and Ca from a pure aluminium melt as well as for removing Na from Al-Mg alloys. The rates for the removal of Na and Ca from a pure aluminium melt are comparable but underestimated by Equation 7.21.

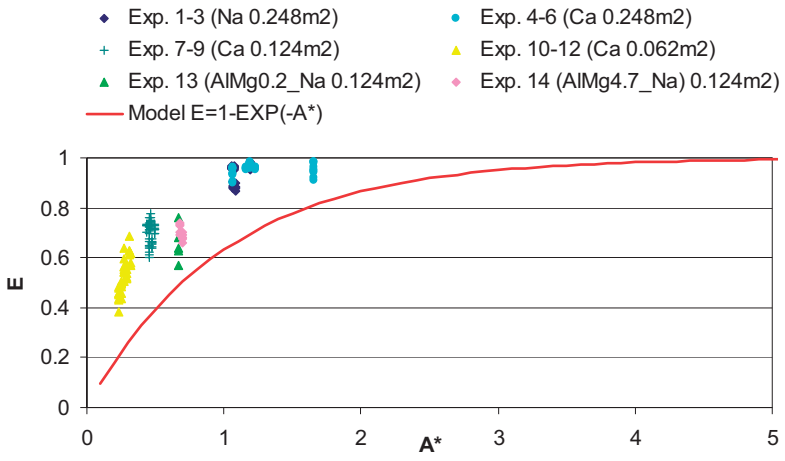

Fig. 7.15 Results of filtration experiments 1–14 as efficiency versus dimensionless contact area A^* for k_c approximated by Equation 7.21 in comparison to the first order kinetic model

7.3.3 Determining the Mass Transfer Coefficients for the Removal of Ca

A more accurate estimate of k_c by Equation 7.21 for the removal of Na and Ca from pure aluminium requires a correction of C (=1.17) in Equation 7.18 (7.20). A^* is proportional to the contact area which requires the introduction of a proportionality constant into Equation 7.7. If the contact area is increased then the proportionality constant increases as well.

A preliminary conclusion in paragraph 7.3.2. was that Equation 7.20 under estimates the removal of Na and Ca throughout experiments 1 – 14. A more accurate estimate of k_c by Equation 7.21 requires a correction of C (=1.17) in Equation 7.20. Therefore a regression analysis has been performed on the model function defined by Equation 7.23 to estimate the value of C. This will give the best description of the experimental data with respect to the dependence on Re_D and Sc. Na is not considered due to the relatively few measurements taken.

$$E = 1 - \exp(-C \cdot x) \tag{7.23}$$

where C is the parameter to be determined and x being the independent variable which according to Equations 7.5 and 7.21 is

$$x = \frac{\mathrm{Re}^{0.585}\, Sc^{1/3} A a_v (1-\varepsilon) HD}{D_p \dot{V}} \tag{7.24}$$

A standard procedure of minimizing the deviations of the model function from the experimental data is the method of least squares. An expression based on elaborations by Press et al. [26] that also takes the weight of the experimental error into account is

$$\chi^2 = \sum_{i=1}^{N} \left[\frac{y_i - y(x_i; C)}{\sigma_i} \right]^2 \tag{7.25}$$

where N is the number of data points;

$$y_i = E_i; \qquad y(x_i; C) = C \frac{\mathrm{Re}^{0.585}\, Sc^{1/3} A a_v (1-\varepsilon) HD}{D_p \dot{V}} = C \cdot x_i$$

Equation 7.23 is not linear in its parameter and therefore the sum of squares must be minimized by an iterative procedure. The best fit is obtained when the model gives the least value for the sum of squared residuals. In the best possible case $\chi^2 = 0$.

The measurements are given as pairs of ($x_i \pm \sigma_{x,i}$; $y_i \pm \sigma_{y,i}$) and according to Guest [27]

$$\sigma_i^2 = \sigma_{y,i}^2 + \left[\frac{dy(x_i; C)}{dx} \right]^2 \sigma_{x,i}^2 \; ; \tag{7.26}$$

The error in E has been taken as its sample standard deviation which for small or moderately-sized samples of a population can be calculated according to Equation 7.27

$$\sigma_{yi} = \left(\frac{1}{N-1} \sum_{i}^{N} (\varepsilon_i - \bar{\varepsilon})^2 \right)^{1/2} \tag{7.27}$$

where E_i is a single value and $\bar{E}$ is the average value of an experiment.

The error $\sigma_{x,i}$ of x defined by Equation 7.24 can, according to Squires [28], be calculated by the following expression

$$\sigma_{x,i} = x_i \sqrt{\left(0.585 \frac{\Delta \mathrm{Re}_i}{\mathrm{Re}_i} \right)^2 + \left(2 \frac{\Delta a_{v,i}}{a_{v,i}} \right)^2 + \left(\frac{\Delta \varepsilon_i}{1-\varepsilon_i} \right)^2 + \left(\frac{\Delta \varepsilon_i}{\varepsilon_i} \right)^2 + \left(\frac{\Delta t_i}{t_i} \right)^2} \tag{7.28}$$

All values that have been used or which are a result of the above calculations are summarized in Tables B.1 and C.1 which can be found in Appendix B an C, respectively.

Figure 7.16 shows the result of the regression analysis where Equation 7.23 (solid line) has been fitted to the experimental points including their individual errors for the removal of Ca throughout experiments 4 – 12. The parameter C has been found to be 3.21 ±0.11 which is larger by almost a factor 3 compared to the original value of 1.17 for C in Equation 7.20. A value of 0.98 for R^2 shows that there is a strong correlation between the independent variable x and the efficiency E [30].

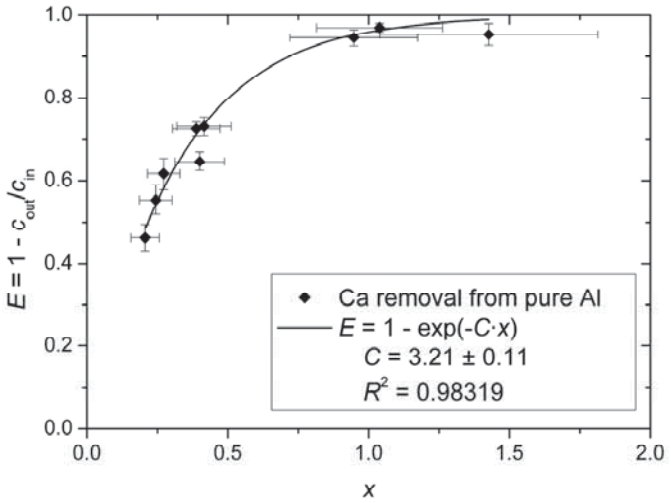

Fig. 7.16 Regression analysis – fitting Equation 7.23 (solid line) to the strongly correlated experimental points including their individual errors for the removal of Ca from pure aluminium throughout experiments 4 – 12 [30]

Figure 7.17 shows that also for experiments 1 – 3 the experimental points for the removal of Na from pure aluminium (red dots) correlate well with the experimental data obtained for experiments 4 – 12. One might expect that Na has a higher removal efficiency than Ca since Na penetrates the filter grains, see Figure 6.16 and 6.17.

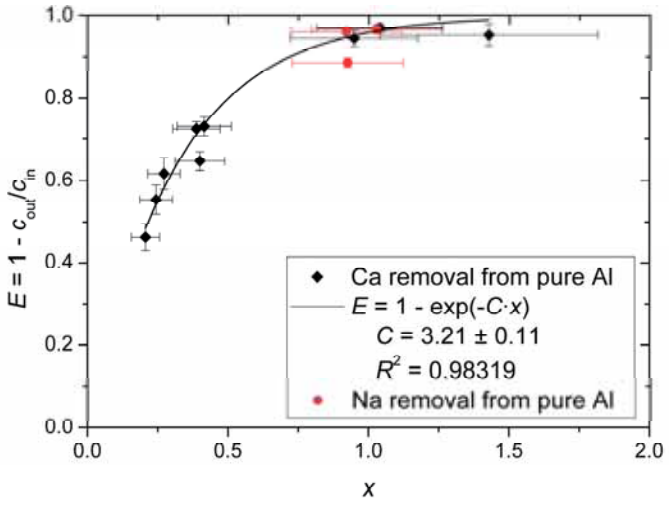

Fig. 7.17 Experiments 1 – 3 (removal of Na from pure aluminium) correlate well with the experimental data obtained for the removal of Ca from pure aluminum (experiments 4 – 12) [30]

Including also the data of experiments 13 – 14 for the removal of Na from an Al-Mg alloy (blue dots) in comparison to experiments 1 – 12 as shown in Figure 7.18 gives a correlation that is less good in comparison to the correlation between experiments 1 – 3 and 4 – 12. That means that the parameter C (=3.21) found can not be applied to describe the removal of Na from an Al-Mg alloy. A parameter C explicitly determined for experiments 13 – 14 would be ~2 since the rates for the removal of Na and Ca from pure aluminium are larger by a factor ~1.5 compared to the rates attained for the removal of Na from an Al-Mg alloy as stated in section 7.3.2. However, increasing Mg concentrations leave the removal efficiency unaffected. It is not attempted to speculate further on the effect of Mg. An exact value of C for those experiments has not been determined due to the scarce data.

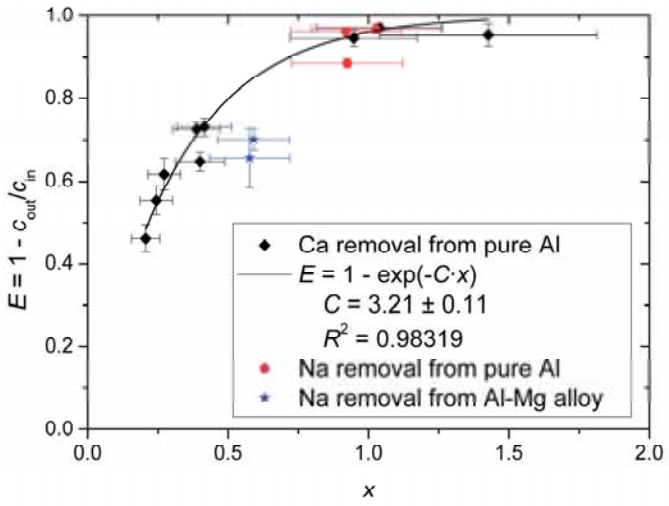

Fig. 7.18 Comparing the correlation of experiments 1 – 3 (Na removal from pure Al), experiments 4 – 12 (Ca removal from pure Al), and experiments 13 – 14 (Na removal from Al-Mg alloy) [30]

As a consequence of the regression analysis Equation 7.21 changes to

$$k_c = \frac{3.21 \mathrm{Re}_p^{0.585}\, Sc^{1/3} D}{D_p} \tag{7.29}$$

7.4 Parametric Study for Industrial Application

As an example the removal of 30ppm Ca from Al scrap at a rate of 10 tonn/hr with 80% efficiency will be calculated. The determination of k_c as well as the characterization of the filter material with respect to ratio of surface to volume, equivalent particle diameter, and void fraction of the packing is a pre-requisite to allow a scale up of the filter to industrial applications.

To illustrate the influence of the equivalent particle diameter, which in this respect could be called a key parameter, Figure 7.21 shows how contact area and mass transfer coefficient of a packed bed depend on its grain size. The calulations are based on a superficial velocity of 0.01m/s. For liquid to solid mass transfer k_c depends on the conditions of fluid flow and therefore is a function of the relative velocity of the fluid

phase and the grain size and shape of the solid phase. Those properties determine the ratio of surface to volume and the tortuosity exhibited by the filter bed. k_c increases approximately with the square root of the velocity. The dependence on the particle diameter is inverse due to the definition of the Sherwood number (Eq. 7.17). This is despite increasing *Re* numbers which according to Equation 7.8 represent the increasing contribution of the forces of convection. As Figure 7.21 shows, both mass transfer coefficient and contact area per cubic meter of reactor (see Eq. 7.13 and 7.14) decrease exponentially with increasing particle diameter. The size of the grains may be reduced to such a degree that the melt will be still able to penetrate the packed bed without considerable pressure drop. A packed bed made of odd/jagged shapes of grains offers a larger ratio of surface to volume as well as increased tortuosity compared to spheres.

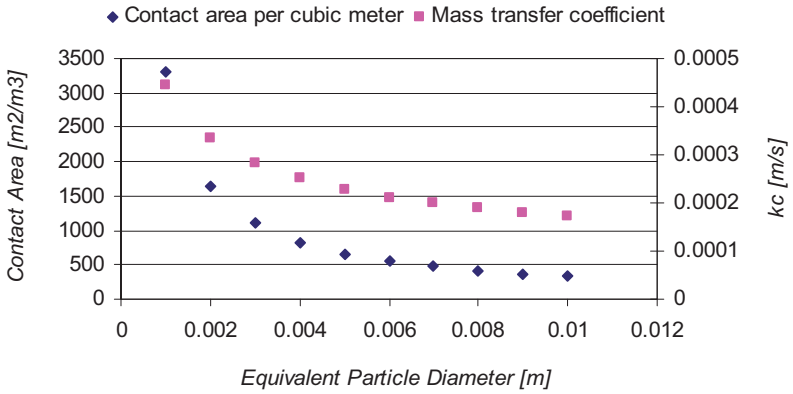

Fig. 7.21 Equivalent particle diameter in a packed bed versus contact area [m^2/m^3] and mass transfer coefficient k_c

According to equation 7.7 a removal efficiency of 80% corresponds to a value of dimensionless contact area of ~ 1.6. For the velocity of interest k_c may be determined experimentally or by calculation as demonstrated. The only value unknown is the necessary thickness of the filter bed which can be calculated with the help of Equation 7.5 introduced earlier.

$$A^* = \frac{k_c A a_v (1-\varepsilon) z}{\dot{V}}$$

A throughput of 10t/h is equivalent to a volume flow of 0.00118m^3/s. The chosen superficial melt velocity of 0.01m/s in the launder translates into a cross section of the filter of 0.118m^2 to accommodate this throughput. The corresponding value of k_c will be ~ 0.00021m/s. The calculation gives a thickness of ~0.12m.

7.5 Conclusion

This work has shown that removal of alkali from aluminium melts by means of filtration is feasible. With concentrations of Na, Ca, and Mg typical for the industry for a filter of hight 0.09m and a residence time of metal 20 seconds

- Na removal was from 6% to 59% for the conventional filter (Al2O3) and from 87.5% to 99% for the AlF3 filter.
- Ca removal was from 5% to 47% for the conventional filter and from 91% to 99% for the AlF3 filter
- Removal efficiencies obtained for Na and Ca seem not to be affected by the Mg content in the Al-Mg alloy.
- The removal rate follows first order kinetics controlled by the resistance in the melt boundary layer
- The mass flow rates that have been determined experimentally are larger by a factor ~3 compared to the predictions based on the use of a diffusion coefficient $D_{Ca} = 5.4 \cdot 10^{-9}$ m^2/s at 1000 K.

7.6 Further work

Further work should proceed concerning diffusion coefficients in molten aluminium. The efficiency of AlF_3 filter beds with respect to removal of inclusions should be investigated further.

Bibliography

[1] Kai Tang, SINTEF Materials and Chemistry, Trondheim, Norway, priv. communication.

[2] Asbjørn Solheim, Åsmund Sterten: *„Activity Data for the System NaF – AlF_3"*. Proceedings of the 9th International Symposium on Light Metals Production, Tromø – Trondheim, Norway, Aug. 18th – 21th, 1997, pp. 225 – 234 http://al.matek.sintef.no/articles/lmp1997/p225/p225-234.htm

[3] A. N. Waernes, S. G. Hansen, J. Kr Tuset, B. Rasch: *"Thermodynamic Computer Programs as an Aid in Refining of Aluminium"*. Light Metals 1999, 1999, pp. 861 – 876.

[4] Michael F. Mattocks, R. A. Frank: *"Recent Quality and Efficiency Improvements through Advances in In-line Refining Technology"*. Aluminium Asia '98, 7-9 May 1998, 1998, pp. 1 – 14.

[5] T. Utigard: *"Thermodynamic Considerations of Aluminum Refining and Fluxing"*. Proceedings of the International Symposium on Extraction, Refining and Fabrication of Light Metals. Ottawa, Ontario, Canada, August 18-21, 1991, p. 356

[6] T. Abel Engh: *"Principles of Metal Refining"*. Oxford University Press, 1992, pp. 46, 50, 94, 116, 179-80

[7] K. Grjotheim: *"Nature and Origin of Impurities in the Hall-Heroult Electrolyte and their Effect on Metal Purity"*. International Seminar on Refining and Alloying of Liquid Aluminium and Ferro-Alloys, August 26-28, 1985, Trondheim, Norway

[8] W. Thiele: *"The Oxidation of Aluminium and Aluminium Alloy melts"*. Aluminium, 38, 1962, pp. 707 – 715.

[9] K. Motzfeldt: *"Discussion of – The Solubility of Sodium in Liquid Aluminum – "*. Metallurgical and Materials Transactions B, Vol. 34B, October 2003, pp. 744 – 746

[10] O. Levenspiel: *"Chemical Reaction Engineering. Second Edition"*. John Wiley & Sons, 1972, pp. 377

[11] R. Pfeffer, J. Happel, *"An analytical study of heat and mass transfer in multiparticle systems at low Reynolds numbers"*. AIChE Journal (1964), 10(5), pp. 605 - 611.

[12] J.Th. Cookson Jr.: *"Removal of Submicron Particles in Packed Beds"*. Environmental Science & Technology, Volume 4, Nr. 2, February 1970, 1970, pp. 128 – 134

[13] R.B. Bird, W.E. Stewart, E.N. Lightfoot: *"Transport Phenomena"*. 2nd ed., John Wiley & Sons, Inc., 2007, pp. 98, 189 – 190, 600

[14] C.J. Geankoplis: *"Transport Processes and Separation Process Principles"*. Prentice Hall, 2003, p. 125

[15] R.S. Brodkey, H.C. Hershey: *"Transport Phenomena – A Unified Approach"*. McGraw-Hill, New York, 1988, pp. 330 – 37; 519; 612 – 622

[16] W.J. Beek, K.M.K. Muttzall: *"Transport Phenomena"*. John Wiley & Sons Ltd., London, 1975, pp. 247; 270

[17] D. Seguin, A. Montillet, D. Brunjail, J. Comiti*: "Liquid-Solid Mass Transfer in Packed Beds of Variously Shaped Particles at Low Reynolds Numbers: Experiments and Model"*. The Chemical Engineering Journal 63, 1996, pp. 1 – 9

[18] T. Miyauchi: *"Film Coefficients of Mass Transfer of Dilute Sphere-Packed Beds in Low Flow Rate Regime"*. Journal of Chemical Engineering of Japan, Vol. 4, No. 3, 1971, pp. 238 – 245 (34 – 41)

[19] W.L. McCabe, J.C. Smith, P. Harriot: *"Unit Operations of Chemical Engineering"*. 6th ed., McGraw Hill, 2001, p. 671

[20] O. Levenspiel: *"The Chemical Reactor Omnibook"*. OSU Book Stores, Inc., Corvallis, Oregon, 1996, pp.11.8, 100.4

[21] T.K. Sherwood, R.L. Pigford, C.R. Wilke: *"Mass Transfer"*. McGraw-Hill, New York, 1975, p. 242

[22] S. Barnett, T.M. Cronin: *"Mathematical Formulae for Engineering and Science Students"*. 4th ed., Longman 1986, p. 5

[23] Octave Levenspiel: *"Chemical Reaction Engineering. Third Edition"*. John Wiley & Sons, 1999, pp. 1 – 5, 401 - 402

[24] *„Principles of Liquid Metal Processing"*. ASM Handbook, Volume 15, Casting (ASM Handbooks Online at ***http://products.asminternational.org/hbk/index.jsp***)

[25] Michael F. Mattocks, R. A. Frank: *"Recent Quality and Efficiency Improvements through Advances in In-line Refining Technology"*. Aluminium Asia '98, 7-9 May 1998, 1998, pp. 1 – 14

[26] W.H. Press, B.P. Flannery, S.A. Teukolsky, W.T. Vetterling: *"Numerical Recipes in C"*. Cambridge University Press 1988, Cambridge, England

[27] P.G. Guest: *"Numerical Methods of Curve Fitting"*. Cambridge University Press 1961, Cambridge, England, pp. 128 – 130

[28] G.L. Squires: *"Practical Physics 3rd ed"*. Cambridge University Press 1985, Cambridge, England, pp. 36, 52 – 53

[29] T.A. Engh: *„Diffusivities in Metals"*. To be published

[30] M. Syversten, SINTEF Materials and Chemistry, Trondheim, Norway, priv. communication.

Appendix

A: PoDFA/PREFIL Evaluation of Melt before and after Filtration

Table A.1 gives an overview of the samples taken for the PoDFA/PREFIL measurements to assess the removal of suspended particles in the "passive" Al_2O_3 and the "active" AlF_3 filter. The quantitative assesment including metallographic preparation of the PoDFA/PREFIL samples was performed at N-Tec Limited (Redditch, England). The results are summarized in two reports provided by N-Tec Limited (No. 050014 & 040107) which are part of this appendix.

Table A.1: Designation of PoDFA/PREFIL samples taken including sample mass.

Before Filtration	**After Filtration**		**Report No.**
	AlF_3 Filter (Mass)	***Al_2O_3 Filter (Mass)***	
			50014
111 (1976g)	211 (1701g)	311 (1260g)	
121 (1645g)	221 (3120g)	321 (2492g)	
			40107
113 (not recorded)	213 (2106g)	313 (2230g)	
123 (not recorded)	223 (1825g)	323 (2369g)	

QUANTITATIVE ASSESSMENT OF PODFA SAMPLES FOR NTNU

REPORT NO. 050014

N-Tec Limited
16 February 2005

Prepared By:
Dr. A. Cushway

N-Tec Limited

Enabling Technologies for the Metals Industry

MOLTEN METAL QUALITY REPORT
N-Tec Limited
Report Ref: 050014

SAMPLE REFERENCE:

Six PoDFA residues were supplied to N-Tec for quantitative evaluation. The samples were identified as 111, 211, 311, 121, 221 and 321.

TECHNIQUES:

Metallographic preparation, photography and quantitative metallographic analysis of the samples.

RESULTS

The principle inclusions in the samples were oxide films and titanium diboride, plus a small amount of carbide and refractory particles.

Sample 121 was very clean (Fig. 1). All the other samples had a high number of oxide films and a variable amount of titanium diboride. A small amount of carbide and refractory particles were present in all the samples. The refractory particles comprised tiny pieces of fibre and/or tiny fragments of lining or coating from walls or tools. Typical inclusions are shown in Fig. 2.

Appendix 1 gives information about the reproducibility of the metallographic analysis and the origins of Inclusions.

Prefil/PoDFA Evaluation Sheet

Customer Trial I.D:	
Customer Name:	Harold Goerner
Sampling Plant:	
Company:	NTNU
Report Date:	16.02.05
Report Number:	050014

Sample I.D:	111	211	311	
Alloy:	Al-99.7	Al-99.7	Al-99.7	
Location:				

Overall Metal Cleanliness

Inclusion Content (mm^2/kg)	0.505	0.080	0.065	
Oxide Film Content (No/kg)	132	183	164	

Oxide Films (Gamma-Al_2O_3)

Number/kg	132	183	164	
Length	Sort, med, long	Sort, med, long	Short, med, long	
Thickness	Thin, thick	Thin, thick	Thin	

Inclusions (mm^2/kg & % of total)

TiB_2/ TiC	0.455 (90%)	0.072 (90%)	0.058 (90%)	
(Ti-V)B_2				
Al_4C_3 < 3□m				
Al_4C_3 > 3□m	0.050 (10%)	0.008 (10%)	0.007 (10%)	
Borocarbides				
MgO				
MgO-cuboids				
$MgAl_2O_4$-spinel				
Dispersed Al_2O_3				
Alumina needles			Trace	
Nitride				
Graphite				
Potential chlorides / micro-gas				
Salt / Fluoride / Bone ash				
Spinel-like / Kaowool / Silicate	Trace	Trace	Trace	

Comments

All samples have a high number of oxide films. The films are decorated with titanium diboride and carbide. Sample 111 in particular has a high level of titanium boride.

Sample information

Filtered weight, kg	1.51	1.52	1.0	
Cord length, mm	11.6	11.9	12.6	
Method	Grid	Grid	Grid	
Magnification	X100	X100	X100	

Prefil/PoDFA Evaluation Sheet

Customer Trial I.D:	
Customer Name:	Harold Goerner
Sampling Plant:	
Company:	NTNU
Report Date:	16.02.05
Report Number:	050014

Sample I.D:	121	221	321	
Alloy:	Al-99.7	Al-99.7	Al-99.7	
Location:				

Overall Metal Cleanliness

Inclusion Content (mm^2/kg)	0.015	0.018	0.344	
Oxide Film Content (No/kg)	7	186	180	

Oxide Films (Gamma-Al_2O_3)

Number/kg	7	186	180	
Length	Short	Short, med, long	Short, med, long	
Thickness	Thick	Thin, thick	Thin	

Inclusions (mm^2/kg & % of total)

TiB_2/ TiC	0.015 (100%)	0.018 (100%)	0.326 (95%)	
(Ti-V)B_2				
Al_4C_3 < 3□m				
Al_4C_3 > 3□m	Trace	Trace	0.018 (5%)	
Borocarbides				
MgO				
MgO-cuboids				
$MgAl_2O_4$-spinel				
Dispersed Al_2O_3				
Alumina needles				
Nitride				
Graphite				
Potential chlorides / micro-gas				
Salt / Fluoride / Bone ash				
Spinel-like / Kaowool / Silicate	Trace	Trace	Trace	

Comments

Sample 121 is very clean. Samples 221 and 321 have a high number of oxide films decorated with titanium diboride, particularly sample 321. A small amount of carbide and refractory inclusions are present in all samples.

Sample information

Filtered weight, kg	1.52	1.52	1.52	
Cord length, mm	12.4	12.1	12.5	
Method	Grid	Grid	Grid	
Magnification	X100	X100	X100	

Fig. 1 Sample 121 X100

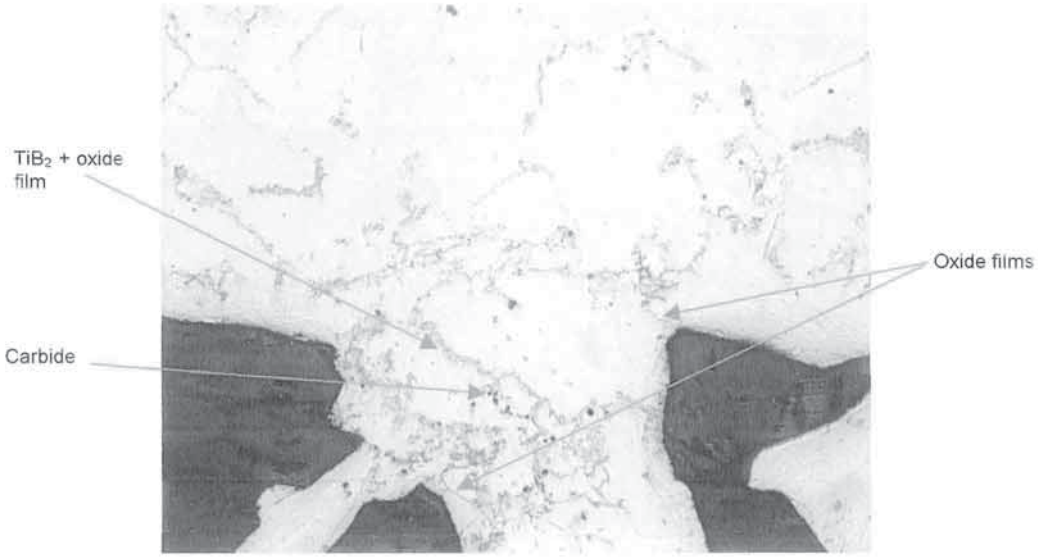

Fig. 2 Sample 321 X200

Appendix 1 Metallographic Analysis

Metallographic Analysis Repeatability

It was established that the repeatability of metallographic analysis is + 16% for an inclusion content over 1.25 mm^2/kg. The precision of the metallographic analysis decreases with an increase of the metal cleanliness. When the inclusion content is less than 0.07 mm^2/kg, repeatability is +40%. [Ref.: Metallographic Evaluation of PoDFA Inclusions Residue, Alcan, ARDC, Method # 2012-96]

Oxide Films

Oxide films are difficult to measure by metallographic means because of the nature of the PoDFA analysis technique. The presence of oxide films in a sample is most probably underestimated. An oxide film is like a paper tissue in its shape, e.g. a flexible plan. When a metallographer looks at a slice of a Prefil sample, what he sees is often just a slice of the oxide film plan. For instance, he may be looking to several slices of different oxide films as well as it may only be several parts of the same film. Because of the nature of this type of analysis, discrimination for fine variation in the content of oxide films is not conceivable. Only changes in the order of magnitude can be confirmed.

Oxide films have a lower density than aluminium and because of the long solidification time of a Prefil crucible, it is likely that oxide films float out of the cake band area just above the filter disk.

Inclusions and Their Origins

Inclusion	*Description*	*Origin*
Carbides Al_4C_3	Tiny platelets or small chunks	Reduction of alumina - Carbon contamination
Dispersed Al_2O_3	Very tiny yellowish needles or clusters	Base metal or scrap contamination
Borocarbides Al_4B_4C	Tiny needles	Chemical reaction from boron in primary aluminum
TiB_2	Clusters of tiny particles	Grain refiner - Act as nuclei in grain size refining
MgO	Dispersed clusters of MgO particles	Chemical reaction between Mg and oxygen in furnace, ladle etc.
Cuboids	MgO particles being transformed in harder crystals	Chemical reaction between MgO and Al_2O_3 after significant time and high temperature
Spinel $MgAl_2O_4$	Hard films or chunks - Large inclusion	Chemical reaction of MgO and Al_2O_3 after significant time and high temperature
Graphite	Small or medium size inclusion	Comes from degradation of graphite equipment (lance, impellers, etc.)
Refractory	Medium to large size inclusion Hard inclusion	Comes from degradation of furnace lining
Nitrides AlN	Relatively hard inclusion - Film distribution	Chemical reaction between Al and air after significant time and high temperature
Chlorides NaCl, $MgCl_2$ etc.	Small voids	Chemical reaction between alkaline and chlorine gas during fluxing operation or chemical flux addition
Oxide films Gamma-Al_2O_3	Elongated films	Oxidation of Al from surface turbulence, splashing, etc.
Oxide films Alpha- Al_2O_3	Thicker film distribution	Oxidation of Al from turbulence after significant time and high temperature

QUANTITATIVE ASSESSMENT OF PODFA/PREFIL SAMPLES FOR SINTEF MATERIALS AND CHEMISTRY

REPORT NO. 040107

N-Tec Limited
21 October 2004

Prepared By:
Dr. A. Cushway

N-Tec Limited

Enabling Technologies for the Metals Industry

MOLTEN METAL QUALITY REPORT
N-Tec Limited
Report Ref: 040107

SAMPLE REFERENCE:

Four PoDFA residues and two PREFIL residues were supplied to N-Tec for quantitative evaluation. The samples were identified as 113, 123, 213, 223, 313, and 323.

TECHNIQUES:

Metallographic preparation, photography and quantitative metallographic analysis of the samples.

RESULTS

The results of the metallographic analyses are shown in the attached table.

All samples contained some refractory inclusions from the furnace walls, linings, tool coatings etc, plus a small amount of carbide. The samples differed principally in the number of oxide films and whether or not the films had thickened, and the amount ot titanium diboride (grain refiner). The thickened oxide films are counted in the category 'MgAl2O4-spinel / thickened oxide' Since the alloy does not contain magnesium the thickened films will not be spinel, so the best I can do is call them thickened oxide. Further work (SEM) would have to be undertaken to reveal more about the chemistry of the thickened films.

Prefil Evaluation Sheet

Customer Trial I.D:	Proj. No. 242789.13
Customer Name:	Harald Goerner
Sampling Plant:	
Company:	SINTEF Materialsteknogi
Report Date:	20.10.04
Report Number:	040107

Sample I.D:	113	213	313	
Alloy:	99.7 Al	99.7 Al	99.7 Al	
Location:				

Overall Metal Cleanliness

Inclusion Content (mm^2/kg)	0.061	0.098	0.166	
Oxide Film Content (No/kg)	10	128	69	

Oxide Films (Gamma-Al_2O_3)

Number/kg	10	128	69	
Length	Long and coiled	Short, Medium	Short	
Thickness	Thin	Thin and Thick	Fine	

Inclusions (mm^2/kg & % of total)

TiB_2/ TiC			0.026 15.7%	
$(Ti-V)B_2$				
Al_4C_3 < 3□m	Trace	Trace	Trace	
Al_4C_3 > 3□m	Trace	Trace	Trace	
Borocarbides				
MgO				
MgO-cuboids				
$MgAl_2O_4$-spinel/Thickened oxide		0.035 35.7%	0.013 7.8%	
Dispersed Al_2O_3				
Alumina needles				
Nitride				
Graphite				
Potential chlorides / micro-gas				
Salt / Fluoride / Bone ash				
Spinel-like / Kaowool / Silicate	0.061 100%	0.063 64.3%	0.127 76.5%	

Comments

113 - Very clean. A few long, thin, coiled oxide films.
123 - Lots of long, thin coiled oxide starting to thicken in places.
213 - Lots of oxide films starting to thicken in places.

Sample information

Filtered weight, kg	1.52	1.52	1.52	
Cord length, mm	12.2	11.9	11.8	
Method	Grid	Grid	Grid	
Magnification	x50/x100	x50/x100	x50/x100	

Prefil Evaluation Sheet

Customer Trial I.D:	Proj. No. 242789.13
Customer Name:	Harald Goerner
Sampling Plant:	
Company:	SINTEF Materialsteknogi
Report Date:	20.10.04
Report Number:	040107

Sample I.D:	123	223	323	
Alloy:	99.7 Al	99.7 Al	99.7 Al	
Location:				

Overall Metal Cleanliness

Inclusion Content (mm^2/kg)	0.239	0.092	0.043	
Oxide Film Content (No/kg)	210	6	16	

Oxide Films (Gamma-Al_2O_3)

Number/kg	210	6	16	
Length	Long and coiled	Short	Short, Med, Long	
Thickness	Thin	Thin	Thin	

Inclusions (mm^2/kg & % of total)

TiB_2/ TiC		0.029 31.5%	0.015 34.9%	
(Ti-V)B_2				
Al_4C_3 < 3□m	Trace	Trace	Trace	
Al_4C_3 > 3□m	Trace	Trace	Trace	
Borocarbides				
MgO				
MgO-cuboids				
$MgAl_2O_4$-spinel/Thickened oxide	0.017 6.6%			
Dispersed Al_2O_3				
Alumina needles				
Nitride				
Graphite				
Potential chlorides / micro-gas				
Salt / Fluoride / Bone ash				
Spinel-like / Kaowool / Silicate	0.239 93.4%	0.063 68.5%	0.028 65.1%	

Comments

223 - Very clean with a small amount of titanium diboride
313 - Similar to 213 but fewer films that have not thickened to the same extent. More refractory inclusions and some titanium diboride.
323 - Similar to 223 with a few more oxide films

Sample information

Filtered weight, kg	0.73	1.52	1.52	
Cord length, mm	12.0	12.0	12.4	
Method	Grid	Grid	Grid	
Magnification	x50/x100	x50/x100	x50/x100	

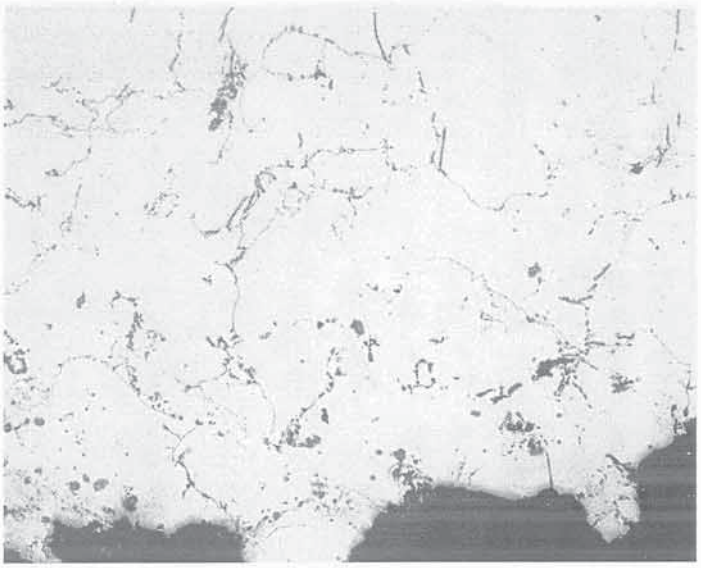

Fig. 1 Sample number 123 x100

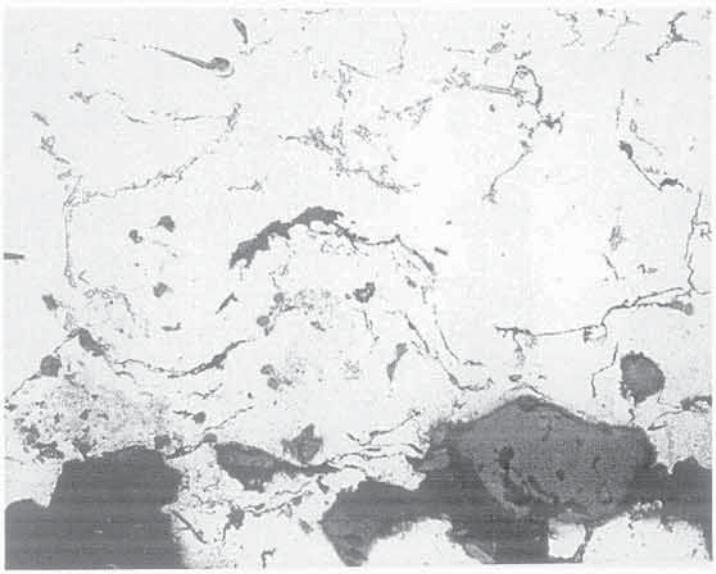

Fig. 2 Sample number 213 x200

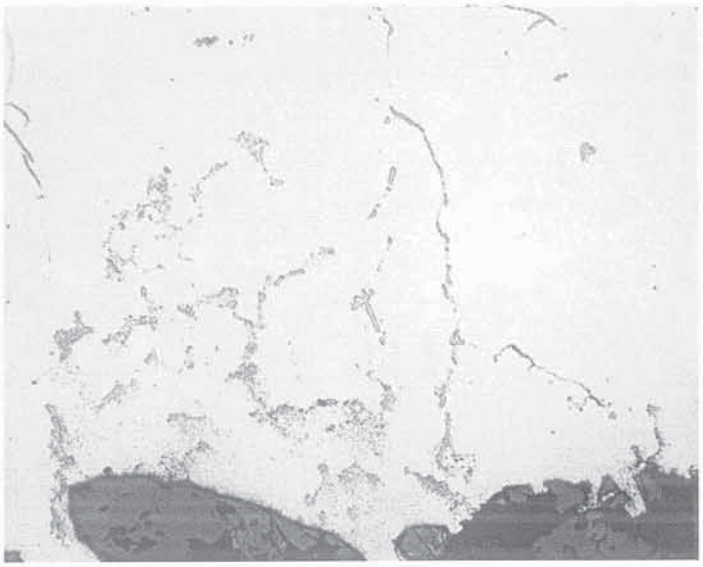

Fig. 3 Sample number 223 x200

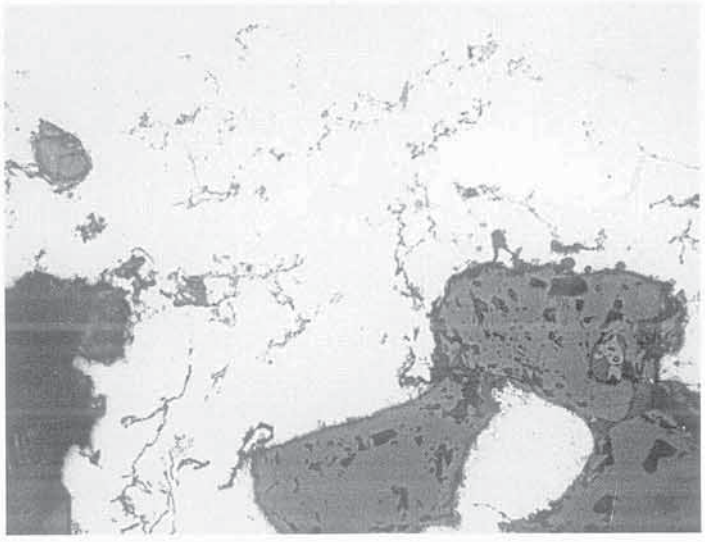

Fig. 4 Sample number 313 x200

Fig. 5 Sample number 323 x200

Appendix 1 – Metallographic Analysis and Prefil Curve Repeatability

Metallographic Analysis Repeatability

It was established that the repeatability of metallographic analysis is + 16% for an inclusion content over 1.25 mm^2/kg. The precision of the metallographic analysis decreases with an increase of the metal cleanliness. When the inclusion content is less than 0.07 mm^2/kg, repeatability is +40%. [Ref.: Metallographic Evaluation of PoDFA Inclusions Residue, Alcan, ARDC, Method # 2012-96]

Prefil Curves Repeatability

±10% error on mass at any time on filtration rate (g/s) curve for fresh A356 at 700°C. [Ref: Prefil specs]. Error due to sample size increases when sample size decreases. [Ref.: Kreyszig E., Advanced Engineering Mathematics, 7th edition, Wiley & sons inc.]

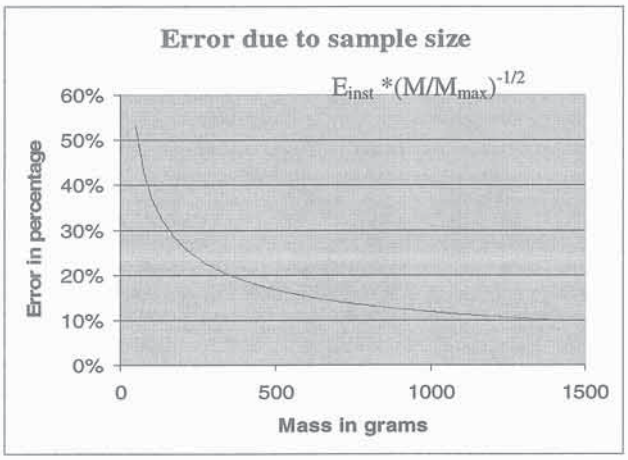

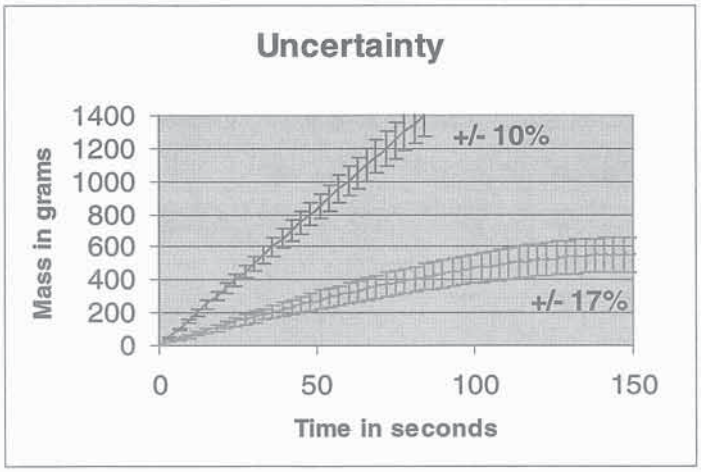

Oxide Films

Oxide films are difficult to measure by metallographic means because of the nature of the PoDFA analysis technique. The presence of oxide films in a sample is most probably underestimated. An oxide film is like a paper tissue in its shape, e.g.: a flexible plan. When a metallographer looks at a slice of a Prefil sample, what he sees is often just a slice of the oxide film plan. For instance, he may be looking to several slices of different oxide films as well as it may only be several parts of the same film. Because of the nature of this type of analysis, discrimination for fine variation in the content of oxide films is not conceivable. Only changes in the order of magnitude can be confirmed.

Oxide films have a lower density than aluminum and because of the long solidification time of a Prefil crucible, it is likely that oxide films float out of the cake band area just above the filter disk.

Based on these facts, the Prefil curve has to be trusted as a better mean of measuring oxide film content than metallographic analysis made by the PoDFA technique or other.

Prefil-Footprinter As A Process Control Tool

The Prefil-Footprinter instrument is designed for process control based on the establishment of industry benchmarks or local references. These benchmarks are valid for a particular alloy and test temperature. A benchmark can be established with many tests made under the same conditions. At least 10 tests are suggested to allow a minimum of confidence in the benchmark[1].
The Prefil-Footprinter curves should be used to see cleanliness tendencies in a batch of liquid metal. For example, when a change in cleanliness occurs in a process, the Prefil curves will get out of the range established for the benchmark. The confidence one may have in the change depends on the number of samples used to confirm the trend. For instance, quality control check based on one sample is questionable when a curve falls out of the benchmark. Conclusion must be drawn only when based on a batch of sample.

[1] A Simard & al, "Cleanliness Measurement Benchmarks of Aluminum Alloys Obtained Directly at-line Using the Prefil-Footprinter Instrument", Light Metals 2000/TMS 2000, Nashville TN.

Inclusions and Their Origins

Inclusion	*Description*	*Origin*
Carbides Al_4C_3	Tiny platelets or small chunks	Reduction of alumina - Carbon contamination
Dispersed Al_2O_3	Very tiny yellowish needles or clusters	Base metal or scrap contamination
Borocarbides Al_4B_4C	Tiny needles	Chemical reaction from boron in primary aluminum
TiB_2	Clusters of tiny particles	Grain refiner - Act as nuclei in grain size refining
MgO	Dispersed clusters of MgO particles	Chemical reaction between Mg and oxygen in furnace, ladle etc.
Cuboids	MgO particles being transformed in harder crystals	Chemical reaction between MgO and Al_2O_3 after significant time and high temperature
Spinel $MgAl_2O_4$	Hard films or chunks - Large inclusion	Chemical reaction of MgO and Al_2O_3 after significant time and high temperature
Graphite	Small or medium size inclusion	Comes from degradation of graphite equipment (lance, impellers, etc.)
Refractory	Medium to large size inclusion Hard inclusion	Comes from degradation of furnace lining
Nitrides AlN	Relatively hard inclusion - Film distribution	Chemical reaction between Al and air after significant time and high temperature
Chlorides NaCl, $MgCl_2$ etc.	Small voids	Chemical reaction between alkaline and chlorine gas during fluxing operation or chemical flux addition
Oxide films Gamma-Al_2O_3	Elongated films	Oxidation of Al from surface turbulence, splashing, etc.
Oxide films Alpha- Al_2O_3	Thicker film distribution	Oxidation of Al from turbulence after significant time and high temperature

B: Values Employed for Error Calculations

Table B.1: Values employed for error calculations

Exp.	Re	ΔRe	Sc	D	$a_v^2 / 6$	Δa_v	$(1-\varepsilon)/\varepsilon$	$\Delta\varepsilon$	t	Δt
1	18.38	0.49	81.40	6.16E-09	216600	106	1.22	0.035	23.82	0.64
2	14.21	1.51	81.40	6.16E-09	216600	106	1.22	0.035	30.79	1.45
3	18.60	0.54	81.40	6.16E-09	216600	106	1.22	0.035	23.54	0.69
4	11.25	0.39	92.78	5.40E-09	216600	106	1.22	0.035	38.92	1.40
5	14.29	1.29	92.78	5.40E-09	216600	106	1.22	0.035	30.87	3.07
6	5.22	1.51	92.78	5.40E-09	216600	106	1.22	0.035	83.75	1.45
7	19.52	1.61	92.78	5.40E-09	216600	106	1.22	0.035	11.28	0.95
8	22.79	1.00	92.78	5.40E-09	216600	106	1.22	0.035	9.61	0.41
9	21.23	1.13	92.78	5.40E-09	216600	106	1.22	0.035	10.33	0.56
10	20.03	2.04	92.78	5.40E-09	216600	106	1.22	0.035	5.52	0.58
11	13.28	1.22	92.78	5.40E-09	216600	106	1.22	0.035	8.30	0.79
12	10.04	0.11	92.78	5.40E-09	216600	106	1.22	0.035	10.89	0.12
13	10.76	2.29	81.40	6.16E-09	216600	106	1.22	0.035	20.33	0.68
14	10.19	0.39	81.40	6.16E-09	216600	106	1.22	0.035	21.50	0.81

C: Uncertainties Calculated for x and E

Table C.1: Uncertainties calculated for x and E

Exp.	x	Δx	c_{in}	Δc_{in}	c_{out}	Δc_{out}	E	ΔE	s (E)
1	0.92	0.20	170.91	12.99	19.45	2.07	88.59	13.39	1.12
2	1.03	0.23	98.11	21.91	3.11	0.93	96.67	41.99	1.15
3	0.92	0.20	156.57	21.78	6.14	1.03	96.08	24.80	0.42
4	1.04	0.22	29.62	2.03	0.88	0.28	97.02	32.67	1.02
5	0.95	0.23	35.04	2.33	1.91	0.73	94.53	37.00	1.99
6	1.43	0.39	26.83	3.13	1.20	0.63	95.33	52.50	2.67
7	0.42	0.10	37.52	2.28	10.07	0.66	73.08	7.87	2.24
8	0.39	0.08	41.32	1.97	11.34	0.47	72.50	5.74	1.71
9	0.40	0.09	47.37	1.89	16.73	1.38	64.70	6.48	2.25
10	0.21	0.05	44.71	1.97	24.04	1.56	46.20	4.16	3.32
11	0.24	0.06	47.21	1.95	21.03	1.35	55.37	4.81	3.51
12	0.27	0.06	41.40	1.36	15.86	1.58	61.68	6.80	3.82
13	0.58	0.14	23.28	2.64	8.16	2.54	65.53	22.98	7.16
14	0.59	0.13	35.59	2.77	10.69	1.50	70.05	12.49	2.61